12-15-2014

Advanced Digital Signal Processing Based Redefined Power Quality Indices, and Their Applications to Wind Power

Md Moinul Islam
University of South Carolina - Columbia

Advanced Digital Signal Processing Based Redefined Power Quality Indices, And Their Applications to Wind Power

by

Md Moinul Islam

Bachelor of Science
Bangladesh University of Engineering and Technology, 2007

Master of Engineering
University of South Carolina, 2011

Submitted in Partial Fulfillment of the Requirements

for the Degree of Doctor of Philosophy in

Electrical Engineering

College of Engineering and Computing

University of South Carolina

2014

Accepted by:

Charles Brice, Major Professor

Enrico Santi, Committee Member

Herbert Ginn, Committee Member

Lingyu Yu, Committee Member

Lacy Ford, Vice Provost and Dean of Graduate Studies

DEDICATION

Dedicated to my wife Navila Rahman, my newborn baby Maahira Islam, my late parents Md Nazrul Islam, and Shirin Akter, and my step mother Shahina Akter.

ACKNOWLEDGMENTS

I would like to thank all of those who contributed their valuable times to help me. A special thanks goes to my academic adviser Dr. Charles Brice who helped me in the strenuous process of my graduation, successful completion of research projects, finishing this dissertation document, and his continuous support to stay focus. I would like to thank Dr. Yong-June Shin as well for teaching me time-frequency analysis technique, and his time for my research publications, and for the support during his stay in the US. Dr. Roger Dougal and Dr. Enrico Santi also helped me through attending my practice presentations for GRid-connected Advanced Power Electronics Systems (GRAPES) center, and with their valuable guidelines and suggestions to make successful presentations and completion of the projects. I would like to thank Dr. Herbert Ginn and Dr. Lingyu Yu for attending my final defense. I would also like to thank Nat Paterson, Burt Ashley, and Hope Johnson for their time and efforts for helping me with official procedures for my dissertation, and research trips. I would like to thank Rich Smart as well for helping me writing my research publications.

I would like to thank the members of the Power IT group in South Carolina. I would like to thank Dr. Phillip E. C. Stone for helping me out in the beginning of my graduate research. I would also like to thank my collaborators Hossein Ali Mohammadpur and Cuong Nguyen for their help and contributions in the successful completion of the projects in a team-environment. Wang Jing-Jang, Mohammed Hassan, Patrick Mitchell, Ryan Lukens, Amin Ghaderi, and Qiu Deng were all members of the same research team, and gave me helpful advice and suggestions throughout my studies. Last, but not least, I would like to thank all of my family and close friends who sacrificed time for me: my wife Navila Rah-

man, my mother Shahina Akter, my siblings Mrs. Rahima Akter, Md Ziaul Islam, Fatema Akter, my uncle Md Monirul Islam, my friends Rassel Raihan, Iftekhar Hossain Shovon, B. M. Farid Rahman, Fazle Rabbi, Sayful Islam, Atikur Rahman, Faisal Jahan, and Ishtiaq Rouf who always supported me, and helped me focus. I would also like to thank all the Bangladeshi faculty members and the rest of the Bangladeshi community in Columbia, SC for wonderful times on different social, religious, and cultural occasions.

The projects that make up this dissertation document have been supported by Industry/University Cooperative Research Center on GRid-connected Advanced Power Electronics Systems (GRAPES) center. I would like to thank all the IAB members, especially Dr. Ram Adapa, involved in the GRAPES for their comments, and suggestions for successful completion of all the projects. Thanks to NREL and AEP for providing us real-world power quality disturbances that which have been utilized in my dissertation for analysis purpose.

ABSTRACT

This dissertation proposes a time-frequency distribution (TFD) based new method to redefine the power quality (PQ) indices for the assessment of PQ disturbances typically present in electric power systems. The redefined PQ indices are applied to various types of synthetic and real-world PQ disturbances in order to verify the efficacy and applicability of the proposed method. The case studies show that the proposed method provides actual results with respect to the existing TFD-based transient PQ indices, and provides much more accurate results than the traditional fast Fourier transform (FFT) based PQ indices under stationary and nonstationary PQ disturbances.

In addition, utilizing the proposed method, the power components contained in the IEEE Standard 1459-2010 are redefined for single-phase, and three-phase power systems under sinusoidal, nonsinusoidal, balanced and unbalanced conditions. Unlike the traditional FFT-based method, the proposed method is able to extract the time information lost in the FFT, and provides very accurate and instantaneous assessment of the power components according to the IEEE Standard 1459-2010. Also, the proposed method will have the advantage of finding the instantaneous direction of time-varying harmonics power flow which can be positive or negative depending on the harmonics flow to the network or to the load. According to the IEEE Standard 1459-2010, the harmonic active power P_H is obtained by subtracting the fundamental active power P_1 from the total active power P $(P_H = P - P_1)$. However, the indirect measurement of the harmonic active power may provide imprecise result since harmonic active power is generally very small part of the total active power. In this dissertation, a direct assessment of the harmonic active power is carried out to obtain accurate result based on the proposed method.

In addition, a new perspective for wind power grid codes is proposed in order to verify that a wind generating plant conforms to grid codes requirements under stationary and non-stationary PQ disturbances, and to obtain supervisory data to protect system reliability. The proposed method is also able to extract the dynamic signature of PQ disturbances introduced by variable speed wind energy conversion systems onto the electrical grid. Also, a TFD-based new method is proposed for the assessment of grid frequency deviation caused by wind power fluctuations in fixed speed wind energy conversion systems.

TABLE OF CONTENTS

LIST OF TABLES

LIST OF FIGURES

CHAPTER 1

INTRODUCTION

1.1 MOTIVATION AND OBJECTIVES

The increase penetration of nonlinear loads and power electronic devices such as distributed generation, variable frequency drives, electric arc furnaces, and flexible ac transmission systems in the existing grid are sources of low electric power quality (PQ) [1]-[7]. Low electric PQ encompasses the loss of 10 billion Euros in Europe, and U.S. 24 billion every year [8]. For assessment purpose of the electric power degradation, PQ indices such as total harmonic distortion (THD), distortion index (DIN), power factor (PF), telephone interference factor (TIF), C message, and K-factor are defined in [9]. The IEEE 519 [10] and IEC 61400-21 [11] are also two examples for the assessment of low electric PQ in electric power systems. The most recommended power theory for the assessment of low electric PQ can be found in IEEE Standard 1459 [12], [13] that defines a set of power components such as displacement power factor, distortion power, harmonic pollution, and total power factor for single-phase, and three-phase electrical power systems under sinusoidal, nonsinusoidal, balanced or unbalanced conditions.

According to the IEEE Standard 1459, the PQ indices are defined based on the "frequency domain" approach utilizing the fast Fourier transform (FFT). The application of the FFT in defining the power components according to the IEEE Standard 1459 is employed for single-phase and three-phase electrical power systems in [14], [15], respectively. However, FFT inherently assumes the signal is periodic, therefore, it can provide accurate results in case of stationary PQ disturbances only. In fact, not all real-world PQ disturbances

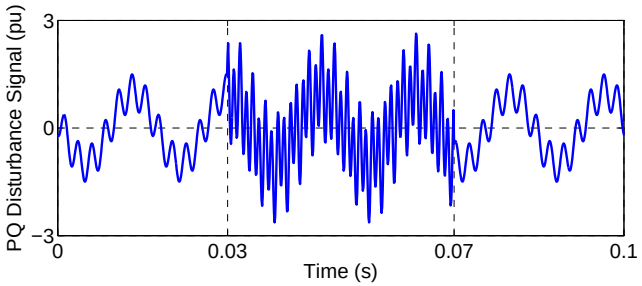

Figure 1.1: A nonstationary PQ disturbance signal comprised of 60 Hz, 7th, and time-varying 15th harmonic components.

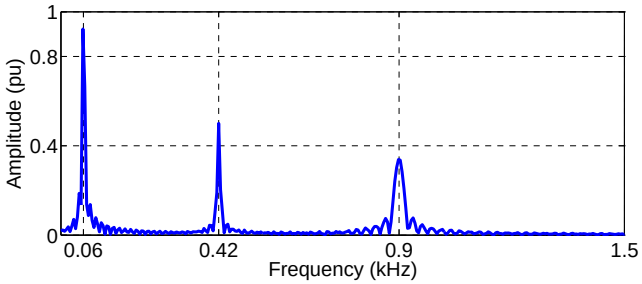

Figure 1.2: FFT of the nonstationary PQ disturbance signal.

such as voltage sag, voltage swell, capacitor switching, etc. result in periodic waveform and exhibit time-varying harmonics characteristics, and can be best described as nonstationary in nature. Therefore, FFT-based method provides erroneous assessment of the PQ indices in the presence of PQ disturbances typically present in electrical power systems due to spectral leakage [16]-[25]. In addition, no time information can be obtained via FFT since the power components are evaluated in the frequency domain. For example, Fig. 1.1 represents a nonstationary PQ disturbance signal which is composed of 60 Hz, 7th harmonic, and time-varying 15th harmonic that persists from 0.03 to 0.07 s. The corresponding FFT in Fig. 1.2 confirms that the PQ disturbance signal is comprised of 60 Hz, 7th, and 15th harmonic components, however, it does not provide any time information regarding the presence of these frequency components in the PQ disturbance signal. Also, side lobes are observed in Fig. 1.2 at other frequency components rather than 60 Hz, 7th, and 15th harmonic components due to spectral leakage phenomenon that causes inaccurate

assessment of nonstationary PQ disturbances.

Regarding the limitations of the FFT, "time domain" techniques based on the Clarke-Park transformation have been utilized for the measurement purpose of the power components in [26]-[31]. The approaches in [29]-[31] are particularly more convenient than the frequency domain technique for the measurement of the power components according to the IEEE Standard 1459 as one can assess the fundamental and positive-sequence components of voltage and current without any spectral analysis. Nonetheless, the assessment of the power components under nonsinusoidal conditions may be erroneous because of the low-pass filters employed in the methods [32]. It has been illustrated in [32] that in order to obtain more accurate results using the methods in [29]-[31], high order filters with specific cut-off frequencies must be employed depending on the grid conditions. Therefore, low-pass filters are replaced in [32] with a recursive algorithm which estimates the average values. The method shows improved assessment precision, however, it suffers from synchronization restrictions for frequency excursions as does the FFT [33].

"Time-frequency domain" is another viable alternative approach for the analysis of PQ disturbances as it can preserve simultaneous time and variable harmonics information of nonstationary PQ disturbance events. One of the time-frequency domain techniques based on wavelet transform has been frequently utilized in assessment, detection, localization, and classification of nonstationary PQ disturbances in [34]-[39]. Also, Morsi et al. redefined the single-phase and three-phase power components in time-frequency domain according to the IEEE Standard 1459 employing discrete wavelet transform, stationary wavelet transform, and wavelet packet transform in [17]-[21], which acquire very accurate results for different types of stationary and nonstationary PQ disturbance events. However, wavelet transform employs long window for low frequency components, and short window for high frequency components, respectively. Therefore, good frequency resolution but low time resolution are obtained for the low frequency components, and good time resolution but low frequency resolution are acquired for the high frequency components

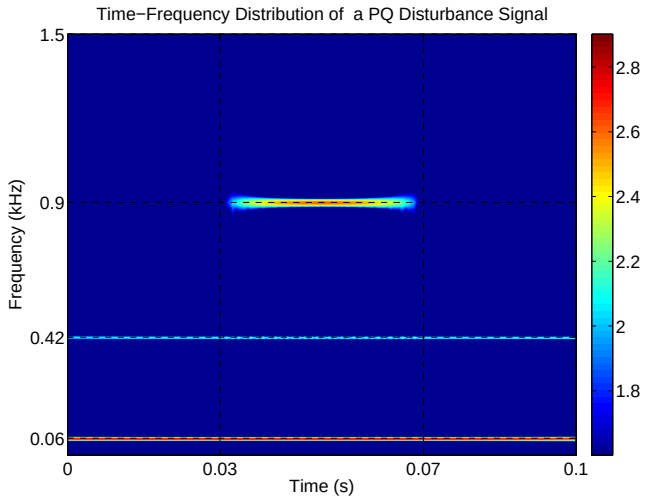

Figure 1.3: Time-frequency distribution of the nonstationary PQ disturbance signal in Fig. 1.1

[40]. Therefore, wavelet transform is particularly convenient for the analysis of nonstationary PQ disturbances when the signal is composed of high frequency components for short duration, and low frequency components for long duration, for example, a signal with transient disturbances [40].

The application of another "time-frequency domain" approach based on time-frequency distribution (TFD) is also motivated as it can provide both time and variable harmonics information of nonstationary PQ disturbances. The time-varying harmonics in electric power systems have been heavily studied in [41]-[58]. However, TFD can also be employed for the purpose of identifying, monitoring, and analyzing the time-varying harmonics of nonstationary PQ disturbances which will be discussed in the scope of the work in this dissertation. For example, Fig. 1.3 represents the TFD of the PQ disturbance signal in Fig. 1.1, and shows the presence of 60 Hz, 7th harmonic, and time-varying 15th harmonic components in the time-frequency domain, and provides good time and frequency resolutions as well for both low and high frequency components. Thus, TFD restores the time information and time-frequency resolution lost in the FFT and wavelet transform, respectively. The following is a brief summary of the previous works for the analysis of stationary and

nonstationary PQ disturbances typically present in electric power systems employing the TFD.

TFD can be classified into linear and bilinear TFDs. A classical linear TFD is the short time Fourier transform (STFT) that computes the FFT of the PQ disturbance signal for a short time duration by a time-localized window [16]. If the time window is sufficiently narrow, the PQ disturbance signal is considered as periodic so that FFT can be employed. Employing the STFT technique, [59]-[63] performed electrical PQ assessment and characterization of distributed PQ disturbance events. Nonetheless, one significant disadvantage of the STFT is the inherent tradeoff between time and frequency resolution [16]. The squared STFT, known as the spectrogram, has been employed for the PQ analysis in [64]-[65]. However, the analytic signal representation of PQ disturbances is considered in these works. Therefore, [64]-[65] provide misleading results as the energy of a original PQ disturbance signal is half the energy of the analytic signal [16].

Bilinear TFDs such as Wigner-Ville (WV), Choi-Williams (CW), reduced interference distribution (RID), Zhao-Atlas-Marks (ZAM), Born-Jordan (BJ), Page are generalized by L. Cohen in [16]. In [66], WV TFD is utilized for the analysis and detection of PQ disturbance events, such as voltage sag, voltage swell and harmonics. However, WV TFD suffers from a severe cross-terms issue since no time-frequency domain filter is employed to minimize the cross-terms. Therefore, the presence of cross-terms leads to misleading sag and swell magnitudes in [66].

In order to minimize the cross-terms low pass time-frequency domain filter, known as kernel, is introduced in CW, RID, ZAM, BJ, Page TFDs [69]-[73]. Employing the CW and RID kernels PQ analysis has been carried out for transient disturbances in [67]-[68], and [22]-[24]. In [22], a set of PQ indices such as instantaneous THD, instantaneous DIN, instantaneous frequency, and instantaneous K-factor are proposed for transient disturbances based on the energy information provided by RID TFD, and these transient PQ indices have been employed for the assessment of wind power PQ disturbances in [23]-[24]. However,

the PQ assessment utilizing the existing transient PQ indices in [22] provide misleading results, as the indices are defined based on the energy instead of rms values [25].

Regarding the limitations of the existing transient PQ Indices, in this dissertation, a solution has been provided based on the RID TFD which redefines the existing transient PQ indices, and provides precise results under different types of stationary and nonstationary PQ disturbances. Also, other PQ indices, such as power factor, telephone interference factor, K-factor, and C message are redefined in the time-frequency domain employing RID TFD. The accuracy of the proposed method has been compared to the traditional FFT-based method which justifies that the proposed method provides much more accurate results than the FFT-based method under nonstationary PQ disturbances.

The second contribution of this dissertation is redefining the PQ indices contained in the IEEE Standard 1459-2010 employing TFD method. Although, TFDs have been frequently utilized for the analysis of PQ disturbance events, there is not yet much work devoted to defining power components for single-phase and three-phase electric power systems under stationary and nonstationary PQ disturbances according to the IEEE Standard 1459-2010. There are two reasons that can limit the application of the TFDs in defining the power components. First, selection of the proper TFD in order to minimize the cross-terms. Second, Cohen's class TFDs cannot provide any phase information for a pair of voltage and current signals [25], [74].

Regarding the limitation of the TFD in obtaining phase information, a new state of the art method cross TFD (XTFD) is proposed in [74] which allows one to obtain time- and frequency-localized phase difference, active power, and reactive power information for PQ disturbances. The XTFD method is employed to capacitor switching direction finding and postural sway behavior in [75], and [76], respectively. However, like cross-terms, cross-power will emerge if a pair of voltage and current PQ disturbance signals are composed of multiple frequency components that has not been addressed in [75], and [76]. Therefore, the presence of cross-power in XTFD may provide inaccurate assessment of phase angle

difference, active power, and reactive power for a pair of voltage and current signals. In this dissertation, the cross-power issue associated with the XTFD has been identified, and a solution has been provided by utilizing the RID and Page TFDs which are able to minimize the cross-terms and cross-power, simultaneously.

Based on the TFD and XTFD, in this dissertation, a new method is proposed for the assessment of power components according to the IEEE Standard 1459-2010 for single-phase and three-phase stationary and nonstationary PQ disturbances. Unlike the FFT, the proposed method is able to estimate the power components precisely under sinusoidal, nonsinusoidal, transient, balanced or unbalanced conditions. Additionally, the technique will allow one to identify the time-varying frequency components responsible for transient disturbances. Also, one can find the direction of transient active and reactive power flow in electric power systems through XTFD. The IEEE Standard 1459 measures the harmonic active power by subtracting the fundamental active power from the total active power. This indirect measurement of the harmonic active power may result in inaccurate assessment since harmonic active power is generally very small part of the total active power [30]. Utilizing the XTFD, in this dissertation, a direct assessment of the harmonic active power is performed to obtain precise result. In addition, this dissertation represents the harmonics active power in the time-frequency domain employing XTFD method which will enable one to monitor, analyze, and identify time-varying harmonics active power typically present in electric power systems.

Finally, in this dissertation, a new perspective for wind power grid codes, issued by the Federal Energy Regulatory Commission (FERC) [77] in the U.S., is proposed utilizing the Page TFD-based three-phase power components under stationary and nonstationary PQ disturbances. The proposed technique provides instantaneous verification of wind power grid codes under various wind PQ disturbances introduced by commonly used variable speed wind energy conversion systems onto the grid. The efficacy of the proposed method has been demonstrated by employing it to three real-world wind PQ disturbances collected

from Trent Mesa wind generating plant in Texas - a voltage sag, a transient, and a oscillatory type PQ disturbances. The analysis results detect large amount of reverse active power flow into the Trent Mesa wind farm in case of voltage sag disturbance. Therefore, disconnections of wind generating plant from the grid may be required in order to protect system reliability. Also, the proposed method is able to extract the dynamic signature of PQ disturbances typically present in wind power systems.

1.2 ORGANIZATION

The organization of this dissertation is as follows:

- In chapter 2 fundamentals of the TFD and cross TFD methods are discussed, rms value, average active power, and reactive power are defined correctly in time-frequency domain utilizing TFD and XTFD, issues associated with the TFD and cross TFD in defining PQ indices are pointed out, and solutions are recommended with the selection of appropriate TFDs.

- Chapter 3 shows the application of the existing transient PQ indices for PQ analysis of variable speed wind energy conversion systems.

- In chapter 4, a TFD-based new method is proposed for the assessment of grid-frequency deviation caused by wind power fluctuations in fixed speed wind energy conversion systems.

- In chapter 5, the limitations of existing transient PQ indices [22] are discussed, and a solution is provided by redefining the existing PQ indices which provide correct assessments, and much more accurate results than the traditional FFT-based method.

- A novel method based on the RID TFD is proposed in chapter 6 for instantaneous assessment of single-phase power components according to IEEE Standard 1459-2010.

- Chapter 7 redefines the three-phase power components according to the IEEE Standard 1459-2010 based on Page TFD which provides more accurate results and faster computational speed than previously used RID method.

- Based on the improved the Page TFD method proposed in the chapter 7, a new perspective for wind power grid codes is proposed in chapter 8 to verify that a wind generating plant conforms to the grid codes requirements, issued by the FERC, under PQ disturbances.

- Finally, conclusions are drawn in chapter 9.

CHAPTER 2

TIME-FREQUENCY DISTRIBUTION, AND ITS ISSUES IN DEFINING POWER QUALITY INDICES

2.1 TIME-FREQUENCY DISTRIBUTION

Traditional fast Fourier transform (FFT) cannot provide time-localized information of the time-varying characteristics of nonstationary PQ disturbances typically present in electrical power systems. Therefore, the application of time-frequency distribution (TFD) is motivated as it has the ability to provide time and variable frequency information of nonstationary PQ disturbances. The first approach in the TFD is the short time Fourier transform (STFT) that takes Fourier transform of nonstationary PQ disturbances for a short time duration specified by a time localized window. The absolute value squared of the STFT is called the spectrogram which is defined for a signal s(t) as follows:

$$SP_s(t,\omega) = |STFT_s(t,\omega)|^2 = |\frac{1}{\sqrt{2\pi}}\int_{-\infty}^{\infty} s(\tau)h(\tau-t)e^{-j\omega\tau}d\tau|^2 \tag{2.1}$$

However, uncertainty principle [78] inhibits the application of STFT for the analysis of PQ disturbances. The uncertainty principle is the product of the time resolution Δt, and frequency resolution $\Delta\omega$, and expressed as follows:

$$\Delta t \cdot \Delta\omega \geq \frac{1}{2} \tag{2.2}$$

The uncertainty principal implies that the product of time resolution and frequency resolution has a lower boundary, therefore, it is not possible to obtain high time resolution and frequency resolution for a signal simultaneously. In other words, there is an inherent tradeoff between time resolution and frequency resolution in case of STFT.

Wigner-Ville (WV) TFD is a prototype distribution function that is qualitatively different from the spectrogram and STFT. The definition of $WV(t,\omega)$ TFD is as follows:

$$WV_s(t,\omega) = \frac{1}{2\pi}\int s^*(u-\frac{\tau}{2})s(u+\frac{\tau}{2})e^{-j\tau\omega}d\tau \tag{2.3}$$

The WV TFD is said to be bilinear in the signal as the signal appears twice in Eq. (2.3). Note that $s(t)$ in the Eq (2.3) is analytic representation of the original signal. The purpose of the analytic signal representation is to consider the positive frequencies only in the TFD [16].

WV TFD is a bilinear transform, and suffers from a severe cross-terms issue if a signal is composed of multiple frequency components. For example, consider the following signal:

$$s(t) = A_1 e^{j\omega_1 t} + A_2 e^{j\omega_2 t} \tag{2.4}$$

According to the Eq. (2.3), WV TFD of the signal s(t) is calculated as follows:

$$\begin{aligned} WV_s(t,\omega) &= \frac{1}{2\pi}\int \left(A_1 e^{j\omega_1(t+\frac{\tau}{2})} + A_2 e^{j\omega_2(t+\frac{\tau}{2})}\right)\left(A_1 e^{-j\omega_1(t-\frac{\tau}{2})} + A_2 e^{-j\omega_2(t-\frac{\tau}{2})}\right)e^{-j\omega\tau}d\tau \\ &= \underbrace{A_1^2\delta(\omega-\omega_1)}_{WV(t,\omega_1)} + \underbrace{A_2^2\delta(\omega-\omega_2)}_{WV(t,\omega_2)} + \underbrace{2A_1A_2\cos((\omega_2-\omega_1)t)\delta(\omega-\frac{\omega_1+\omega_2}{2})}_{\textbf{cross-terms}} \end{aligned} \tag{2.5}$$

We see that the WV TFD of the sum of the two signals is not the sum of the WV distribution of each signal but has the cross-term. Regarding the limitation of WV TFD, Choi-Williams [69] suggested, and Jeong and Williams provided the reduced interference distribution (RID) [70] function by introducing a two dimensional low pass filter in the time-frequency domain. The definition of CW TFD is as follows:

$$CW_s(t,\omega;\sigma) = \frac{1}{4\pi^{\frac{3}{2}}}\int_{-\infty}^{\infty}\int_{-\infty}^{\infty}\frac{1}{\sqrt{\tau^2/\sigma}}s^*(u-\frac{\tau}{2})s(u+\frac{\tau}{2})e^{-\sigma(u-t)^2/\tau^2-j\tau\omega}dud\tau \tag{2.6}$$

The CW TFD of the signal in the Eq. (2.4) is as follows:

$$CW_s(t,\omega;\sigma) = A_1^2\delta(\omega-\omega_1) + A_2^2\delta(\omega-\omega_2) + 2A_1A_2\cos((\omega_2-\omega_1)t)\eta(\omega,\omega_1,\omega_2,\sigma) \tag{2.7}$$

where

$$\eta(\omega,\omega_1,\omega_2,\sigma) = \sqrt{\frac{1}{4\pi(\omega_1-\omega_2)^2/\sigma}}e^{-(\omega-\frac{1}{2}(\omega_1+\omega_2))^2/4(\omega_1-\omega_2)^2/\sigma} \tag{2.8}$$

Table 2.1: Kernels of Cohen's class TFDs

Name	Kernel $\phi(\theta,\tau)$
Spectrogram	$s^*(u-\frac{\tau}{2})s(u+\frac{\tau}{2})e^{-j\theta u}du$
WV	1
CW	$e^{-\theta^2\tau^2/\sigma}$
RID	2D symmetric low poss filter
ZAM	$g(\tau)\lvert\tau\rvert\frac{sin\alpha\theta\tau}{\alpha\theta\tau}$
BJ	$\frac{\sin\frac{1}{2}\theta\tau}{\frac{1}{2}\theta\tau}$
Page	$e^{j\theta\lvert\tau\rvert}$

We can see that cross-term can be minimized significantly with the selection of small value of σ, however, they cannot be minimized completely.

Besides CW TFD, there are other TFDs, such as reduced interference distribution (RID), Zhao-Altas-Marks (ZAM), Born-Jordan (BJ), Page, etc that are utilized to minimize the cross-terms in time-frequency domain [16]. All TFDs can be obtained from the definition of Cohen's class as [16]:

$$TFD_s(t,\omega;\phi)=\frac{1}{4\pi^2}\int\int\int s^*(u-\frac{\tau}{2})s(u+\frac{\tau}{2})\phi(\theta,\tau)e^{-j\theta t-j\tau\omega+j\theta u}d\theta d\tau du \qquad (2.9)$$

where $s(t)$ is the analytic (complex) representation of a signal, and $s^*(t)$ is the complex conjugate of $s(t)$, respectively. The variable θ represents a frequency domain shift and τ a time domain shift. The two dimensional function $\phi(\theta,\tau)$ is known as a kernel which is basically two dimensional low pass filter employed in the time-frequency domain in order to minimize the cross-terms. Some examples of the kernels, that belongs to Cohen's class TFD, are provided in the Table 2.1.

The time-frequency representation of a signal will depend on the selection of the kernel $\phi(\theta,\tau)$. For the selection of the kernel, we will focus on the two significant properties of the TFD, time and frequency marginal properties, in defining PQ indices for PQ disturbances. The time and frequency marginal properties of the TFD are expressed in the following

manner [16]:

Time Marginal of TFD:

$$TM_s = \int TFD_s(t,\omega;\phi)d\omega = |s(t)|^2; \quad \{\text{for } \phi(\theta,\tau=0)=1\} \tag{2.10}$$

Frequency Marginal of TFD:

$$FM_s = \int TFD_s(t,\omega;\phi)dt = |S(\omega)|^2; \quad \{\text{for } \phi(\theta=0,\tau)=1\} \tag{2.11}$$

where $S(\omega)$ denotes the Fourier transform of the time domain signal s(t). Therefore, TFD collapses to absolute value squared time domain signal for the time marginal with the kernel requirement such that $\phi(\theta,\tau=0)=1$, and absolute value squared Fourier transform for the frequency marginal with the kernel requirement $\phi(\theta=0,\tau)=1$. Note that Parseval's theorem provides the physical validity of FFT-based PQ indices for periodic waveforms, In the same way, time and frequency marginal properties confirm the physical validity of TFD-based PQ indices which we will redefine in this dissertation for PQ disturbances.

2.2 Issues Associated with TFD in Defining PQ Indices

In this section, we will point out the potential issues associated with TFD in defining PQ indices for PQ disturbances. At first, we will focus on defining rms value appropriately utilizing the TFD.

Defining RMS Value

The rms value of a signal $s(t)$ is defined as follows:

$$S = \sqrt{\frac{1}{T}\int_0^T s(t)^2 dt} \tag{2.12}$$

However, TFD utilizes the analytic signal representation instead of the original signal, and provides energy information of the analytic signal $E_a = |s(t)|^2$ according to the time-marginal property. The spectrum of the original real signal satisfies $|S(\omega)| = |S(-\omega)|$, and

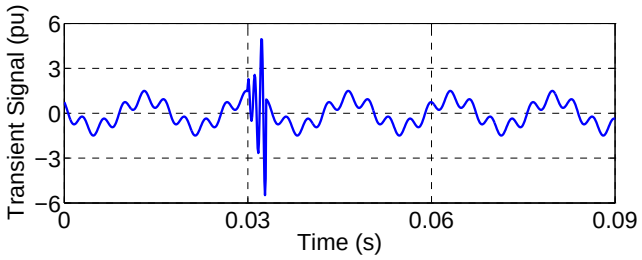

Figure 2.1: (a) A transient PQ disturbance.

therefore the energy of the original signal E_{org} is as follows:

$$E_{org} = \int_{-\infty}^{\infty} |S(\omega)|^2 d\omega = 2\int_{0}^{\infty} |S(\omega)|^2 d\omega = \frac{1}{2}\int |2S(\omega)|^2 d\omega = \frac{1}{2}E_a \tag{2.13}$$

Therefor, one can define the rms value based on the time marginal property of the TFD as follows:

$$S^{TFD} = \frac{1}{\sqrt{2}}\sqrt{\frac{1}{T}\int_{0}^{T}\int_{\omega} TFD_s(t,\omega;\phi)d\omega dt} \tag{2.14}$$

The scale factor $\frac{1}{\sqrt{2}}$ is introduced in the TFD-based rms Eq. (2.14) as the energy of the original signal is half the energy of the analytic signal. In [64]-[65], the scale factor is missing in the rms definition which leads to erroneous assessments of rms values of PQ disturbances. Therefore, one should be careful in utilizing TFD-based rms value for the assessment of PQ disturbances because of the scale factor $\frac{1}{\sqrt{2}}$.

Cross-terms

Cohen's class TFDs are bilinear transform, therefore, cross-terms will be emerged in case of a signal composed of multiple frequency components. Therefore, the selection of the TFD should be carefully investigated in defining PQ indices utilizing TFDs since the presence of cross-terms may lead to erroneous assessment of PQ disturbances. Fig. 2.1 shows a transient PQ disturbance signal which is composed of 60 Hz, 5th harmonic, and time-varying 15th harmonic component that appears at $t = 0.03$ s. The corresponding TFDs utilizing the WV and RID are shown in Fig. 2.2(a) and (b), respectively. As seen in the

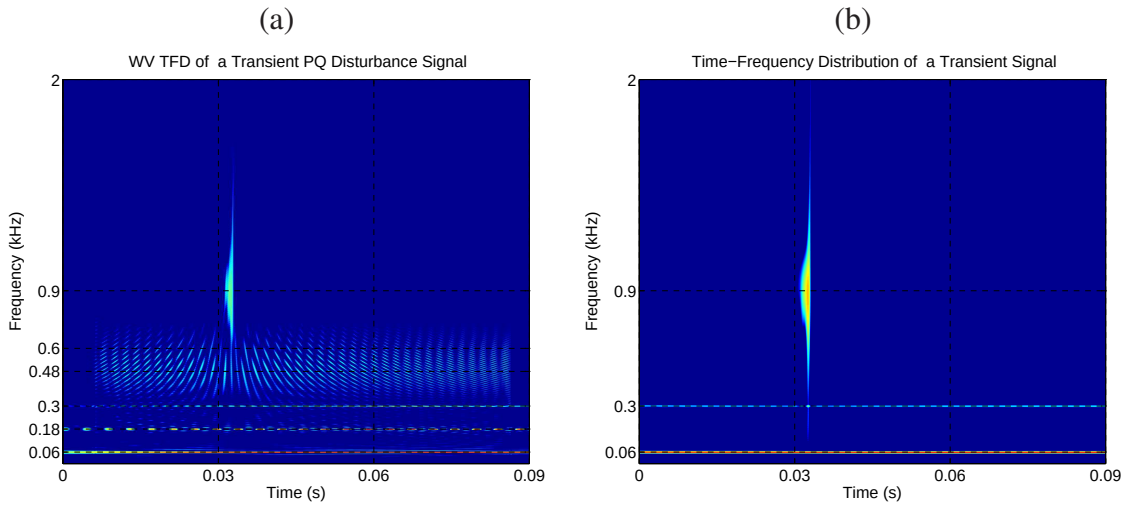

Figure 2.2: TFD of the transient signal utilizing (a) WV TFD, and (b) RID TFD.

Fig. 2.2(a), we can see the presence of cross-terms at 180 Hz in between 60 Hz and 5th harmonic, and cross-terms with center frequencies of 480 Hz, and 600 Hz in between 5th harmonic and 15th harmonic components. However, utilizing the RID, the cross-terms are minimized, therefore, only the original frequency components 60 Hz, 5th harmonic and time-varying 15th harmonic are observed in the TFD as seen in Fig. 2.2(b).

Phase Information

The self-conjugate terms $s^*(u-\frac{\tau}{2})s(u+\frac{\tau}{2})$ in the Cohen's Eq. (2.9) basically provide energy information $|s(t)|^2|$ of a signal according to the time marginal property, therefore cannot provide any phase information for a pair of voltage and current PQ disturbances. Thus, active power, and reactive power information cannot be obtained utilizing Cohen's class TFDs. In order to obtain phase information, self conjugate terms $s(u+\frac{\tau}{2})s^*(u-\frac{\tau}{2})$ in the Eq. (2.9) are replaced by a pair of PQ voltage and current disturbance signals as $v(u+\frac{\tau}{2})i^*(u-\frac{\tau}{2})$. The state-of-the-art, known as cross time-frequency distribution (XTFD), is introduced in [74], and expressed as follows:

$$XTFD_{vi}(t,\omega;\phi) = \frac{1}{4\pi^2}\int\int\int v(u+\frac{\tau}{2})i^*(u-\frac{\tau}{2})\phi(\theta,\tau)e^{-j\theta t-j\tau\omega+j\theta u}d\theta d\tau du \qquad (2.15)$$

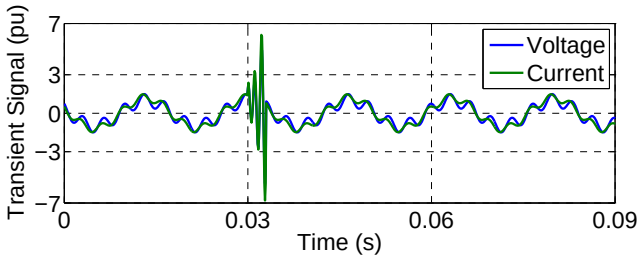

Figure 2.3: Transient PQ voltage and current disturbances.

Thus, time-frequency complex power according to the Eq. (2.15) can be expressed in the following manner [74]:

$$XTFD_{vi}(t,\omega;\phi) = |XTFD(t,\omega;\phi)|e^{j\Theta_{vi}(t,\omega;\phi)} \tag{2.16}$$

where $\Theta_{vi}(t,\omega;\phi)$ is the time-frequency phase spectrum of phase angle difference between voltage and current signals as:

$$\Theta_{vi}(t,\omega;\phi) = \Theta_v(t,\omega;\phi) - \Theta_i(t,\omega;\phi) \tag{2.17}$$

Note that the phase difference between voltage and current is localized in terms of "time" and "frequency" simultaneously, and corresponds to the classical power angle. In addition, the time and frequency marginal properties of the XTFD breakdown to the classical notations of power either in the time domain or in the frequency domain as follows:

Time Marginal of Cross TFD:

$$TM_{vi} = \int XTFD_{vi}(t,\omega,\phi)d\omega = v(t)\cdot i^*(t) \tag{2.18}$$

Frequency Marginal of Cross TFD:

$$FM_{vi} = \int XTFD_{vi}(t,\omega,\phi)dt = V(\omega)\cdot I^*(\omega) \tag{2.19}$$

where $V(\omega)$ and $I(\omega)$ are Fourier transform of the voltage and current signals $v(t)$ and $i(t)$, respectively. Based on the time marginal property of the XTFD, one can obtain instantaneous active power P, reactive power Q, and apparent power S for a pair of voltage and

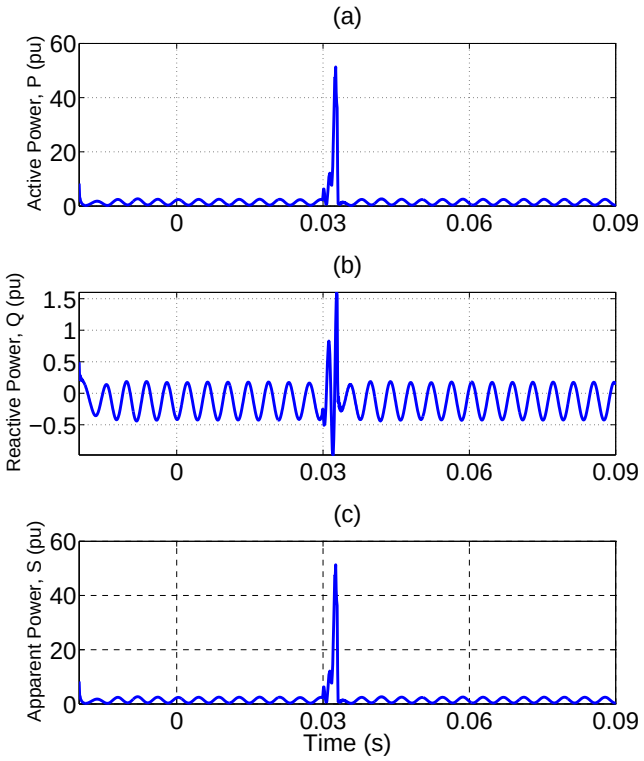

Figure 2.4: (a) Active power P, (b) Reactive power Q, and (c) Apparent power S obtained via RID.

current signals as follows:

$$P(t) = \Re\left\{\int XTFD_{vi}(t,\omega,\phi)d\omega\right\} \tag{2.20}$$

$$Q(t) = \Im\left\{\int XTFD_{vi}(t,\omega,\phi)d\omega\right\} \tag{2.21}$$

$$S(t) = abs\left\{\int XTFD_{vi}(t,\omega,\phi)d\omega\right\} \tag{2.22}$$

Fig. 2.4 represents an example of the instantaneous active power P, reactive power Q, and apparent power S for a pair of transient voltage and current disturbance signals shown in Fig. 2.3 obtained via RID.

Obtaining Average Active Power and Reactive Power

Like time marginal property of the TFD, XTFD utilizes the analytic signal representation of a pair of voltage and current signals, and provides complex power with time based on

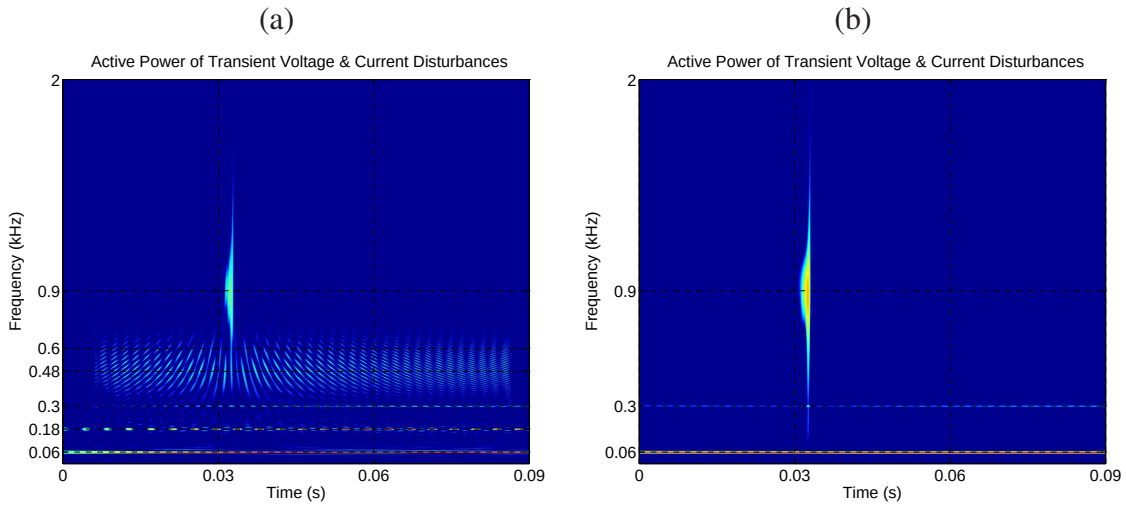

Figure 2.5: Active power of the voltage and current PQ disturbances utilizing (a) WV TFD, and (b) RID TFD

the time marginal property of XTFD. However, complex power of the original signal S^*_{org} will be half the complex power of analytic signal S^*_a as follows:

$$S^*_{org} = \int_{-\infty}^{\infty} V(\omega)I^*(\omega)d\omega = 2\int_{0}^{\infty} V(\omega)I^*(\omega)d\omega = \frac{1}{2}\int (2V(\omega))(2I^*(\omega))d\omega = \frac{1}{2}S^*_a \quad (2.23)$$

Therefore, based on the XTFD, one can define the average active power and reactive power as follows:

$$P^{XTFD} = \frac{1}{2}\cdot\frac{1}{T}\int_0^T \Re\left\{\int_\omega XTFD_{vi}(t,\omega;\phi)d\omega\right\}dt \quad (2.24)$$

$$Q^{XTFD} = \frac{1}{2}\cdot\frac{1}{T}\int_0^T \Im\left\{\int_\omega XTFD_{vi}(t,\omega;\phi)d\omega\right\}dt \quad (2.25)$$

Note that the scale factor $\frac{1}{2}$ is introduced in the average active power and reactive power definitions as the complex power of the original voltage and current signals is half the complex power of the analytic voltage and current signals.

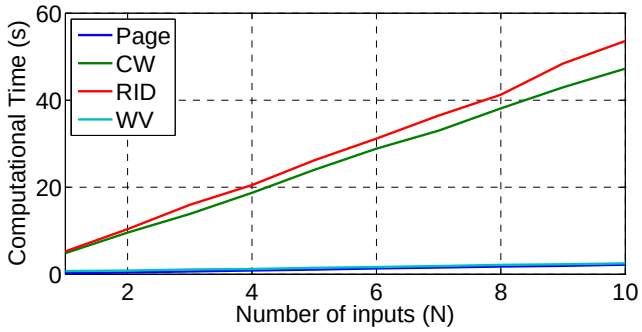

Figure 2.6: Computational time associated with WV, CW, RID, and Page TFDs with an increase number of inputs.

Cross-Power

Like cross-term, cross-power will emerge in the XTFD if a voltage and a current PQ disturbance signals are composed of multiple frequency components. For example, Fig. 2.3 shows a pair of voltage and current PQ transient disturbances which are composed of 60 Hz, 5th and time-varying 15th harmonic components. Utilizing the WV TFD in Fig. 2.5 (a), we can see the presence of cross-power at 3rd harmonic, and in between 5th and 15th harmonic components with center frequencies of 8th and 10th harmonic components. Thus, the presence of cross-power may provide erroneous assessment in [75]-[76] that utilize WV TFD for direction finding of capacitor switching and postural sway behavior. However, cross-power can be minimized by proper selection of the TFD. For example, Fig. 2.5(b) justifies that utilizing the RID cross power are minimized in the time-frequency domain. Therefore, cross-power in the XTFD should be carefully treated in defining PQ indices, and to obtain accurate results.

Computational Complexity

Cohen's class TFDs are bilinear transforms of the signal, and suffer from a high computational complexity [79]. However, computational complexity can be reduced by selecting a suitable TFD for the assessment of PQ indices for PQ disturbances. The computational

time associated with WV, CW, RID, and Page TFDs are shown Fig. 2.6 which justifies that WV and Page TFDs provide much lower computational time than the CW and RID with an increase number of inputs. Therefore, for faster computational speed one can select the WV and Page TFDs, however, WV TFD suffers from cross-terms and cross-power issues, therefore, for faster computational speed we will employ Page TFD in this dissertation.

In this chapter, we introduce the TFD method, and identify the significant issues associated with TFD and XTFD in defining PQ indices for PQ disturbances. It can be concluded that STFT, SP, and WV TFDs are not suitable TFDs in defining the PQ indices as there is an inherent tradeoff between time and frequency resolution in STFT, SP does not satisfy the marginal properties [16], and WV suffers from a severe cross-terms and cross-power issues. Therefore, the application of other TFDs such as CW, RID, ZAM, BJ, and Page TFDs are recommended in defining PQ indices as they employ two dimensional low-pass filter to minimize the cross-terms, and cross-power, provide good time and frequency resolution, and satisfy the marginal properties of the TFD and XTFD. Also, rms value of a PQ disturbance signal, and active and reactive power for a pair of voltage and current PQ disturbance signals are defined correctly by introducing the scale factors. Utilizing the TFD method, in this dissertation, we will redefine the existing RID-based transient PQ indices [22], PQ indices for single-phase and three-phase electric power systems according to the IEEE Standard 1459-2010 [13], and will propose a new perspective for wind power grid codes utilizing the three-phase PQ indices. At first, we will review and demonstrate the applications of RID-based existing PQ indices in chapter 2 and chapter 3, and redefine these indices for accurate assessment of PQ disturbances in chapter 4.

CHAPTER 3

POWER QUALITY ANALYSIS OF VARIABLE SPEED TURBINE GENERATORS

3.1 REVIEW OF EXISTING RID-BASED PQ INDICES

In this chapter, at first we will review the existing RID-based transient PQ indices defined in [22]. After the review of existing transient PQ indices, we will apply the PQ indices for PQ analysis of two commonly used variable speed wind energy conversion systems.

In [22], four PQ indices, such as instantaneous THD (ITHD), instantaneous DIN (IDIN), instantaneous frequency (IF), and instantaneous K-factor (IK) are proposed for the analysis of transient PQ disturbances. The PQ indices are defined based on the signal decomposition method in [22]. To illustrate the decomposition method briefly, consider the following transient PQ disturbance s(t):

$$\begin{aligned} s(t) &= A_1\cos(\omega_1 t+\theta_1)+A_5\cos(5\omega_1 t+\theta_5) \\ &\quad +Ke^{-\frac{(t-t_1)}{\tau}}A_{15}\cos(15\omega_1(t-t_1))(u(t_2)-u(t_1)) \\ &= s_1(t)+\underbrace{s_5(t)+s_{15}(t)}_{s_{D(t)}} \end{aligned} \tag{3.1}$$

The transient PQ indices are defined based on the separation of the fundamental component $s_1(t)$ and disturbance component $s_D(t)$ of the transient signal $s(t)$. The method estimates the amplitude A_1 and phase θ_1 of the fundamental frequency component from the TFD at the fundamental frequency $TFD(t,\omega_1)$, and a curve fitting routine, $\theta_1 = arg_\theta \min |s(t)-s_1(t)|^2$, respectively. The disturbance component $s_D(t)$ is then obtained by subtracting the fundamental component $s_1(t)$ from the PQ disturbance signal $s(t)$. After the

separation of the fundamental and disturbance components, the four PQ indices are defined based on the RID as follows:

Instantaneous THD

The definition of ITHD provides a time-varying assessment of the PQ as an energy ratio of the disturbance frequencies to the fundamental frequency as follows:

$$ITHD = \{\frac{\int TFD_D(t,\omega;\phi)d\omega}{\int TFD_F(t,\omega;\phi)d\omega}\}^{1/2} \times 100\% \tag{3.2}$$

where $TFD_F(t,\omega;\phi)$, and $TFD_D(t,\omega;\phi)$ are the TFDs of the fundamental, and disturbance components, respectively which provide energy associated with the fundamental and disturbance components according to the time marginal property.

Instantaneous DIN

Instantaneous DIN is the defined based on the energy ratio of the disturbance component to the energy of the fundamental plus disturbance components, and expressed as follows:

$$IDIN = \{\frac{\int TFD_D(t,\omega;\phi)d\omega}{\int TFD_F(t,\omega;\phi)d\omega + \int TFD_D(t,\omega;\phi)d\omega}\}^{1/2} \times 100\% \tag{3.3}$$

Instantaneous Frequency

Another RID-based transient PQ index is the instantaneous frequency (IF). This metric prioritizes higher frequencies typically present in transient disturbances. It identifies the local frequency content of a signal, and is defined as:

$$IF(t) = \{\frac{\int \omega \cdot TFD_s(t,\omega;\phi)d\omega}{\int TFD_s(t,\omega;\phi)d\omega}\} \times 100\% \tag{3.4}$$

where $TFD_S(t,\omega;\phi)$ is the time-frequency distribution of a transient PQ disturbance signal s(t).

Instantaneous K-factor

The other transient PQ index is the instantaneous K-factor, and is defined based on the second order moment of the TFD. The IK is expressed as follows:

$$IK(t) = \{\frac{\int \omega_N^2 \cdot TFD_s(t,\omega;\phi)d\omega}{\int TFD_s(t,\omega;\phi)d\omega}\} \times 100\% \tag{3.5}$$

where ω_N is the normalized frequency.

In order to quantify the transient PQ indices as a single value, "principal average" [22] of the time-frequency PQ indices, $\overline{TFPQ}$ as an average of the time-frequency based PQ index function over a fundamental period T is defined as follows:

$$\overline{TFPQ} = \frac{1}{T}\int_{t_0-\frac{T}{2}}^{t_0+\frac{T}{2}} TFPQ(t)dt \tag{3.6}$$

where $t_0 = argmax_t TFPQ(t)$ denotes the time at which maximum value of the transient PQ indices is obtained. Out of these four transient PQ indices, we will employ ITHD, and IF for PQ analysis of variable speed wind energy conversion systems. At first we will discuss the PQ issues associated with wind energy conversion systems, and the variable speed wind energy conversion system models utilized in this chapter for the analysis of PQ disturbances.

3.2 Power Quality of Wind Power

Wind energy can play an important role in mitigating the increasing demands of power generation on the electrical grid. However, WTGs are problematic in the sense that they introduce voltage and current disturbances which may lower the PQ of a grid. Transient voltage disturbances are introduced by WTGs when they are connected to or disconnected from the grid [80] and by such events as capacitors switching [81]. Furthermore, power electronics used in the power converters necessary to connect variable speed WTGs to the

grid can inject harmonics. Also, voltage sags may be caused by uneven power production from wind turbine installation or a power system fault. Studying and understanding the PQ impact of such disturbances through modeling and simulation is a prerequisite for the actual connection of a WTG to the electrical supply grid. It is required to identify the causes of the disturbances and quantify them as well in order to attenuate their detrimental effects by designing compensating devices such as harmonic filter.

The converter of a DFIG wind turbine is typically designed to approximately 25% of the turbine rated power [82]. Although, this partial-scale frequency converter makes the wind turbine DFIG more attractive than the wind turbine SG from an economic point of view, further investigation is required to analyze the performance from a PQ point of view.

The current PQ standard for wind turbines, issued by the IEC, defines the parameters of the wind turbine behavior in terms of the quality of power. The IEC standard also provides recommendations to carry out measurements and assess the PQ characteristics of grid-connected WTGs [11]. According to the IEC recommendations, PQ measurements for variable speed WTGs are discussed in [83]. Voltage fluctuations and harmonics caused by variable speed WTGs are analyzed in [84]-[85] as well. [86] has proposed a control algorithm recently to keep a WTG in operation successfully under unbalanced and/or harmonically distorted grid voltage conditions. However, identifying and quantifying time-varying frequency characteristics can add further stimulus to the PQ analysis of grid-connected WTGs.

3.3 Wind Energy Conversion System

In this section, we will briefly discuss the two variable speed WTGs models, a WT DFIG, and a WT SG, utilized in this chapter for PQ analysis utilizing the exiting transient PQ indices ITHD, and IF.

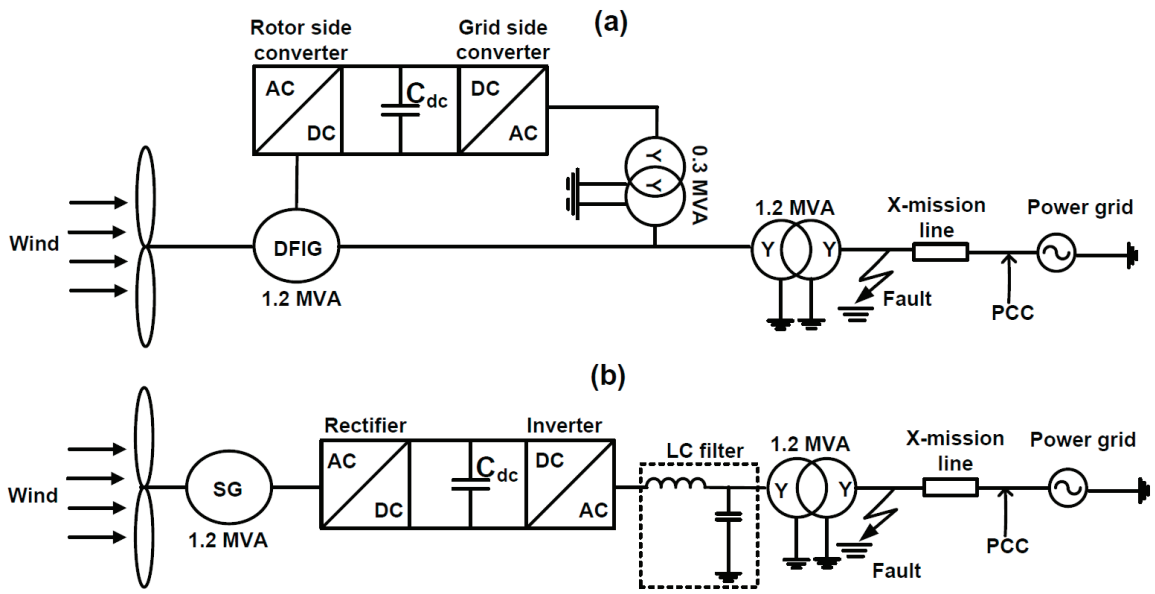

Figure 3.1: Block diagram of a variable speed (a) Wind turbine DFIG and, (b) Wind turbine SG.

Wind Turbine DFIG

The DFIG concept with a partial-scale frequency converter on the rotor circuit is shown in Fig. 3.1(a). The partial-scale frequency converter performs the reactive power compensation and enables a smoother grid connection. In this model, a 1.2 MVA DFIG is driven by a wind turbine, and is connected to the grid through a transformer with turns ratio of 0.69:22.9 and a 10 km long transmission with line impedance of $(0.182 + j0.392)$ [ohm/km]. The short circuit capacity of the grid is 68.38 MVA. The line-to-neutral voltage and frequency of the DFIG are 1.195 kV and 60 Hz, respectively. The details of the rotor side converter control system and its concept can be found in [87].

Wind Turbine SG

The variable speed wind turbine SG connection to the grid through a full-scale frequency converter is shown in Fig. 3.1(b). The frequency converter consist of an uncontrolled rectifier and a voltage source inverter performs the reactive power compensation and the

smoother grid connection. In this work, a direct driven wind turbine SG is connected to the grid through a transformer with turns ratio of 1.195:22.9, and a transmission line. The transmission line impedance and the grid short circuit capacity of the wind turbine SG are kept same as wind turbine DFIG. The line-to-neutral voltage and frequency of the SG are 1.1 kV and 60 Hz, respectively.

3.4 IEC PQ STANDARDS

The need for consistent and replicable documentation, IEC 61400-21 [11] describes procedures for determining the PQ characteristics of the wind turbines. According to the IEC, the sudden voltage reduction (d) may be assessed as follows:

$$d = 100 k_u(\psi_k) \frac{S_n}{S_k} \tag{3.7}$$

where S_n and S_k are the rated and short-circuit apparent power of a wind turbine and grid respectively, and $k_u(\psi_k)$ is the voltage change factor caused by a single switching operation. This factor is a function of a network impedance phase angle, ψ_k.

Another potential PQ issue of variable speed WTGs is the harmonic distortion. As mentioned in [11], the total harmonic distortion of a variable speed WTG is measured at the point of common coupling (PCC) and is defined as follows:

$$V_{THD} = \frac{\sqrt{\sum_{n=2}^{40} V_n^2}}{V_1} \tag{3.8}$$

where V_n and V_1 are n^{th} harmonic voltage and fundamental voltage, respectively.

The IEC PQ standards defined above may not be able to provide any information about when and which frequency components are responsible for a WTG disturbance. Moreover, grid short circuit capacity, WTG ratings, impedance angle etc. are required for PQ assessment according to IEC PQ standards. However, time-frequency analysis of a WTG disturbance may provide some advantages over existing IEC PQ standards. Consider a disturbance caused by a wind turbine DFIG startup. The disturbance signal normalized by

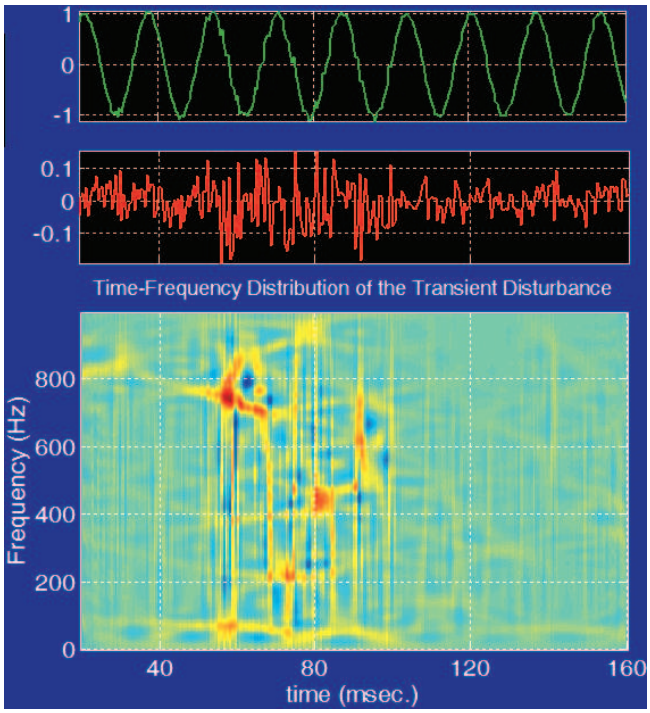

Figure 3.2: Instantaneous voltage, extracted disturbance, and time-frequency distribution of the disturbance due to introduction of a wind turbine DFIG.

its steady state peak value is shown in the top axis of Fig. 3.2. The second and the third axes of the figure show the extracted disturbance and the time-frequency distribution of the disturbance, respectively. From the time-frequency distribution, the presence of high frequency components (750 Hz and 450 Hz) are noticed during the transient duration from 60 ms to 100 ms. There are some other frequency components which have low energy content compared to these two frequency components (750 Hz and 450 Hz). Thus, time-frequency based PQ indices can play an important role to identify and quantify the time-varying frequency characteristics of the variable speed WTGs which is discussed in details in the next section.

3.5 PQ Analysis of wind turbine DFIG and SG

Power quality analysis of the wind turbine DFIG and SG via time-frequency analysis for two case studies, a wind turbine generator trip and recovery, and a three-phase-to-ground

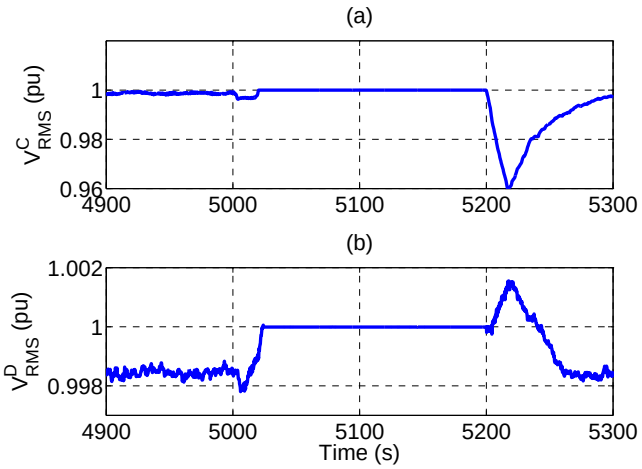

Figure 3.3: PCC RMS voltage of (a) WTG DFIG and (b) WTG SG for generator trip.

fault, are presented in this section. The sampling frequency of the case studies is 4 kHz. Due to presence of the low-order harmonics, time-frequency distributions for the wind turbine DFIG are shown for down sample of 0.8 kHz for high resolution in the case studies.

In this case study, the WTG trips at 5 s and is reconnected to the system at 5.2 s. Fig. 3.3 shows the RMS values of the voltages at the PCC for both types of variable speed WTGs to their respective grids. As seen in the figure, the RMS voltage variation caused by WTG disconnection and connection transient disturbance is very low and does not provide any time-varying frequency information.

WTG Trip and Recovery

Transient voltage and current disturbances may occur due to capacitor switchings, lighting, adjustable speed drive trips and malfunctions of other electronically controlled loads. In addition, if the wind speed exceeds the cut-out speed (i.e., 25 m/s), the WTG can no longer deliver power. This may happen during a storm, for instance. In this work, in order to see the impact of a variable speed WTG connection and disconnection to the grid, a transient disturbance caused by such an event is analyzed, and compared for both types of WTGs.

The phase A transient voltage events at the PCC introduced by the wind turbine DFIG

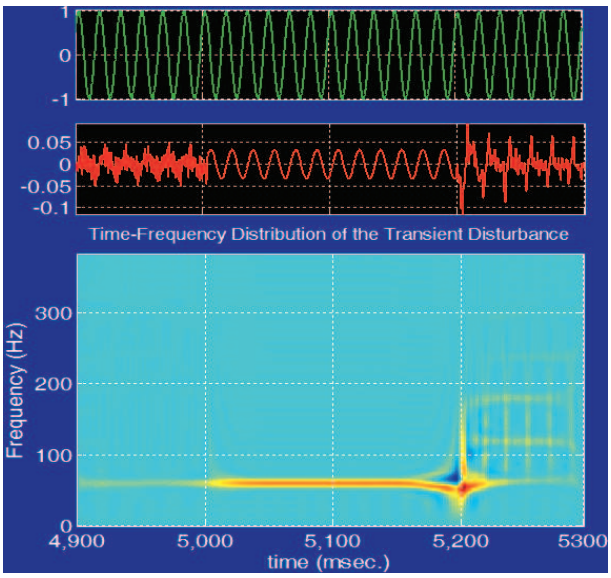

Figure 3.4: Instantaneous voltage, extracted disturbance, and time-frequency distribution of the disturbance introduced by wind turbine DFIG trip.

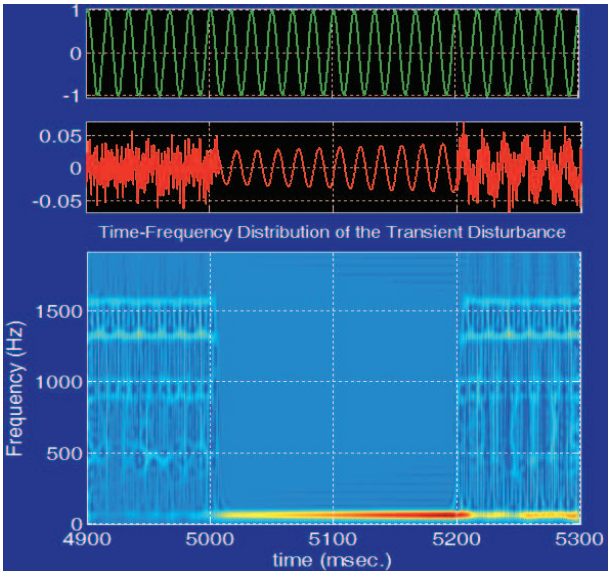

Figure 3.5: Instantaneous voltage, extracted disturbance, and time-frequency distribution of the disturbance introduced by wind turbine SG trip.

and the wind turbine SG trip and recovery are shown in the top axes of Fig. 3.4 and Fig. 3.5, respectively. The extracted disturbances and the time-frequency distributions of the disturbances are shown in the second and the bottommost axes of the figures, respectively. The time-frequency distributions shown in Fig. 3.4 exhibit the DFIG voltage disturbance con-

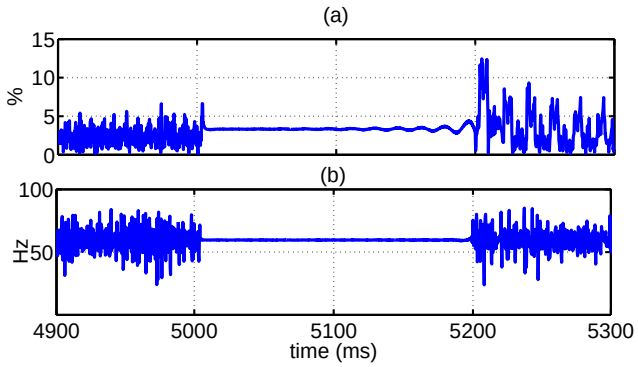

Figure 3.6: (a) Instantaneous THD (ITHD(t)) and (b) Instantaneous frequency (IF(t)) for wind turbine DFIG trip.

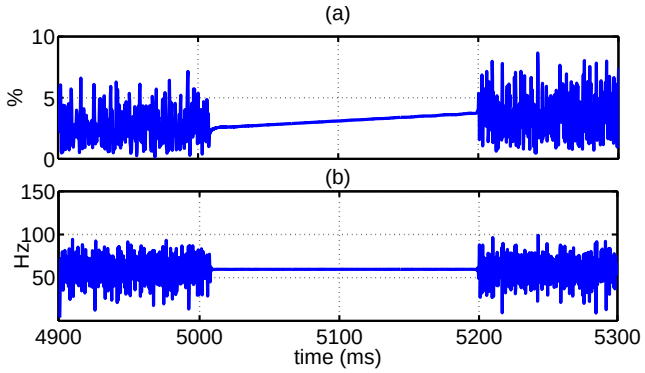

Figure 3.7: (a) Instantaneous THD (ITHD(t)) and (b) Instantaneous frequency (IF(t)) respectively for wind turbine SG trip.

tains relatively low-order frequency (2nd and 3rd) components when the generator comes on-line and the energy content of these frequencies decreases in magnitude as the PCC voltage becomes stable. For the wind turbine SG, the 7th harmonic and some high-order harmonics 15th, 17th, 23rd, and 26th have high energy content. That is, the wind turbine SG transient disturbance contains high order harmonics whereas low order harmonics are observed for the DFIG.

Fig. 3.6 and Fig. 3.7 show the two PQ indices for the wind turbine SG and the wind turbine DFIG phase voltages, respectively. As shown in these figures, the variation of the PQ indices indicates presence of time-varying harmonics in the variable speed WTGs. In the case of the wind tubine DFIG, the peak value of ITHD(t) is 12.44% whereas it is 8.65%

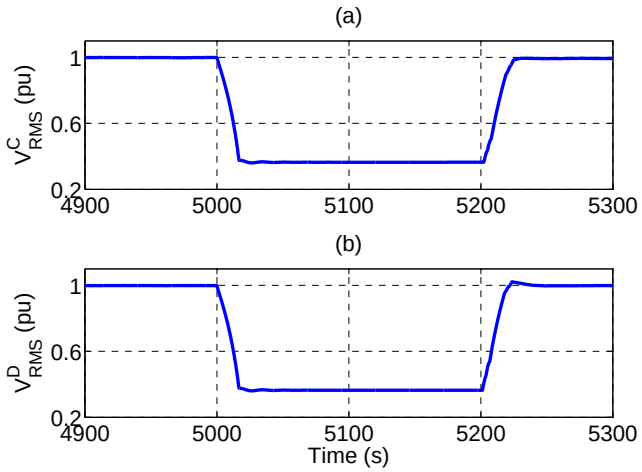

Figure 3.8: PCC RMS voltage of (a) Wind turbine DFIG and (b) wind turbine SG for a three phase line-to-ground fault.

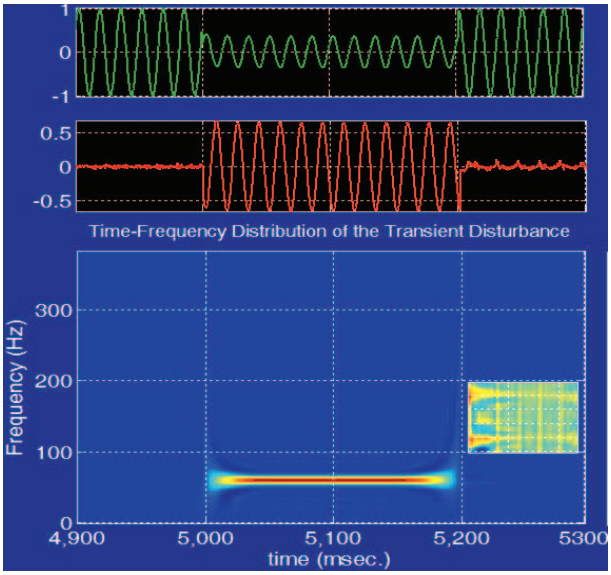

Figure 3.9: Instantaneous voltage, extracted disturbance, and time-frequency distribution of the disturbance introduced by a three-phase-to-ground fault applied to a wind turbine DFIG.

for the wind turbine SG. Due to the presence of the high frequency components in the wind turbine SG, the peak value (100.01 Hz) of IF(t) is higher than that (85.05 Hz) of the wind turbine DFIG.

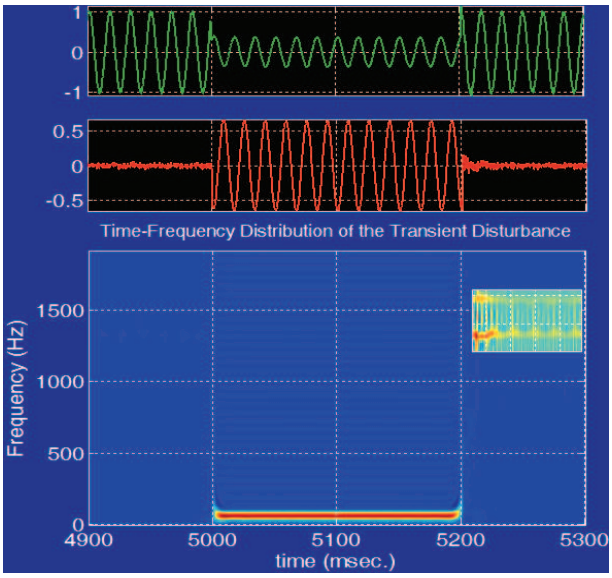

Figure 3.10: Instantaneous voltage, extracted disturbance, and time-frequency distribution of the disturbance introduced by a three-phase-to-ground fault applied to wind turbine SG.

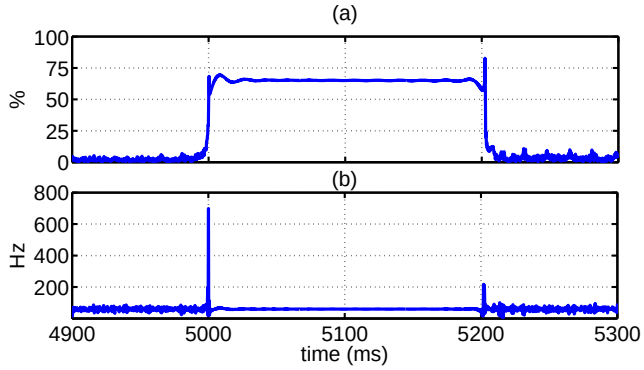

Figure 3.11: (a) Instantaneous THD (ITHD(t)), and (b) Instantaneous frequency (IF(t)) for a fault applied to a wind turbine DFIG.

Three-Phase-to-Ground Fault Analysis

Power system fault is a common type of PQ disturbance. In the past, WTGs were allowed to disconnect from the system during a fault. Due to the increase in penetration of wind power, now-a-days grid code requires WTGs remain connected to the grid during a fault. In this work, a three-phase-to-ground fault is applied at the both WTGs terminals, and the WTGs maintain connection to the system during the fault (5 s to 5.2 s).

The PCC RMS voltages of the both WTGs decrease below 0.4 pu during the fault as

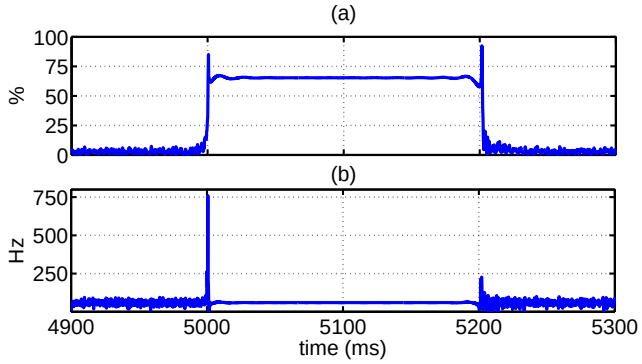

Figure 3.12: (a) Instantaneous THD (ITHD(t)) and (b) Instantaneous frequency (IF(t)) for a fault applied to wind turbine SG.

Table 3.1: PQ indices for transient disturbance

PQ indices		DFIG	SG
ITHD	peak value (%)	12.44	8.65
	peak time (ms)	5204	5242
	principal avg	4.88	3.51
IF	peak value (Hz)	85.05	100.01
	peak time (ms)	5237	5242
	principal avg	58.96	58.88

shown in Fig. 3.8. Fig. 3.9 and Fig. 3.10 show the time-frequency distributions of the instantaneous disturbances for the both WTGs due to a three-phase-to-ground fault. When the fault is cleared, the transient introduced by wind turbine SG has high frequency (23rd and 26th harmonics) energy content which decreases in magnitude with time as the system becomes stable, whereas the low-order harmonics (2nd and 3rd) are present in the DFIG fault transient disturbance.

The peak value of ITHD(t) for the WTG SG is 92.32% at the instant of the fault clearance which is higher than that of the wind turbine DFIG (82.75%), and are shown in Fig. 3.11 and Fig. 3.12, respectively. And the peak values of IF(t) are 698.69 Hz and 759.88 Hz for the wind turbine DFIG and the wind turbine SG, respectively.

Table 3.2: PQ indices for three-phase-to-ground fault

PQ indices		DFIG	SG
ITHD	peak value (%)	82.75	92.32
	peak time (ms)	5202	5202
	principal avg	35.99	36.88
IF	peak value (Hz)	698.69	759.88
	peak time (ms)	5000	5000
	principal avg	64.65	78.16

The results of the PQ analysis discussed above are summarized in Table 3.1 and Table 3.2. Comparing the PQ indices for the disturbance case studies, it can be concluded that the peak value of IF(t) of the SG is always higher than that of the DFIG because of high order harmonics presence. The DFIG performs better than the SG from the PQ point of view except for ITHD(t) of WTG trip and recovery case study.

3.6 Conclusion

This chapter focuses on the limitation of Fourier transform based traditional PQ indices in quantifying the time-varying disturbances caused by variable speed WTGs. Therefore, time-frequency distribution based PQ indices are utilized as an effective way to identify, quantify and compare the time-varying frequency characteristics of variable speed WTGs. In addition, based on the analyses shown in this chapter, designing appropriate passive or an active filter, particular harmonics can be eliminated, and compensating devices such as energy storage can be applied to damp the transient disturbance in order to improve the PQ of grid-connected WTGs.

CHAPTER 4

ASSESSMENT OF FUNDAMENTAL FREQUENCY DEVIATION OF FIXED SPEED WIND ENERGY CONVERSION SYSTEM

4.1 INTRODUCTION

In this chapter we will utilize the existing PQ index instantaneous frequency for the assessment of grid frequency deviation caused by fixed speed wind energy conversion systems. Currently, 2.3% of the total energy in the US is generated from wind power, and it has been estimated to be increased to 20% by 2030 [88]. The increase interest of wind energy has lead to the integration of large wind energy conversion systems (WECS) to the existing grid. Although, variable speed wind turbine generators (WTGs) are currently the most used WECS, fixed speed WTGs are still a significant part of the rapidly growing wind power markets [89].

Fixed speed WTGs have the advantages of being simple, robust, and reliable with simple and inexpensive electric systems. However, due to the fixed operation, all fluctuations in wind speed are transmitted into the mechanical torque and further, as electrical fluctuations, into the grid which affect the power grid frequency [90]. Excessive power frequency variation may lead to power system blackout if frequency relays trip the circuit breakers [91]-[93]. Therefore, it is necessary to estimate the power frequency deviation, and take necessary steps to control the power frequency in order to avoid power system blackout.

Several methodologies have been proposed to estimate the grid frequency variation caused by wind power fluctuation [91]-[93]. In these works, grid frequency deviation is measured based on the analysis of 1-hour deterministic wind power fluctuation. How-

ever, the stochastic power fluctuation of the wind farm is not considered in these studies at all. Therefore, [94] has proposed stochastic system analysis for the assessment of grid frequency deviation due to wind power fluctuation based on time-frequency method. The method obtains power spectral density of grid frequency deviation in frequency domain from time series wind power fluctuation via Fourier transform (FT), and finally, applies inverse FT to restore the grid frequency deviation in time domain. Thus, the method involves three stages of "Time $\rightarrow$ Frequency $\rightarrow$ Time" transformation which will eventually increase the computational cost. Also, FT-based assessment of grid frequency may be erroneous due to spectral leakage as wind power fluctuation is aperiodic in nature.

In this chapter, we employ time-frequency analysis technique in order to assess the grid frequency deviation caused by the wind speed change of fixed speed wind energy conversion systems. The proposed method interprets the effects of power fluctuation caused by the wind speed change in terms of voltage/current signal energy. In case of fixed speed wind energy conversion systems, the variation of the energy caused by wind power fluctuation is associated with the fundamental frequency component only. Therefore, by exploring the frequency localization via time-frequency analysis, the severity of the wind power fluctuation caused by the wind speed change is estimated in terms of frequency. The method can estimate the instantaneous frequency regardless of the wind speed data, and involves one stage of "Time-Frequency" transformation only. For the assessment of instantaneous frequency, we employ WV TFD as it provides faster computational speed than the RID. Note that in fixed speed wind energy conversion systems, voltage/current signal is composed of fundamental frequency component only, therefore, cross-terms won't appear in the assessment of fundamental frequency deviation.

4.2 Studied Wind Energy Conversion System

Power extracted from wind by a wind turbine is given by the following equations [95]:

$$P_{wind} = \frac{1}{2}\rho A C_p(\lambda, \beta) V^3 \tag{4.1}$$

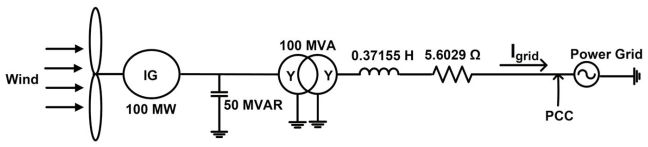

Figure 4.1: One line diagram of a fixed speed wind energy conversion system.

$$C_p(\lambda,\beta) = 0.5(\lambda - 0.022\beta^2 - 5.6)e^{-0.17\lambda} \tag{4.2}$$

where P_{wind} is the captured power from the wind [W], ρ is the air density [kg/m^3], A is the rotor area [m^2], V is the wind speed [m/s], and C_p is the power coefficient which is a function of both tip speed ratio (λ) and pitch angle (β) [deg]. Tip speed ratio is defined as follows:

$$\lambda = \frac{\omega R}{V} \tag{4.3}$$

where ω is the rotational speed [rad/s] and R is rotor radius [m]. The fixed speed wind energy conversion system studied in this work is shown in Fig 4.1. The wind energy conversion system provided in the figure is the aggregation of 135 small 0.74 MW self-excited double-cage induction generators according to [96]. A shunt capacitor is added to the wind farm terminal for the reactive power compensation of the induction generator, and the transmission line for the wind farm model is derived from the IEEE first benchmark model as in [97]. We will be studying this wind farm model for the estimation of the fundamental frequency deviation caused by wind speed change in the next section. The parameters of the aggregated 100 MW wind energy conversion are given as follows:

It is worth to address the grid code while estimating the the fundamental frequency deviation caused by the wind power fluctuation. According to the grid code of the wind power in USA, the fundamental frequency deviation caused by the wind turbine generator at the point of common coupling should be within the limit of $\pm$ 1 Hz [77]. Therefore, in our study, we will also verify the grid code while power fluctuation caused by the wind speed change is introduced into the grid.

Table 4.1: Parameters of single 0.746 MW and aggregated 100 MW Fixed Speed wind energy conversion system

Rated wind speed, V_r	10.33 [m/s]	10.33 [m/s]
Rated power, P_r	0.746 MW	100 MW
Rated voltage, V_r	26 kV	26 kV
Stator leakage reactance, X_{ls}	0.091 pu	0.091 pu
Rotor leakage reactance, X_{lr}	0.0539 pu	0.0539 pu
Magnetizing reactance, X_m	0.01418 pu	0.01418 pu
Stator resistance, R_s	0.015 pu	0.015 pu
Rotor resistance, R_r	0.0507 pu	0.0507 pu
Inertia constant, H_g	0.5 s	0.5 s

4.3 Case Studies

In this section, we will consider three different wind speeds for the estimation of the fundamental frequency deviation caused by fixed speed wind energy conversion system. The three wind speeds - a ramp, a gust and a random wind speeds are applied to the wind turbine using PSCAD/EMTDC simulation software, and the fundamental frequency variation of the grid current signal is analyzed employing the WV time-frequency analysis technique. The parameters of ramp, gust, and random wind speeds are provided as follows:

Table 4.2: Ramp and Gust Wind Speed Data

Parameters	Ramp	Gust
Total number	1	1
Maximum velocity	2 [m/s]	1 [m/s]
Ramp period	1 [s]	1 [s]
Ramp start time	5 [s]	5 [s]

Table 4.3: Random Wind Speed Data

Mean wind speed, V_r	10 [m/s]
Random amplitude controlling parameter, A_n	1 [rad/s]
Number of noise components, n	50
Random seed number	8
Surface drag coefficient, K	0.0192
Time interval for random generation, t	0.0006 [s]
Turbulence scale, H	10 [m]

Ramp Wind Speed

A ramp wind speed with peak velocity of 2 [m/s] applied to the wind turbine is provided in Fig. 4.2(a), and the corresponding rotor speed, power delivered to the grid and grid current are shown in Fig. 4.2(b), (c) and (d), respectively. The ramp wind speed applied at 5 s goes up to 12.33 m/s from the rated speed of 10.33 m/s within 1 s duration. When wind speed is restored to its rated speed at 6 s, the rotor speed exhibits oscillatory behavior and comes to steady state after a while as seen in Fig. 4.2(b). It is observed in the figure, the fluctuation in the wind speed is transmitted as fluctuation in the rotor speed and then as fluctuation in the electrical power on the grid. The power variation in turn leads to large current fluctuation as shown in Fig. 4.2(d). The fluctuation in the current signal indicates the variation of the energy associated with 60 Hz frequency component which can be best observed from TFD of the signal itself.

The TFD of the grid current signal is shown in Fig. 4.3. As seen in the figure, no energy fluctuation of 60 Hz frequency component is observed in the steady state. As a ramp wind speed is applied at 5 s, the energy content of 60 Hz frequency tends to increase, and have the highest energy content at 6 s. This is because, when the wind speed is restored to its rated speed at 6 s, the rotor speed and the power delivered to the grid have the largest fluctuations as observed in Fig. 4.2(b) and (c), respectively. The large variation of the power delivered to the grid causes a large variation of the energy content of the 60 Hz

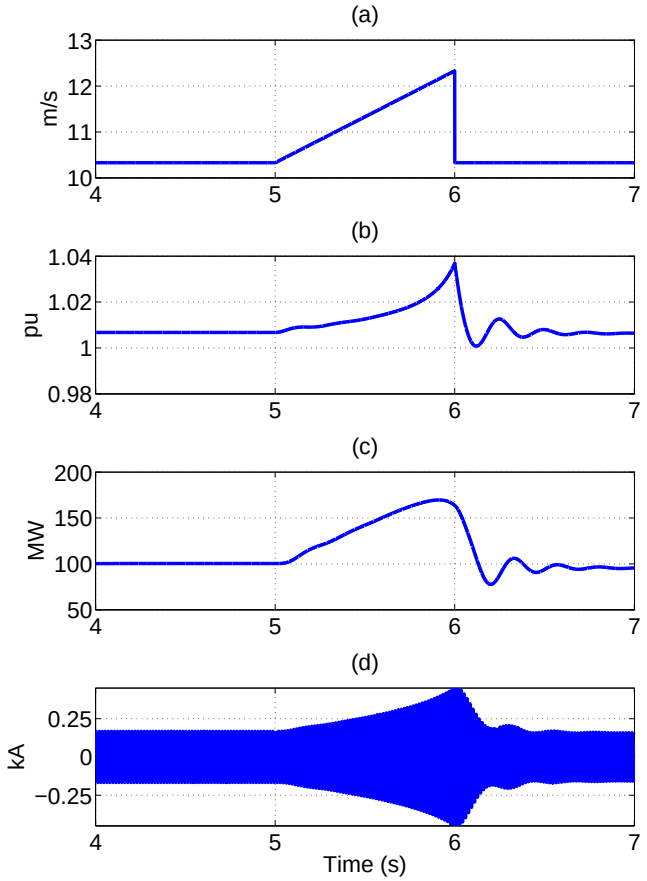

Figure 4.2: (a) Ramp wind speed, (b) Rotor speed, (c) Power delivered to the grid, and (d) Grid current signal.

frequency component current signal as seen in Fig. 4.3. However, the energy content of 60 Hz frequency component decreases gradually after 6 s as the oscillation in the power delivered to the grid dies out with time.

The instantaneous frequency of the grid current signal in Fig. 4.4 shows the variation of the fundamental frequency around 60 Hz. The maximum value of the fundamental frequency of the grid current signal is 60.21 Hz at 6.005 s, while the minimum value is 59.20 Hz at 6.205 s. The maximum and the minimum values of the fundamental frequency correspond to the highest and lowest power fluctuation to the grid at 6.005 s and 6.205 s, respectively. However, the fundamental frequency variation does not exceed the limit of $\pm$I Hz as mentioned in the wind power grid code requirements.

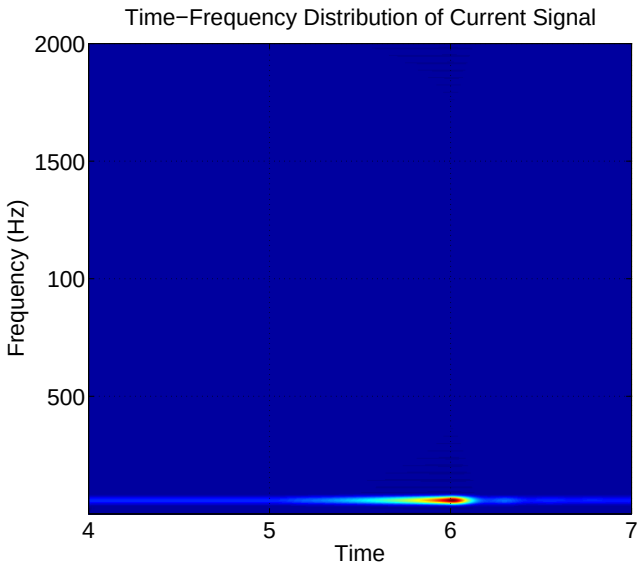

Figure 4.3: TFD of the grid current signal.

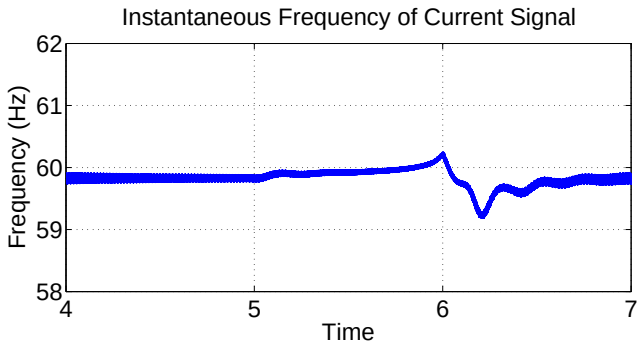

Figure 4.4: Instantaneous frequency of the grid current signal.

Gust Wind Speed

In this case study, a gust wind speed with peak velocity of 1 [m/s] is applied to the wind turbine at 5 s and shown in Fig. 4.5(a). The variation of the rotor speed, power delivered to the grid and the grid current as a result of the gust wind speed are provided in Fig. 4.5(b), (c) and (d), respectively. As seen in the figure, the rotor speed and the power delivered to the grid reach the peak values of 1.015 pu and 150 MW, respectively during the gust period (5 s to 6 s), and increases the grid current to the maximum value of 0.25 kA consequently. A very small oscillation is observed in the rotor speed, delivered power and the grid current

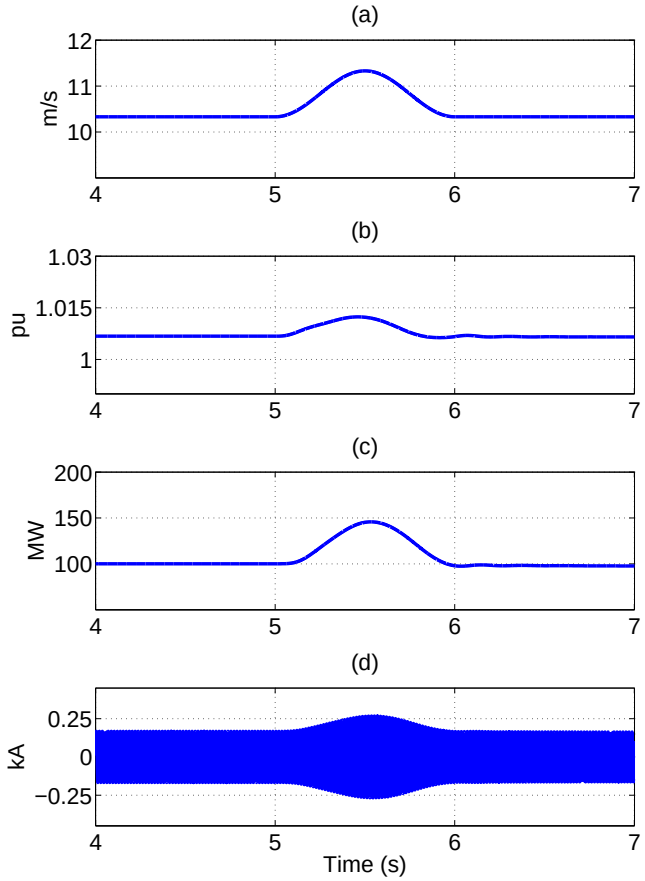

Figure 4.5: (a) Ramp wind speed, (b) Rotor speed, (c) Power delivered to the grid, and (d) Grid current signal.

signal as well after the wind speed is restored to its rated speed at 6 s, and these small fluctuations die out with time eventually as the wind energy conversion system becomes stable.

The variation of the power delivered to the grid causes the fluctuation of the fundamental frequency energy content of the grid current signal, which in turn leads to the fundamental frequency deviation from the normal operating condition. The time-frequency distribution of the current signal in Fig. 4.6 shows the fundamental frequency component has the highest energy content at the instant of the maximum power delivered to the grid. The energy variation of the 60 Hz frequency component becomes in steady state as soon as wind speed is restored to the rated speed and power fluctuation caused by the gust wind

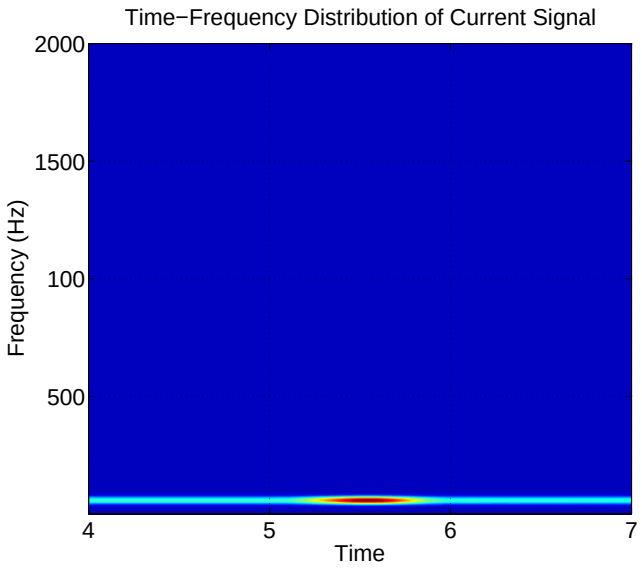

Figure 4.6: TFD of the grid current signal.

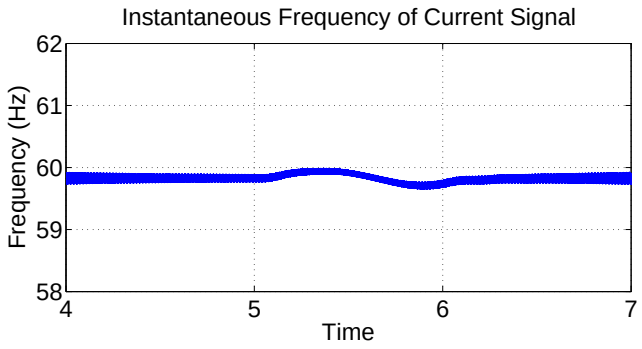

Figure 4.7: Instantaneous frequency of the grid current signal.

speed dies out with time.

The instantaneous frequency of the grid current signal in Fig. 4.4 shows the variation of the fundamental frequency with time caused by the gust wind speed. The maximum and minimum values of the fundamental frequency are 59.96 Hz and 59.64 Hz, respectively. Therefore, the frequency deviation is within the limit imposed by the grid code. However, the frequency deviation in this case study is smaller than that of the ramp wind speed. This is because of the peak value of the gust wind speed is 1 m/s, while it is 2 m/s in case of the ramp wind speed. As a result of the higher ramp wind speed, the maximum power

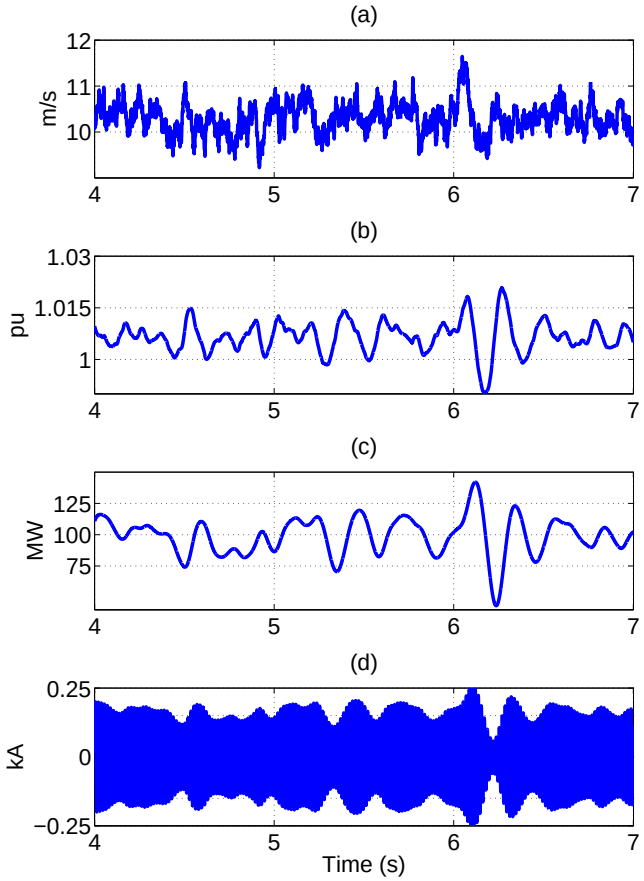

Figure 4.8: (a) Random wind speed, (b) Rotor speed, (c) Power delivered to the grid, and (d) Grid current signal.

delivered to the grid is more than 150 MW, while it is 150 MW in the case of gust wind speed. Therefore, power fluctuation caused by the ramp wind speed is higher than that of the gust wind speed. As a result, the higher fundamental frequency deviation is observed in the case of ramp wind speed.

Random Wind Speed

In the final case study, a noise wind speed, V_n is applied to the wind turbine according to [98] as follows:

$$V_n = 2\sum_{n=1}^{n}\sqrt{S_v(\omega_n)\cdot A_n}\cdot\cos(\omega_n\cdot t+\phi_n) \tag{4.4}$$

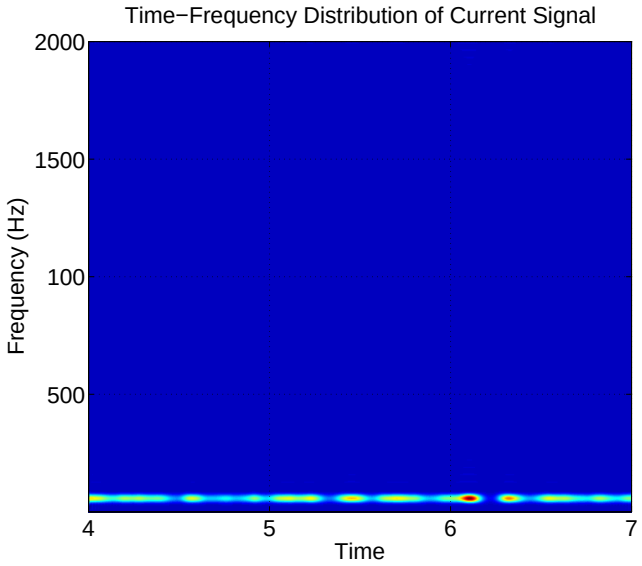

Figure 4.9: TFD of the grid current signal.

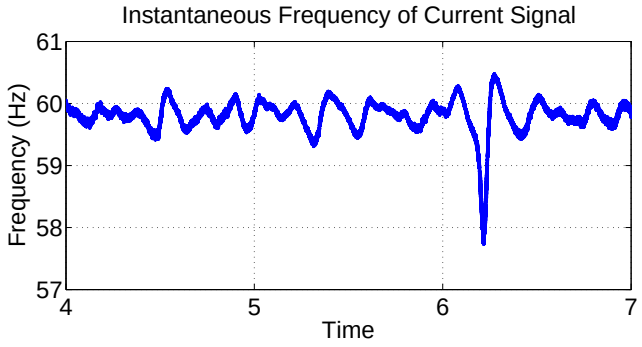

Figure 4.10: Instantaneous frequency of the grid current signal.

where

$$\omega_n = (n-0.5)A_n \tag{4.5}$$

$$S_v(\omega_n) = \frac{2\cdot K\cdot H^2\cdot \omega_n}{\pi^2[1+(\frac{H\cdot\omega_n}{V_r\cdot\pi})^2]^{\frac{4}{3}}} \tag{4.6}$$

where A_n, ϕ_n, K, H and V_r are noise amplitude controlling parameter in [rad/s], random variable on the interval 0 to 2π, surface drag coefficient, turbulence scale in [m] and mean wind speed in [m/s], respectively. The random wind speed is generated using wind source component available in PSCAD/EMTDC simulation software.

The random wind speed, and corresponding simulation results of the rotor speed, power delivered to the grid and the grid current are shown in Fig. 4.8(a), (b), (c), and (d), respectively. The simulation results show the fluctuations of the rotor speed, power delivered to the grid and the current signal as the wind speed changes with time. The random variation of the power delivered to the grid causes the rapid energy change of grid current signal as seen in the TFD of the current signal in Fig. 4.9. From the time-frequency distribution, it can be observed that the fundamental frequency component has the highest energy after 6 s because of the large wind power fluctuation.

The instantaneous frequency of the grid current signal in Fig. 4.10 shows the rapid variation of 60 Hz frequency components as wind speed varies with time. The maximum and minimum values of the fundamental frequency are 60.44 Hz at 6.271s, and 57.73 Hz at 6.218 s, respectively. Unlike the ramp and gust wind speeds, random wind speed case study shows the violation of the grid code as the fundamental frequency drops below 59 Hz, while fundamental frequency remains within the range from 59 Hz to 60 Hz in case of the ramp and gust wind speed case studies. However, the fundamental frequency deviation may vary depending on the severity of the ramp, gust and random wind speeds.

4.4 Conclusion

This chapter presents a time-frequency based new assessment method for fundamental frequency deviation of grid current for three different wind speed changes - a ramp, a gust and a random wind speed. The IEEE first benchmark model has been utilized in order to justify the efficacy of the proposed method for fixed speed wind energy conversion systems. The simulation results and the analysis shown in this chapter justify that the proposed time-frequency based instantaneous frequency estimates grid frequency deviation accurately, and requires less computational complexity as well. Therefore, the proposed method can be a viable alternative for the assessment of grid frequency deviation caused by fixed speed wind energy conversion systems.

CHAPTER 5

REDEFINED EXISTING REDUCED INTERFERENCE DISTRIBUTION BASED POWER QUALITY INDICES FOR STATIONARY AND NONSTATIONARY POWER QUALITY DISTURBANCES

5.1 INTRODUCTION

In chapter 2, and 3, we show the applications of existing transient PQ indices for the analysis of variable speed wind PQ disturbances, and assessment of grid frequency deviation caused by fixed speed wind energy conversion systems. Although, existing PQ indices are good indication of transient disturbances, they cannot provide actual values of the PQ indices [25]. As regards this shortcoming, in this chapter, we will redefine them to provide accurate assessment of PQ disturbances. To validate the efficacy of the redefined PQ indices, we will compare them to traditional FFT-based PQ indices for stationary and nonstationary PQ disturbances.

5.2 LIMITATIONS OF EXISTING TRANSIENT PQ INDICES

In this section, we will discuss the limitations of existing transient PQ indices ITHD, IDIN, IF, and IK proposed in [22] as follows:

- The decomposition method assumes the power system frequency to be constant at 50/60 Hz. In fact, power system frequency deviates from nominal to off nominal

frequency in real-world PQ disturbances.

- The PQ indices provide misleading results [25] of ITHD, IDIN as these two indices are defined based on the energy ratio of the fundamental and disturbance components instead of rms value. Although, IF, which is a first order moment of TFD [16], and a good indication of the presence of high frequency components in transient disturbances, it cannot provide any useful information for stationary PQ disturbances. In addition, IK is a second order moment of TFD [16] that basically provides squared frequency bandwidth of a signal, and does not result in actual value of K-factor.

- Finally, the PQ indices are quantified as a single value employing "principal average" which evaluates average of the transient PQ indices over one fundamental cycle centered around the peak value. Thus, principal average provides high value for transient disturbances, however, cannot afford true values of PQ indices for the assessment of PQ disturbances.

To further illustrate the limitations, the transient PQ indices in [22] are represented in Fig. 5.1 for a stationary PQ voltage disturbance signal $v(t) = \cos(\omega_1 t + 30^o) + 0.2\cos(\omega_3 t + 60^o) + 0.15\cos(\omega_5 t + 120^o)$. Note that true values of THD, DIN, and K-factor for the stationary PQ disturbance $v(t)$ are 0.25, 0.2425, and 0.9318 pu, respectively. However, Figs. 1(a), (b), and (c) justify that employing the method in [22], IDIN, ITHD, and IK provide oscillating results instead of the true values.

Regarding the limitations of the existing PQ indices discussed above, we will redefine the existing PQ indices ITHD, IDIN, and IK, and also reformulate other PQ indices PF, TIF, and C-message for stationary and nonstationary PQ disturbances. At first we will modify the decomposition method to overcome the limitations of decomposition method utilized in [22]. Then, RID method will be applied to redefine PQ indices in order to obtain correct assessment of PQ disturbances.

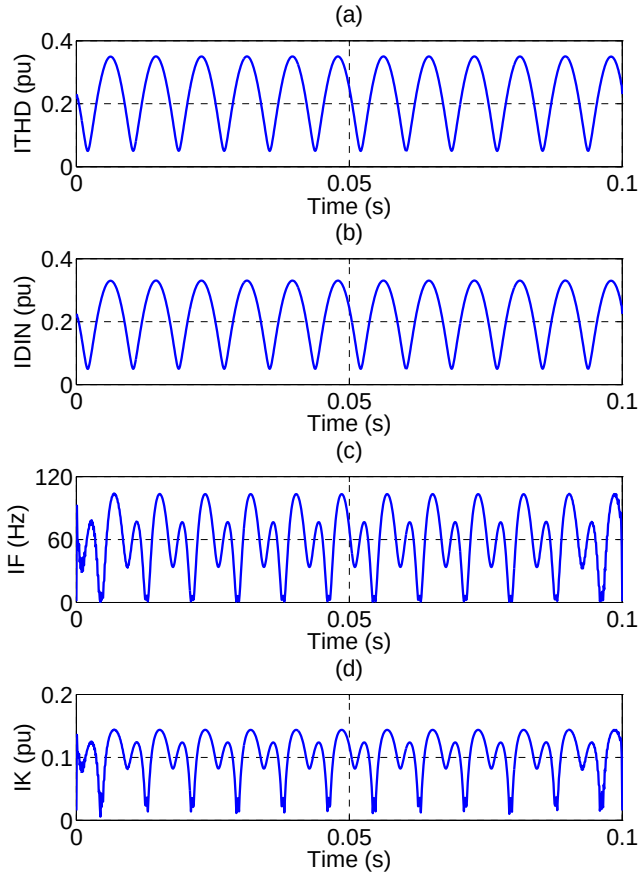

Figure 5.1: Transient PQ indices (a) ITHD, (b) IDIN, (c) IF, and (d) IK according to the [22].

5.3 Redefined PQ Indices

The existing PQ indices are redefined based on the modified decomposition method of fundamental and harmonic components which is discussed step by step as follows:

- Step 1: First step starts with the frequency energy spectrum obtained via frequency marginal-property of TFD in order to assign bandwidth (B) for each frequency component in a PQ disturbance signal. By assigning the bandwidth for each frequency component, the modified decomposition method eliminates the assumption of constant power system frequency.

- Step 2: In step 2, energy associated with each frequency bandwidth is calculated

from TFD as follows:

$$E_1 = \int_{B_{\omega_1}} TFD(t,\omega;\phi)d\omega; \quad E_3 = \int_{B_{\omega_3}} TFD(t,\omega;\phi)d\omega; \tag{5.1}$$

$$E_5 = \int_{B_{\omega_5}} TFD(t,\omega;\phi)d\omega; \tag{5.2}$$

.....

$$E_n = \int_{B_{\omega_n}} TFD(t,\omega;\phi)d\omega; \tag{5.3}$$

- Step 3: In step 3, the instantaneous rms values of the fundamental and each harmonic component are defined based on the energy information obtained in Step 2 as follows:

$$S_1 = \frac{1}{\sqrt{2}}\sqrt{\frac{1}{T}\int_{t-T}^{t} E_1 dt}; \quad S_3 = \frac{1}{\sqrt{2}}\sqrt{\frac{1}{T}\int_{t-T}^{t} E_3 dt} \tag{5.4}$$

$$S_5 = \frac{1}{\sqrt{2}}\sqrt{\frac{1}{T}\int_{t-T}^{t} E_5 dt} \tag{5.5}$$

.....

$$S_n = \frac{1}{\sqrt{2}}\sqrt{\frac{1}{T}\int_{t-T}^{t} E_n dt}; \tag{5.6}$$

Based on the rms values of the fundamental component S_1 and harmonic components S_3, S_5, ...S_n, obtained via TFD one can redefine PQ indices, such as THD, DIN, TIF, C message, and K factor for stationary and nonstationary PQ disturbances. Note that TFD considers analytic expression of a signal [16], therefore, scale factor $\frac{1}{\sqrt{2}}$ is introduced in the rms equations as energy of the original signal is half the energy of analytic signal.

- Step 4: Phase information for a pair of voltage and current signal can be obtained from XTFD as:

$$\theta_{vi} = atan^{-1}\frac{\Re\{XTFD_{vi}(t,\omega;\phi)\}}{\Im\{XTFD_{vi}(t,\omega;\phi)\}} \tag{5.7}$$

From the phase information obtained via Eq. (5.7), one can define PF for a pair of voltage and current stationary and nonstationary PQ disturbance events.

However, the decomposition method will have the limitation due to the presence of cross-terms since there is no TFD that can minimize the cross-terms completely [16] in time-frequency domain. Among various TFDs, RID shows the most suitable properties for the minimization of cross-terms employing a two dimensional low pass filter in time-frequency domain [70], [99]. Therefore, in this work, we employ RID method to redefine PQ indices which is discussed in the following subsections.

Total Harmonic Distortion

The voltage and current THDs are ratio of rms fundamental and harmonic components, and defined as follows:

$$THD_V^{RID} = \frac{\sqrt{\frac{1}{T}\int_{t-T}^{t}\sum_{n\neq 1}^{n} E_{V_n} dt}}{\sqrt{\frac{1}{T}\int_{t-T}^{t} E_{V_1} dt}} \tag{5.8}$$

$$THD_I^{RID} = \frac{\sqrt{\frac{1}{T}\int_{t-T}^{t}\sum_{n\neq 1}^{n} E_{I_n} dt}}{\sqrt{\frac{1}{T}\int_{t-T}^{t} E_{I_1} dt}} \tag{5.9}$$

where E_{V_1}, and E_{V_n} are energy associated with fundamental and harmonic voltage, respectively, and E_{I_1}, and E_{I_n} are energy associated with fundamental and harmonic current, respectively.

Distortion Index

The DIN is utilized to overcome the difficulty of the nonexistence of fundamental component, and is defined for voltage and current signals based on the RID TFD as:

$$DIN_V^{RID} = \frac{\sqrt{\frac{1}{T}\int_{t-T}^{t}\sum_{n\neq 1}^{n} E_{V_n} dt}}{\sqrt{\frac{1}{T}\int_{t-T}^{t}\sum_{n=1}^{n} E_{V_n} dt}} \tag{5.10}$$

$$DIN_I^{RID} = \frac{\sqrt{\frac{1}{T}\int_{t-T}^{t}\sum_{n\neq 1}^{n} E_{I_n} dt}}{\sqrt{\frac{1}{T}\int_{t-T}^{t}\sum_{n=1}^{n} E_{I_n} dt}} \tag{5.11}$$

where E_{V_n}, and I_{V_n} are energy associated with the PQ voltage and current disturbances, respectively.

Power Factor

The PF for a pair of voltage and current PQ disturbances can be obtained in the following manner utilizing the Eq. (5.7):

$$PF = \cos\theta_{vi} = \frac{\int_{t-T}^{t} \int \Re\{XTFD_{vi}(t,\omega;\phi)\} d\omega dt}{\int_{t-T}^{t} \int abs\{XTFD_{vi}(t,\omega;\phi)\} d\omega dt} \tag{5.12}$$

Telephone Interference Factor

The TIF based on the RID can be defined in the following manner:

$$TIF_V^{RID} = \frac{\sqrt{\frac{1}{T}\int_{t-T}^{t} \sum_{n\neq 1}^{\infty} w_n^{TIF} E_{V_n} dt}}{\sqrt{\frac{1}{T}\int_{t-T}^{t} E_{V_1} dt}} \tag{5.13}$$

$$TIF_I^{RID} = \frac{\sqrt{\frac{1}{T}\int_{t-T}^{t} \sum_{n\neq 1}^{\infty} w_n^{TIF} E_{I_n} dt}}{\sqrt{\frac{1}{T}\int_{t-T}^{t} E_{I_1} dt}} \tag{5.14}$$

where W_n^{TIF} is the TIF weights that can be found in [10]. Similarly, C message for voltage and current PQ disturbances can be obtained by replacing TIF weights W_n^{TIF} by C message weights W_n^C that can be found in [10] as well.

K-Factor

The voltage and current K-factor are obtained as:

$$K_V^{RID} = \frac{\sqrt{\frac{1}{T}\int_{t-T}^{t} \sum_{n\neq 1}^{\infty} n^2 E_{V_n} dt}}{\sqrt{\frac{1}{T}\int_{t-T}^{t} E_{V_1} dt}} \tag{5.15}$$

$$K_I^{RID} = \frac{\sqrt{\frac{1}{T}\int_{t-T}^{t} \sum_{n\neq 1}^{\infty} n^2 E_{I_n} dt}}{\sqrt{\frac{1}{T}\int_{t-T}^{t} E_{I_1} dt}} \tag{5.16}$$

In order to quantify the redefined PQ indices as a single value, the PQ indices are assessed over a fundamental period T instead of a running window according to the Eqs. (5.8)-(5.16). Thus, redefined PQ indices correspond to "true average", and can be utilized to

justify the efficacy of the redefined PQ indices by comparing them to the traditional FFT-based PQ indices. For example, the true average of redefined PQ ($\overline{TAPQ}$) indices for THD_V^{RID} can be obtained as follows:

$$\overline{TAPQ_{THD_V}^{RID}} = \frac{\sqrt{\frac{1}{T}\int_0^T \sum_{n\neq 1}^{n} E_{V_n} dt}}{\sqrt{\frac{1}{T}\int_0^T E_{V_1} dt}} \tag{5.17}$$

Similarly, other RID-based redefined PQ indices can be quantified as a single value according to the Eq. (5.17)

5.4 Case Study Analysis

In this section, we will analyze four synthetic stationary and nonstationary PQ disturbances in order to justify the efficacy of redefined PQ indices in Sec. 5.3. The synthetic PQ disturbances are considered as we will have prior information of the actual values of PQ indices.

Synthetic Stationary PQ Disturbance

In stationary PQ disturbance, we consider the same voltage signal that is used to illustrate the limitations of existing transient PQ indices in Fig. 5.1. The following signal is considered for the current disturbance:

$$i(t) = \cos(\omega_1 t) + 0.3\cos(\omega_3 t + 30^o) + 0.2\cos(\omega_5 t + 60^o) \tag{5.18}$$

Fig. 5.2 represents the instantaneous redefined PQ indices obtained via RID. Unlike the existing transient PQ indices shown in Fig. 5.1, employing the redefined PQ indices actual values of voltage THD, DIN, and K-factor are obtained after the first cycle as shown in Figs. 5.2(a), (b), and (e), respectively. Also, two other PQ indices PF and voltage TIF in Figs. 5.2(c), and (d) result in actual values.

Table 5.1 summarizes the redefined PQ indices obtained via $\overline{TAPQ}$ as single values which are compared to the FFT-based method. As seen in the table, RID-based redefined

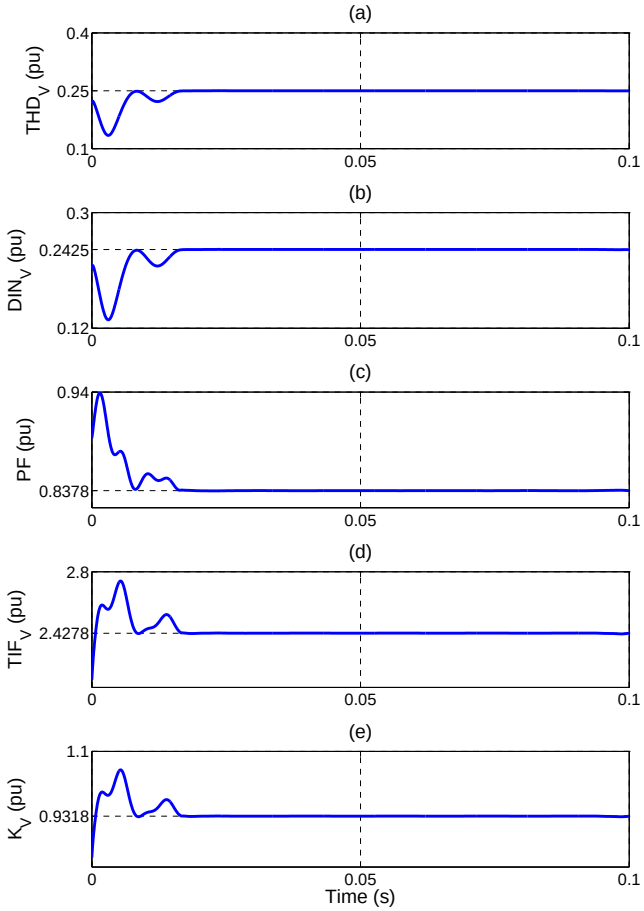

Figure 5.2: (a) Voltage THD, (b) Voltage DIN, (c) PF, (d) Voltage TIF, and (e) Voltage K-factor for stationary PQ disturbance.

PQ indices provide very accurate results, and result in smaller percentage errors (ε) compared to the FFT-based method. In stationary PQ disturbance, FFT-based method is competitive to the proposed RID-based method as the voltage and current signals are periodic in stationary PQ disturbances.

Synthetic Transient PQ Disturbance

In synthetic transient PQ analysis, transient disturbance is introduced in voltage and current signals at $t = 0.05$ and persists for a short duration of $t = 0.015$ s as shown in Fig. 5.3. The PQ indices obtained via modified RID method are incorporated in Fig. 5.4. Fig. 5.4 shows that all the PQ indices increase due to transient voltage and current PQ disturbances.

Table 5.1: Power Quality Analysis Results (pu) for Stationary Example

PQ Indices	Actual	FFT	RID	FFT %$\|\varepsilon\|$	RID %$\|\varepsilon\|$
THD_V	0.2500	0.2498	0.2499	0.0800	0.0400
THD_I	0.3606	0.3606	0.3606	0	0
DIN_V	0.2425	0.2424	0.2424	0.0412	0.0412
DIN_I	0.3392	0.3392	0.3392	0	0
PF	0.8378	0.8379	0.8379	0.0119	0.0119
TIF_V	2.4278	2.4278	2.4282	0	0.0165
TIF_I	3.2178	3.2137	3.2142	0.1274	0.1119
K_V	0.9318	0.9317	0.9318	0.0107	0
K_I	1.2656	1.2641	1.2643	0.1185	0.1027

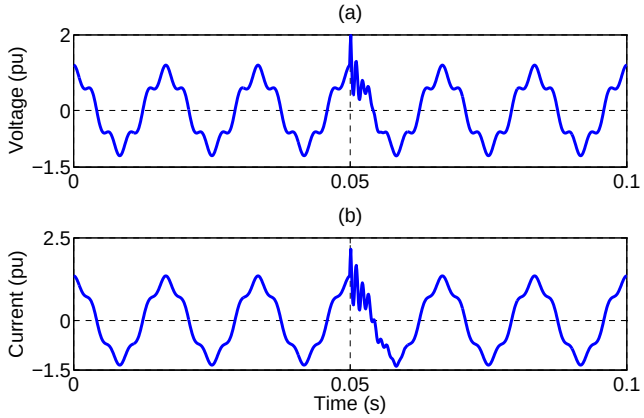

Figure 5.3: A transient PQ (a) Voltage, and (b) Current disturbance waveforms.

The redefined PQ indices take one cycle to reach steady state value after the transient is cleared, as they are assessed over a moving window of one fundamental cycle $T = 0.0167$ s according to the Eqs. (5.8)-(5.16). Therefore, in Fig. 5.4, the PQ indices becomes steady state condition at $t = 0.065 + 0.0167 = 0.0817$ s approximately. Note that the dynamic signature of the redefined PQ indices will depend on the time-varying nature of nonstationary PQ disturbances, and will be different for different types of PQ disturbances.

Table 5.2 summarizes the redefined PQ indices quantified as a single value via $\overline{TAPQ}$

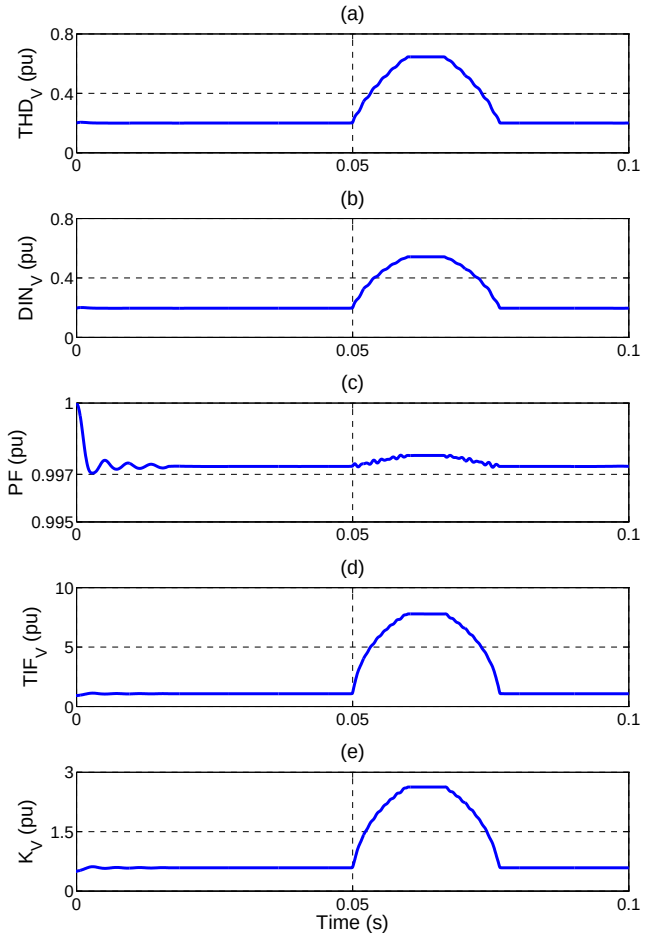

Figure 5.4: (a) Voltage THD, (b) Voltage DIN, (c) PF, (d) Voltage TIF, and (e) Voltage K-factor for transient PQ disturbance.

in order to compare with the traditional FFT-based method, and to justify the efficacy of the redefined PQ indices under the transient PQ disturbance. Table 5.2 validates that the proposed RID-based redefined PQ indices provide very accurate results, and percentage errors associated with the redefined PQ indices are smaller than the traditional FFT-based method for the transient PQ disturbance.

Synthetic Voltage Swell PQ Disturbance

A voltage swell and corresponding current PQ disturbance waveforms are provided in Fig. 5.5 where voltage increases and current increases at $t = 0.05$ s. Fig. 5.6 represents the

Table 5.2: Power Quality Analysis Results (pu) for Transient Example

PQ Indices	Actual	FFT	RID	FFT %|ε|	RID %|ε|
THD_V	0.2187	0.2230	0.2185	1.9662	0.0914
THD_I	0.1450	0.1505	0.1444	3.7931	0.4138
DIN_V	0.2137	0.2176	0.2135	1.8250	0.0936
DIN_I	0.1435	0.1489	0.1430	3.7631	0.2340
PF	0.9971	0.9974	0.9970	0.0301	0.0100
TIF_V	6.3338	7.2174	6.1952	13.9506	2.1883
TIF_I	5.0832	5.8804	4.9588	15.6830	2.4473
K_V	1.6077	1.7851	1.5808	11.0344	1.6732
K_I	1.2411	1.4093	1.2155	13.5525	2.0627

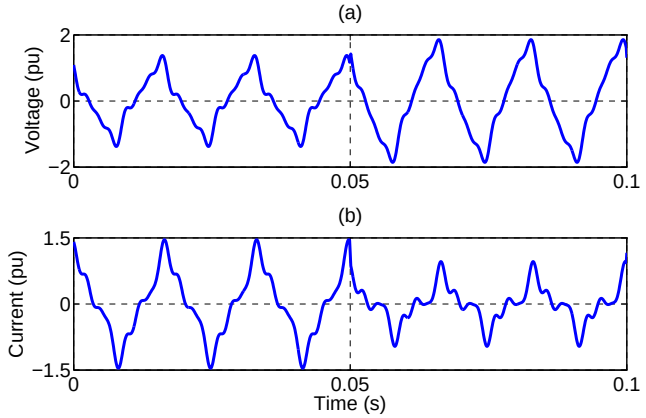

Figure 5.5: A (a) Voltage swell, and corresponding (b) Current PQ disturbance waveforms.

PQ indices based on RID for the synthetic voltage swell PQ disturbance. In voltage swell PQ disturbance, RID-based voltage PQ indices decrease due to increase in fundamental frequency component caused by voltage swell PQ disturbance. In the same way, current PQ indices increase due to decrease in fundamental current.

Table 5.3 justifies that RID-based PQ indices result in musch smaller percentage errors than the traditional FFT-based method which justify the efficacy of proposed RID-based PQ assessment method.

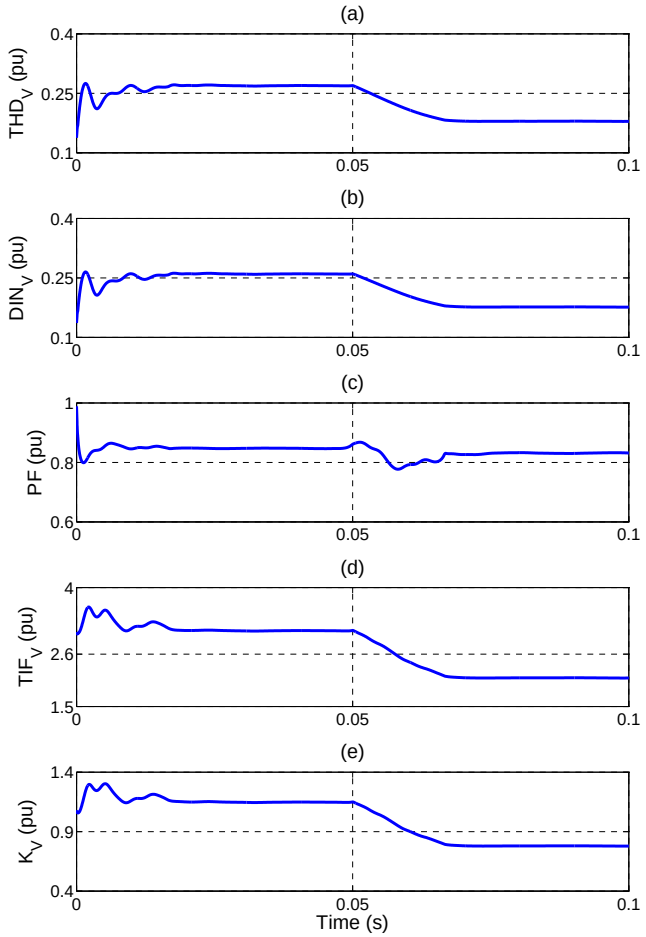

Figure 5.6: (a) Voltage THD, (b) Voltage DIN, (c) PF, (d) Voltage TIF, and (e) Voltage K-factor for voltage swell PQ disturbance.

Synthetic Voltage Sag Disturbance

In final example, we consider a voltage sag PQ disturbance whose voltage and current waveforms are shown in Fig. 5.7. In this figure, sag disturbance is introduced at $t = 0.05$ s, and cleared at $t = 0.08$ s. The corresponding PQ indices for the synthetic voltage sag disturbance are incorporated in Fig. 5.8 which represents dynamic behavior of PQ indices under voltage sag disturbance. Also, the voltage PQ indices such as THD_V, DIN_V, TIF_V, and K_v in Fig. 5.8 increase during the voltage sag as the sag disturbance is caused by the decrease in fundamental frequency component.

The $\overline{TAPQ}$ of RID-based PQ indices are summarized in Table 5.4. Table 5.4 justi-

Table 5.3: PQ Analysis Results (pu) for Voltage Swell Example

PQ Indices	Actual	FFT	RID	FFT %|ε|	RID %|ε|
THD_V	0.2112	0.2648	0.2121	25.3788	0.4261
THD_I	0.2418	0.2968	0.2430	22.7461	0.4963
DIN_V	0.2067	0.2560	0.2075	23.8510	0.3870
DIN_I	0.2350	0.2845	0.2361	21.0638	0.5322
PF	0.7458	0.8615	0.7461	15.5135	0.0402
TIF_V	2.7420	3.4050	2.7520	24.1794	0.3647
TIF_I	4.3201	3.5096	4.3272	18.7611	0.1643
K_V	0.9122	1.1313	0.9156	24.0189	0.3727
K_I	1.4977	1.2175	1.5003	18.7087	0.1736

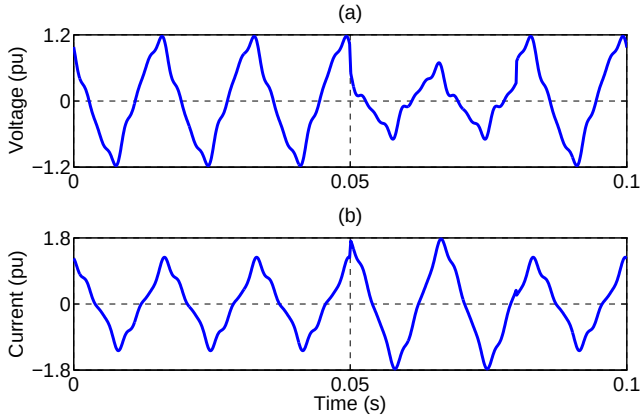

Figure 5.7: A (a) Voltage sag, and corresponding (b) Current disturbance waveforms

fies that the redefined PQ indices provide much more accurate assessment of voltage sag disturbance than the traditional FFT-base PQ indices. The maximum percentage error associated with the FFT-based PQ indices is 12.3916% whereas maximum error in redefined PQ indices is only 0.1958%.

Four case study analyses verify that the redefined PQ indices provide more accurate results than the FFT-based method under nonstationary PQ disturbances. Also, dynamic behavior of the PQ indices are extracted which provides actual value of PQ indices with

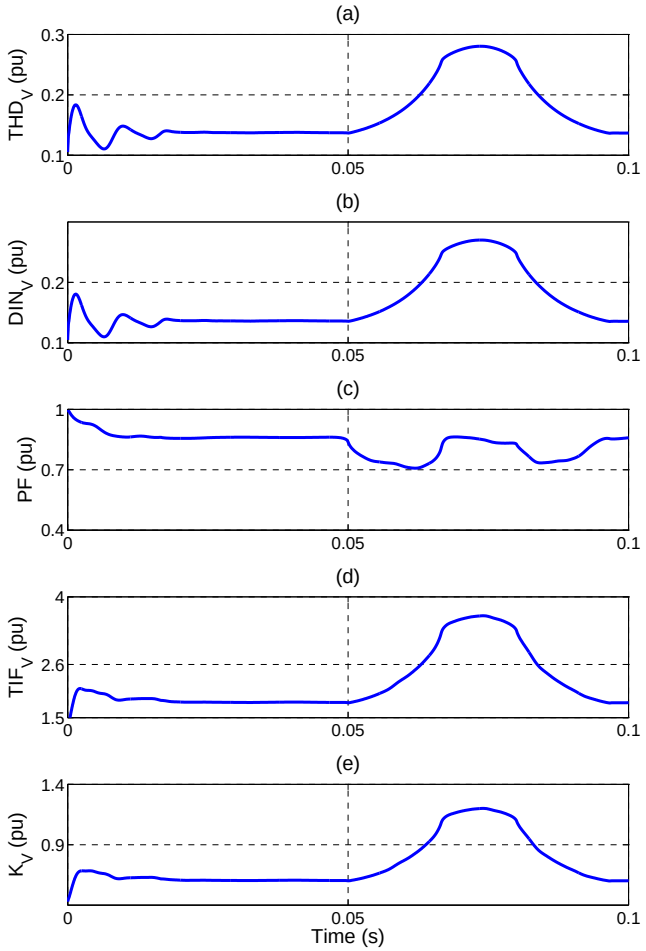

Figure 5.8: (a) Voltage THD, (b) Voltage DIN, (c) PF, (d) Voltage TIF, and (e) Voltage K-factor for voltage sag PQ disturbance.

time under PQ disturbances. Therefore, the proposed PQ indices can be a viable alternative for the assessment of PQ disturbances in electric power systems.

5.5 Conclusion

This chapter focuses on the limitations of decomposition method, and transient PQ indices proposed in [22]. Regarding the limitations of the decomposition method in [22], in this work, an improved decomposition method is proposed by defining tolerant frequency bandwidth in TFD for each frequency component which does not require any assumption of power system frequency.

Table 5.4: PQ Analysis Results (pu) for Voltage Sag Example

PQ Indices	Actual	FFT	RID	FFT %|ε|	RID %|ε|
THD_V	0.1580	0.1420	0.1586	10.1266	0.3797
THD_I	0.1622	0.1822	0.1629	12.3305	0.4316
DIN_V	0.1560	0.1406	0.1567	9.8718	0.4487
DIN_I	0.1601	0.1792	0.1608	11.9300	0.4372
PF	0.7660	0.8382	0.7675	9.2559	0.1958
TIF_V	2.3617	2.1280	2.3707	9.8954	0.3811
TIF_I	2.0247	1.9258	2.0321	4.8847	0.3655
K_V	0.7387	0.8369	0.7515	10.0176	0.3790
K_I	0.6803	0.7646	0.6828	12.3916	0.3675

Based on the improved decomposition method, the transient PQ indices ITHD, IDIN, and IK [22] are redefined correctly which provide accurate results under stationary and non-stationary PQ disturbances. Other PQ indices PF, TIF, and C message are redefined in the time-frequency domain as well for the assessment of PQ disturbances.

Also, in order to justify the efficacy of the redefined PQ indices, the PQ indices are quantified as a single value by a new index "true average" which replaces the "principal average" defined in [22], and provides very accurate values for stationary and non-stationary PQ disturbances. The "true average" of redefined PQ indices are compared to the traditional FFT-based method for four synthetic stationary and nonstationary PQ disturbances. The analysis results prevail that the redefined PQ indices provide very accurate values, and the percentage errors associated them are much smaller than the traditional FFT-based method under nonstationary PQ disturbances. Therefore, the new PQ indices can be viable alternative solution for the assessment of PQ disturbances under stationary and nostationary PQ disturbances.

Utilizing the proposed PQ indices, one can extract dynamic signature of PQ disturbances, thus, detect and classify PQ disturbance events typically present in electric power

systems. Furthermore, one can reformulate the single phase and three-phase power components according to the IEEE Standard 1459-2010 under sinusoidal, nonsinusoidal, balanced or unbalanced conditions for stationary and nonstationary PQ disturbances which we will discuss in the next two chapters.

CHAPTER 6

SINGLE-PHASE INSTANTANEOUS POWER COMPONENTS FOR TRANSIENT DISTURBANCES ACCORDING TO THE IEEE STANDARD 1459-2010

6.1 INTRODUCTION

In order to assess electric PQ and develop proper compensation techniques, the IEEE Standard 1459-2010 defines a set of power components for measuring PQ factors, such as displacement power factor, harmonic pollution and total power factor [13]. In this chapter, we will redefine the power components for PQ disturbances based on the time-frequency analysis method utilizing the RID.

6.2 DEFINITIONS OF POWER COMPONENTS

In a single-phase system, non-sinusoidal voltage and current can be expressed as follows:

$$v(t) = v_1(t) + v_h(t) \tag{6.1}$$

$$= \sqrt{2}V_1 \sin(\omega_1 t - \alpha_1) + V_0(t) + \sqrt{2}\sum_{h\neq 1} V_h \sin(h\omega_1 t - \alpha_h) \tag{6.2}$$

$$i(t) = i_1(t) + i_h(t) \tag{6.3}$$

$$= \sqrt{2}I_1 \sin(\omega_1 t - \beta_1) + I_0(t) + \sqrt{2}\sum_{h\neq 1} I_h \sin(h\omega_1 t - \beta_h) \tag{6.4}$$

where h stands for the integer and non-integer number harmonics, α_1 and β_1 are fundamental voltage and current phase angle, respectively, and α_h and β_h are harmonic voltage and current phase angle, respectively.

Fundamental Power Components: According to the IEEE Standard 1459-2010 [13], the rms voltage and current are defined as:

$$V = \sqrt{\frac{1}{T}\int_0^T v(t)^2 dt} = \sqrt{(V_1^2 + V_H^2)} \tag{6.5}$$

$$I = \sqrt{\frac{1}{T}\int_0^T i(t)^2 dt} = \sqrt{(I_1^2 + I_H^2)} \tag{6.6}$$

where V_1 and I_1 are fundamental voltage and current, respectively.

The fundamental apparent power, active power, reactive power and displacement power factor are defined as:

$$S_1 = V_1 I_1 \tag{6.7}$$

$$P_1 = V_1 I_1 \cos(\alpha_1 - \beta_1) = V_1 I_1 \cos\theta_1 \tag{6.8}$$

$$Q_1 = V_1 I_1 \sin(\alpha_1 - \beta_1) = V_1 I_1 \sin\theta_1 \tag{6.9}$$

$$PF_1 = \frac{P_1}{S_1} = \cos\theta_1 \tag{6.10}$$

Non-Fundamental And Combined Power Components: The harmonic rms voltage and current are defined as:

$$V_H = \sqrt{V_0^2 + \sum_{h\neq 1} V_h^2} = P - P_1; \quad I_H = \sqrt{I_0^2 + \sum_{h\neq 1} I_h^2} \tag{6.11}$$

Total harmonic distortion factors for voltage and current are:

$$THD_V = \frac{V_H}{V_1}; \quad THD_I = \frac{I_H}{I_1} \tag{6.12}$$

The voltage distortion power D_V, current distortion power D_I, harmonic apparent power S_H and non-fundamental apparent power S_N are defined as follows:

$$D_V = V_H I_1 = S_1 \cdot THD_V \tag{6.13}$$

$$D_I = V_1 I_H = S_1 \cdot THD_I \tag{6.14}$$

$$S_H = V_H I_H = S_1 \cdot THD_V \cdot THD_I \tag{6.15}$$

$$S_N^2 = D_V^2 + D_I^2 + S_H^2 \tag{6.16}$$

The harmonic active power and the harmonic distortion power are expressed in the following equations:

$$P_H = V_0 I_0 + \sum_{h \neq 1} V_h I_h \cos\theta_h; \quad D_H = \sqrt{S_H^2 - P_H^2} \tag{6.17}$$

The total apparent power, active power and non-active power are defined as:

$$S^2 = S_1^2 + D_V^2 + D_I^2 + S_H^2 \tag{6.18}$$

$$P = P_1 + P_H; \quad N = \sqrt{S^2 - P^2} \tag{6.19}$$

Finally, the harmonics pollution level and total power factor can be calculated as:

$$HP = \frac{S_N}{S_1}; \quad PF = \frac{P}{S} \tag{6.20}$$

Note that according to the IEEE Standard 1459, harmonic active power is assessed as:

$$P_H = P - P_1 \tag{6.21}$$

This indirect assessment of harmonic active power may provide erroneous result as harmonic active power is usually very small part of the total active power [30].

6.3 Redefined Power Components

In this section, the power components are redefined based on the TFD and XTFD of the fundamental and disturbance components of transient voltage and current signals.

Time-Frequency Based Instantaneous Fundamental Power Components: Time-frequency (TF) based fundamental power components such as fundamental rms voltage, rms current, apparent power, active power, reactive power, and displacement power factor

are defined as follows:

$$V_1^{TF} = \frac{1}{\sqrt{2}}\sqrt{\frac{1}{T}\int_{t-T}^{t}\int_{\omega} TFD_{v_1}(t,\omega;\phi)d\omega dt} \tag{6.22}$$

$$I_1^{TF} = \frac{1}{\sqrt{2}}\sqrt{\frac{1}{T}\int_{t-T}^{t}\int_{\omega} TFD_{i_1}(t,\omega;\phi)d\omega dt} \tag{6.23}$$

$$S_1^{TF} = V_1^{TF}\cdot I_1^{TF} \tag{6.24}$$

$$P_1^{TF} = \frac{1}{2}\cdot\frac{1}{T}\int_{t-T}^{t}\Re\left\{\int_{\omega} XTFD_{v_1 i_1}(t,\omega;\phi)d\omega\right\}dt \tag{6.25}$$

$$Q_1^{TF} = \frac{1}{2}\cdot\frac{1}{T}\int_{t-T}^{t}\Im\left\{\int_{\omega} XTFD_{v_1 i_1}(t,\omega;\phi)d\omega\right\}dt \tag{6.26}$$

$$PF_1^{TF} = \frac{P_1^{TF}}{S_1^{TF}} \tag{6.27}$$

where $TFD_{v_1}(t,\omega;\phi)$ and $TFD_{i_1}(t,\omega;\phi)$ are the TFDs of the fundamental voltage and fundamental current, respectively, and $XTFD_{v_1 i_1}(t,\omega;\phi)$ is the cross TFD of the fundamental voltage and current. The scale factors $\frac{1}{\sqrt{2}}$ and $\frac{1}{2}$ are introduced in the Eqs. (6.22)-(6.23), and Eqs. (6.25)-(6.26), respectively because of the energy and complex power of the original signal being half the energy and complex power of the analytic signal, respectively.

Time-Frequency Based Instantaneous Non-Fundamental And Combined Power Components: The TF based disturbance rms voltage and current are defined as:

$$V_D^{TF} = \frac{1}{\sqrt{2}}\sqrt{\frac{1}{T}\int_{t-T}^{t}\int_{\omega} TFD_{V_D}(t,\omega;\phi)d\omega dt} \tag{6.28}$$

$$I_D^{TF} = \frac{1}{\sqrt{2}}\sqrt{\frac{1}{T}\int_{t-T}^{t}\int_{\omega} TFD_{I_D}(t,\omega;\phi)d\omega dt} \tag{6.29}$$

where $TFD_{V_D}(t,\omega;\phi)$ and $TFD_{I_D}(t,\omega;\phi)$ are the TFDs of the voltage and current disturbances, respectively.

The voltage and current THD formed on the TF are as follows:

$$THD_V^{TF} = \frac{V_D^{TF}}{V_1^{TF}}; \quad THD_I^{TF} = \frac{I_D^{TF}}{I_1^{TF}} \tag{6.30}$$

The TF based voltage distortion power, current distortion power, disturbance apparent power and non-fundamental apparent power are expressed as:

$$D_V^{TF} = V_D^{TF} I_1^{TF} = S_1^{TF} \cdot THD_V^{TF} \tag{6.31}$$

$$D_I^{TF} = V_I^{TF} I_D^{TF} = S_1^{TF} \cdot THD_I^{TF} \tag{6.32}$$

$$S_D^{TF} = V_D^{TF} I_D^{TF} = S_1^{TF} \cdot THD_V^{TF} \cdot THD_I^{TF} \tag{6.33}$$

$$(S_N^{TF})^2 = (D_V^{TF})^2 + (D_I^{TF})^2 + (S_D^{TF})^2 \tag{6.34}$$

The TF based disturbance active power and disturbance distortion power are obtained as follows:

$$P_D^{TF} = \frac{1}{2} \cdot \frac{1}{T} \int_{t-T}^{t} \Re\left\{ \int_{\omega} XTFD_{V_D I_D}(t, \omega; \phi) d\omega \right\} dt \tag{6.35}$$

$$D_D^{TF} = \sqrt{(S_D^{TF})^2 - (P_D^{TF})^2} \tag{6.36}$$

Note that the disturbance active power P_D^{TF} is assessed directly from the cross time-frequency distribution of the voltage and current disturbances $XTFD_{V_D I_D}(t, \omega; \phi)$.

Therefore, the TF based total apparent power, active power and non-active power can be obtained as:

$$(S^{TF})^2 = (S_1^{TF})^2 + (D_V^{TF})^2 + (D_I^{TF})^2 + (S_D^{TF})^2 \tag{6.37}$$

$$P^{TF} = P_1^{TF} + P_D^{TF}; \quad N^{TF} = \sqrt{(S^{TF})^2 - (P^{TF})^2} \tag{6.38}$$

Finally, the disturbance pollution (DP) level and total power factor based on the TF method can be calculated as:

$$DP^{TF} = \frac{S_N^{TF}}{S_1}; \quad PF^{TF} = \frac{P^{TF}}{S^{TF}} \tag{6.39}$$

Note that owing to the time marginal property $\int TFD_s(t, \omega; \phi) d\omega = |s(t)|^2$ for a signal $s(t)$, the transient power components proposed in this chapter will correspond to traditional FFT-based power components, if the disturbance is periodic in steady state.

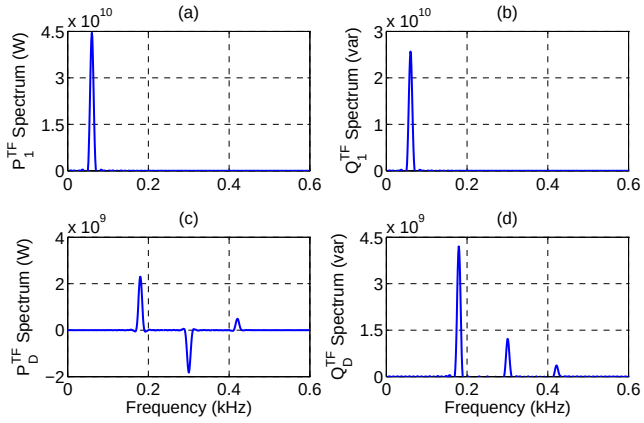

Figure 6.1: TF based fundamental (a) Active power, (b) Reactive power, and non-fundamental (c) Active power and (d) Reactive power spectra of the steady state signal, respectively.

6.4 Case Study Analysis

In this section, we will assess TF based power components for three different PQ disturbance events - first two waveforms are simulated steady state and transient disturbance waveforms, and the other waveform is a real-world transient disturbance waveform. The purpose of the simulated case study analysis is to demonstrate the efficacy of the proposed method under steady state and transient condition. The sampling frequency of the simulated waveforms is 10 kHZ.

Simulated Steady State Case Study

The per unit (pu) voltage and current ($S_{base} = 100$ MVA, $V_{base} = 138$ kV) waveforms considered for the steady state case study are expressed as:

$$v(t) = \cos(\omega_1 t + 30^o) + 0.3\cos(3\omega_1 t + 60^o) + 0.2\cos(5\omega_1 t + 150^o) + 0.1\cos(7\omega_1 t + 30^o) \tag{6.40}$$

$$i(t) = \cos(\omega_1 t) + 0.3\cos(3\omega_1 t) + 0.2\cos(5\omega_1 t) + 0.1\cos(7\omega_1 t) \tag{6.41}$$

Fig. 6.1 shows the active and reactive power spectra of the fundamental and disturbance components obtained through frequency marginal property of the XTFD. As seen in the

Table 6.1: Stationary Case Study Results

Fundamental Power Components		
Actual Value (pu)	TF Based Value (pu)	Percentage Error (%)
$V_1 = 0.70711$	$V_1^{TF} = 0.70710$	0.00142
$I_1 = 0.70711$	$I_1^{TF} = 0.70710$	0.00142
$S_1 = 0.50000$	$S_1^{TF} = 0.49999$	0.00200
$P_1 = 0.43301$	$P_1^{TF} = 0.43300$	0.00231
$Q_1 = 0.25000$	$Q_1^{TF} = 0.25000$	0.00000
$PF_1 = 0.86602$	$PF_1^{TF} = 0.86601$	0.00115
Non-Fundamental And Combined Power Components		
Actual Value (pu)	TF Based Value (pu)	Percentage Error (%)
$V_H = 0.26458$	$V_D^{TF} = 0.26460$	0.00756
$I_H = 0.26458$	$I_D^{TF} = 0.26460$	0.00756
$THD_V = 0.37417$	$THD_V^{TF} = 0.37420$	0.00802
$THD_I = 0.37417$	$THD_I^{TF} = 0.37420$	0.00802
$D_V = 0.18708$	$D_V^{TF} = 0.18710$	0.01069
$D_I = 0.18708$	$D_I^{TF} = 0.18710$	0.01069
$S_H = 0.07000$	$S_D^{TF} = 0.06999$	0.01429
$S_N = 0.27367$	$S_N^{TF} = 0.27370$	0.01096
$P_H = 0.009510$	$P_D^{TF} = 0.009508$	0.02103
$D_H = 0.06935$	$D_D^{TF} = 0.06934$	0.01442
$S = 0.57000$	$S^{TF} = 0.57000$	0.0000
$N = 0.35927$	$N^{TF} = 0.35929$	0.00557
$HP = 0.54734$	$DP^{TF} = 0.54741$	0.01279
$PF = 0.77635$	$PF^{TF} = 0.77633$	0.00258

Figs. 6.1(a)-(d), the active power of 5th harmonic component flows opposite to the fundamental active power, while active power of 3rd and 7th harmonic components and reactive power of 3rd, 5th, and 7th harmonic components flow in the same direction as the funda-

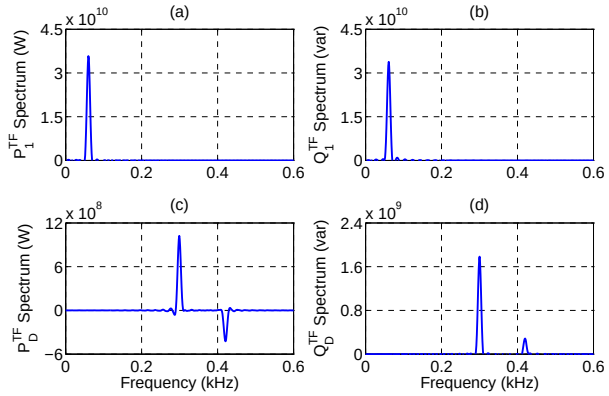

Figure 6.2: TF based fundamental and non-fundamental active power and reactive power spectra of the transient disturbance signal.

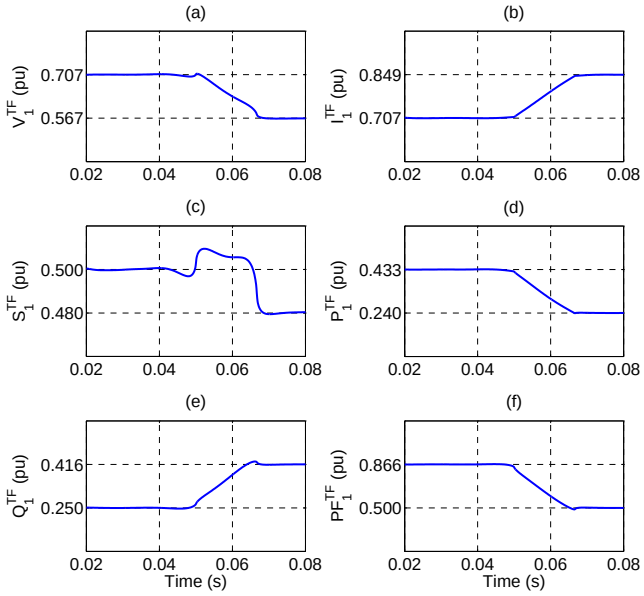

Figure 6.3: TF based fundamental power components of the transient disturbance signal.

mental components according to the phase difference in the Eqs. (6.40)-(6.41).

In this study, the power components are constant over the time after the first cycle. Therefore, instead of providing instantaneous power components, the constant values of the TF based power components are provided in the Table 6.1 indicates that the percentage errors associated with the TF based power components are very small, and justifies the effectiveness of the TF based power components estimation method in the steady state.

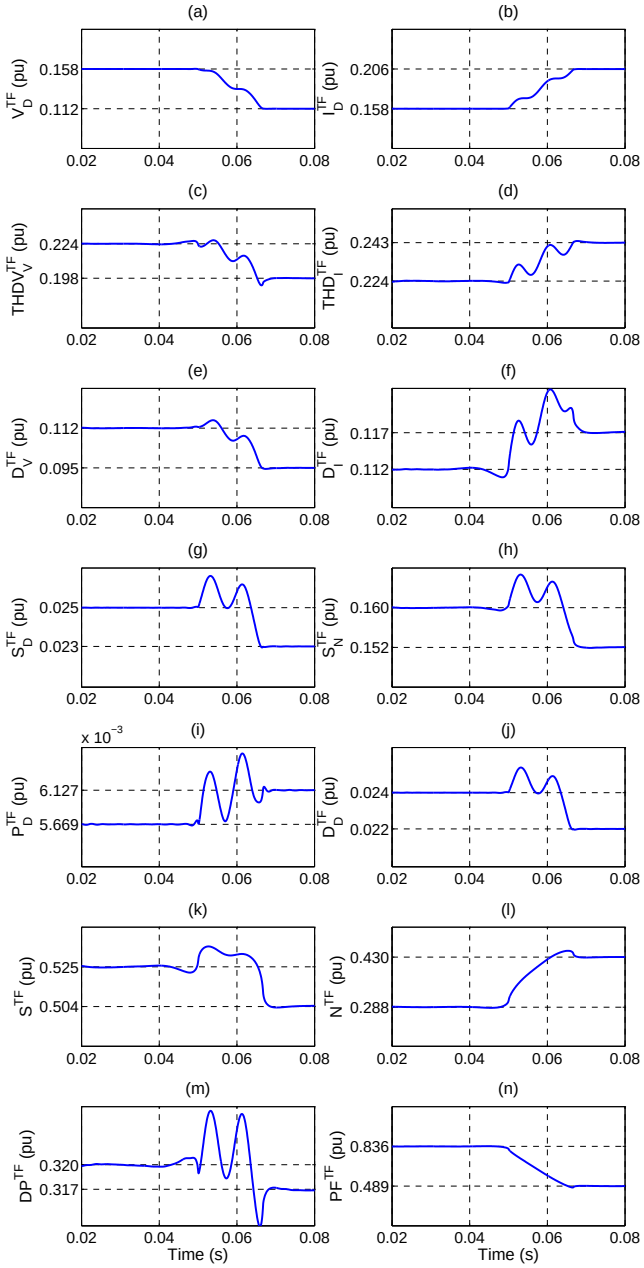

Figure 6.4: Instantaneous non-fundamental and combined power components of the transient disturbance signal.

Simulated Transient Disturbance Case Study

In the transient case study, the fundamental and harmonic components of the transient voltage and current waveforms change with time at $t = 0.05$ s, and are expressed in pu

values as follows:

$$v(t) = \cos(\omega_1 t + 30^o) + 0.2\cos(5\omega_1 t + 60^o) + 0.1\cos(7\omega_1 t + 150^o)\{\text{for } 0 < t \leq 0.05\} \tag{6.42}$$

$$i(t) = \cos(\omega_1 t) + 0.2\cos(5\omega_1 t) + 0.1\cos(7\omega_1 t)\{\text{for } 0 < t \leq 0.05\} \tag{6.43}$$

$$\begin{aligned} v(t) &= 0.8\cos(\omega_1 t + 60^o) + 0.15\cos(5\omega_1 t + 60^o) \\ &\quad + 0.05\cos(7\omega_1 t + 150^o)\{\text{for } 0.05 \leq t < 0.1\} \end{aligned} \tag{6.44}$$

$$i(t) = 1.2\cos(\omega_1 t) + 0.25\cos(5\omega_1 t) + 0.15\cos(7\omega_1 t)\{\text{for } 0.05 \leq t < 0.1\} \tag{6.45}$$

Figs. 6.2(a)-(d) show that the reactive power of the 5th harmonic flows opposite to the active and reactive power of all other frequency components as estimated according to the Eqs. (6.42)-(6.45). The TF based instantaneous fundamental, non-fundamental and combined power components of the simulated transient case study are summarized in Figs. 6.3 and 6.4, respectively where the middle two axes indicate the actual value of the power components prior and after the transient disturbance. As seen in these figures, the TF based assessment of the power components agrees with the values calculated with the Eqs. (6.42)-(6.45). However, transients are observed in between two steady state values due to the change in the voltage and current waveforms at $t = 0.05$ s according to the Eqs. (6.42)-(6.45). The power components take one cycle to reach steady state values since the TF based power components are assessed over a moving window of one fundamental cycle $T = 0.0167$ s. The transient behavior of the TF based power components will vary for different types of PQ disturbance events depending on the time-varying nature of the signals.

Real-World Transient Disturbance Case Study

The real-world transient disturbance signal is provided by the National Renewable Energy Laboratory (NREL), and is collected from Trent Mesa Wind Farm in Texas. The sampling

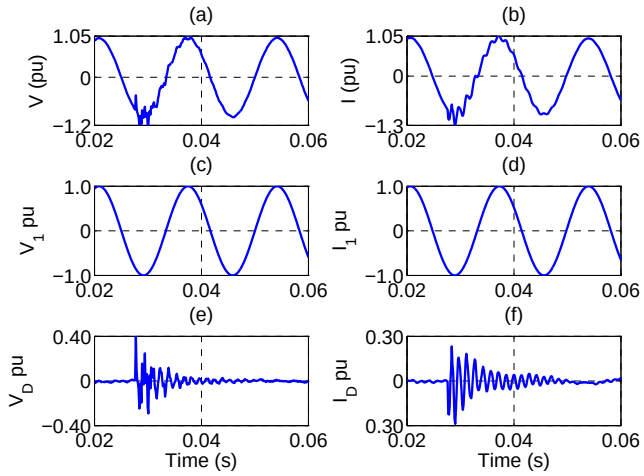

Figure 6.5: Capacitor switching (a) Voltage waveform, (b) Current waveform, separated (c) Fundamental voltage, (d) Fundamental current, (e) Voltage disturbance, and (f) Current disturbance, respectively.

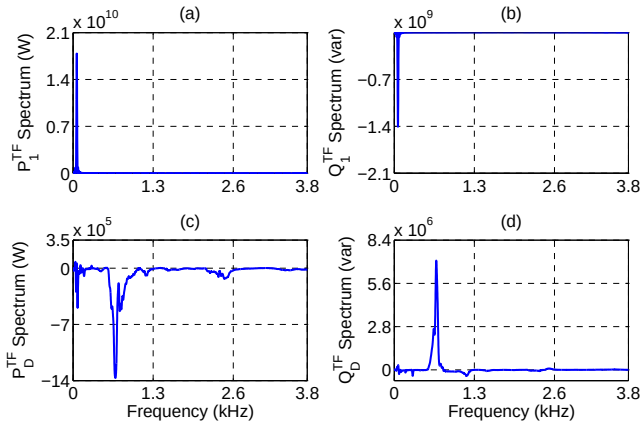

Figure 6.6: TF based fundamental and non-fundamental active power and reactive power spectra of the real-world transient disturbance case study.

frequency of the recorded transient disturbance waveform is 7.676 kHz. The transient voltage and current disturbance waveforms in pu ($S_{base} = 70$ MVA, $V_{base} = 115$ kV), extracted fundamental and disturbance components are shown in Fig. 6.5.

The active power and reactive power spectra of the fundamental and disturbance components, attained using frequency marginal property of the XTFD, are shown in Fig. 6.6(a)-(d). It is observed in Figs. 6.6(c)-(d) that the maximum disturbance active power and reactive power are generated over the frequency range of 0.3-0.9 kHz, and flow in the opposite

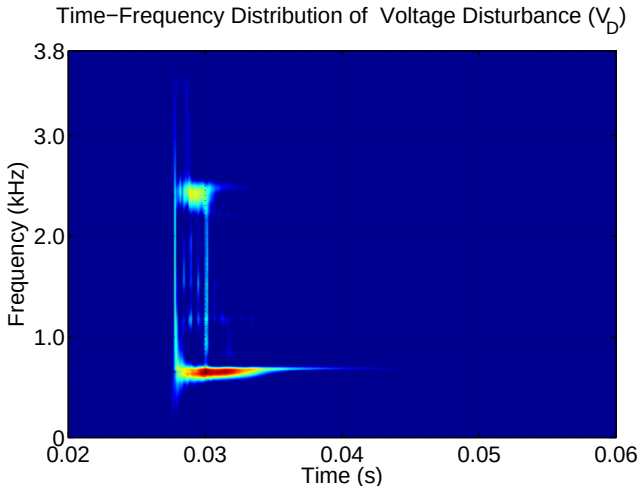

Figure 6.7: Time-frequency distribution of transient voltage disturbance.

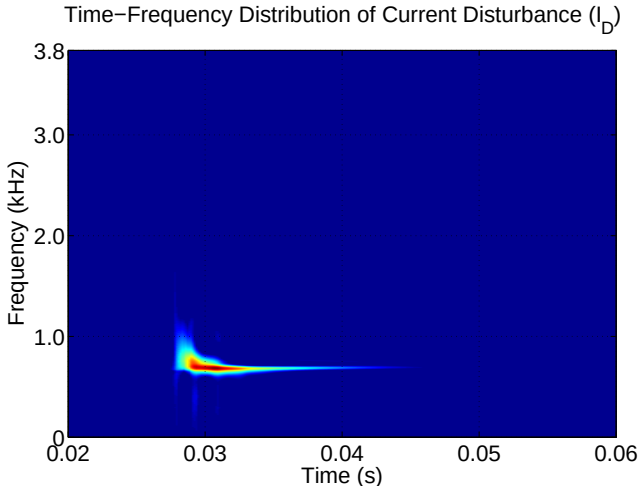

Figure 6.8: Time-frequency distribution of transient current disturbance.

direction.

The TFDs of the voltage and current disturbances in Fig. 6.7 and Fig. 6.8 show that the time-varying voltage disturbance energy exists approximately in between two frequency ranges of 0.3-0.9 kHz and 2.1-2.7 kHz, and the current disturbance energy occurs only in the frequency range of approximately 0.3-0.9 kHz during 0.027-0.038 s. The real part of the cross time-frequency distribution which provides transient disturbance active power is obtained time marginal property of the XTFD, and shown in Fig. 6.9. As seen in the figure,

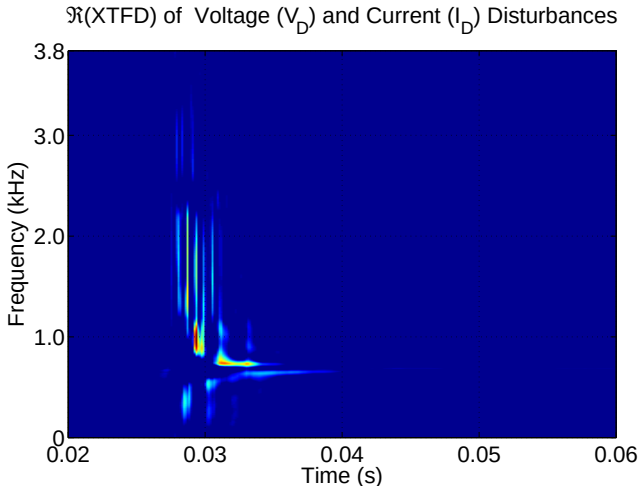

Figure 6.9: Disturbance active power in time-frequency domain obtained via XTFD.

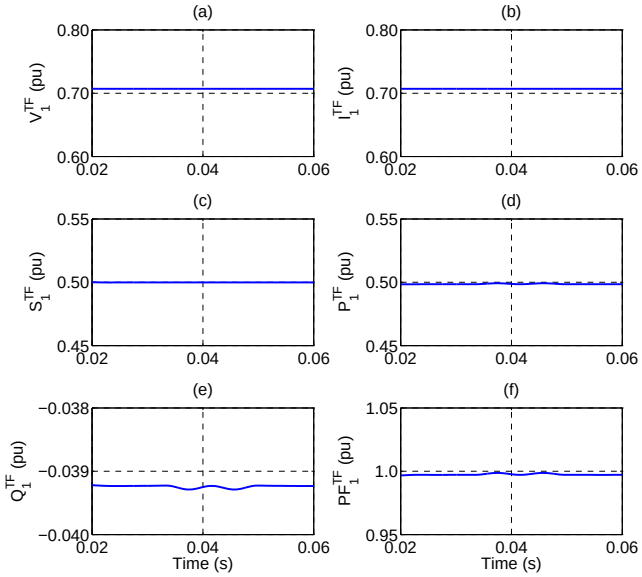

Figure 6.10: Instantaneous fundamental power components of the real-world transient disturbance case study.

the time-varying disturbance active power is distributed over the frequency range of 0.3-2.6 kHz approximately during the transient disturbance.

The TF based instantaneous fundamental power components for the transient disturbance case study are obtained through Eqs. (6.22)-(6.27), and presented in Figs. 6.10(a)-(f). As seen in these figures, the fundamental power components are almost constant over

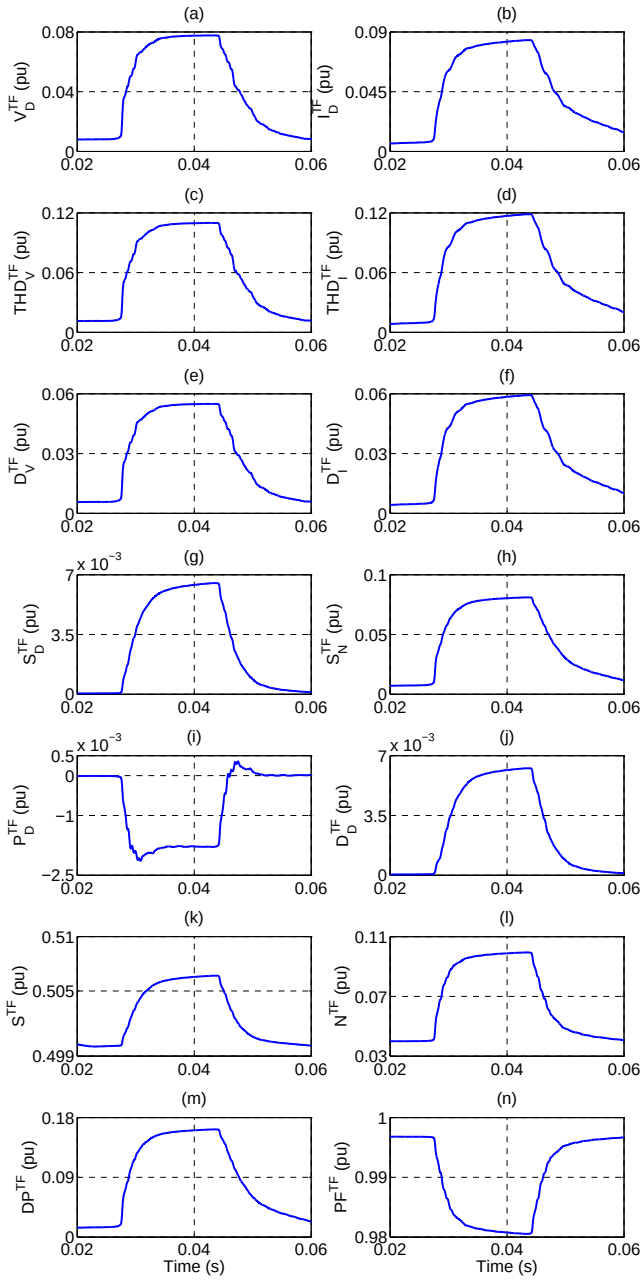

Figure 6.11: Instantaneous non-fundamental and combined power components of the real-world transient disturbance case study.

time since the transient disturbance has very small impact on the fundamental frequency component. Figs. 6.10(d)-(e) show that the fundamental active is power positive, and flows from wind farm to the grid while the reactive power flows in the opposite direction i.e. from grid to the wind farm. Also, the displacement power factor under the transient condition is

close to the unity as observed in Fig. 6.10 (f).

Figs. 6.11(a)-(n) summarize the TF based instantaneous non-fundamental and combined power components which are obtained via Eqs. (6.28)-(6.39). As seen in these figures, unlike the fundamental power components, the non-fundamental power components change with time due to the change of non-fundamental frequency components under the transient condition. During the transient disturbance, the voltage distortion power and current distortion power go up to 0.06 pu approximately as seen in Figs. 6.11(e)-(f). Fig. 6.11(i) shows that the disturbance active power flows in the opposite direction of the fundamental active power i.e. from grid to the wind farm during the transient disturbance. Finally, in Figs. 6.11(m)-(n), we can see that the transient disturbance increases the disturbance pollution up to approximately 0.18 pu and decreases the total power factor to almost 0.98 pu.

The reactive power associated with other frequency components may superimpose on the fundamental reactive power in the presence of PQ disturbance events, and result in errors [21]. Therefore, in this chapter, the fundamental reactive power is extracted, identified and quantified which represents the total reactive power with time under sinusoidal operating conditions only. The direction of the fundamental reactive power will depend on the instantaneous phase angle between fundamental voltage and current obtained through cross time-frequency distribution. Thus, the TF based instantaneous power components discussed in this chapter can be interpreted as the assessment of time-varying power components under transient condition. For example, Fig. 6.11(i) shows that the time-varying disturbance active power is approximately zero in the steady state, however, is negative and flows from grid to the wind farm during the transient condition. Thus, the proposed technique can resolve a lot of transient phenomena which have not been fully investigated yet.

The TF based power components proposed in this chapter can be employed to quantify the PQ disturbance accurately, estimate the associated economic impacts on the distribution

system and decide a cost-effective PQ compensation technique. For example, in the wind power where time-varying PQ disturbances are big concerns, the TF based active power and reactive power information can be employed to design energy storage system and reactive power compensator to enhance the PQ at distribution level for the economic considerations.

6.5 Conclusion

In this chapter, the limitations of the traditional FFT-based power components assessment method adopted in the IEEE Standard 1459-2010, which intrinsically requires periodicity of the disturbance signal, have been resolved by the use of time-frequency and cross time-frequency distributions simultaneously. Employing the time- and frequency-localization of the time-frequency and cross time-frequency distributions, a new method is proposed for transient disturbances which redefines all the power components and provides instantaneous assessment of the power components contained in the IEEE Standard 1459-2010. The efficacy of the proposed method has been demonstrated by the use of simulated and real-world transient disturbance case studies.

Based on the proposed method one can determine the direction of active and reactive power flow in electric power systems. In addition, the disturbance active power is measured directly utilizing the cross time-frequency distribution of the voltage and current disturbances which provides accurate result under steady state and transient condition. Frequency components responsible for a transient disturbance can also be identified from time-frequency distribution of transient disturbances as discussed in the chapter. Therefore, the proposed method can be considered as a viable alternative for assessment of the power components under transient condition.

CHAPTER 7

REDEFINED THREE-PHASE POWER COMPONENTS ACCORDING TO IEEE STANDARD 1459-2010 UNDER NONSINUSOIDAL, BALANCED AND UNBALANCED CONDITIONS

7.1 INTRODUCTION

In this chapter, we redefine the three-phase power components according to the IEEE Standard 1459-2010 [13] under stationary and nonstationary PQ disturbances. The power components are redefined based on the time marginal property of the Page TFD. Utilizing the time-marginal property, Page TFD preserves simultaneous time and variable frequency information, and redefines the three-phase power components in the time-frequency domain. The efficacy of the proposed method is demonstrated by employing it to a stationary and a nonstationary PQ disturbances. In addition, the accuracy of the proposed Page TFD-based method is compared to the CW and previously used RID methods for the PQ disturbances in [22]-[25].

7.2 REVIEW OF THREE-PHASE POWER COMPONENTS

In this section, we will review the definitions of the three-phase power components according to the IEEE Standard 1459-2010 [13] for three-phase power systems with nonsinusoidal

conditions. The three-phase line-to-neutral voltages are expressed as follows:

$$\begin{aligned} v_a(t) &= \sqrt{2}V_{a1}\sin(\omega_o t) \\ &\quad +\sqrt{2}\sum_{h\neq 1} V_{ah}\sin(h\omega_o t+\alpha_{ah}) \end{aligned} \tag{7.1}$$

$$\begin{aligned} v_b(t) &= \sqrt{2}V_{b1}\sin(\omega_o t-120^o) \\ &\quad +\sqrt{2}\sum_{h\neq 1} V_{bh}\sin(h\omega_o t-\alpha_{bh}-120^o h) \end{aligned} \tag{7.2}$$

$$\begin{aligned} v_c(t) &= \sqrt{2}V_{c1}\sin(\omega_1 t+120^o) \\ &\quad +\sqrt{2}\sum_{h\neq 1} V_{ch}\sin(h\omega_o t+\alpha_{ch}+120^o h) \end{aligned} \tag{7.3}$$

Three-phase line currents are:

$$\begin{aligned} I_a(t) &= \sqrt{2}I_{a1}\sin(\omega_1 t) \\ &\quad +\sqrt{2}\sum_{h\neq 1} I_{ah}\sin(h\omega_o t+\alpha_{ah}) \end{aligned} \tag{7.4}$$

$$\begin{aligned} I_b(t) &= \sqrt{2}I_{b1}\sin(\omega_1 t-120^o) \\ &\quad +\sqrt{2}\sum_{h\neq 1} I_{bh}\sin(h\omega_o t-\alpha_{bh}-120^o h) \end{aligned} \tag{7.5}$$

$$\begin{aligned} I_c(t) &= \sqrt{2}I_{c1}\sin(\omega_1 t+120^0) \\ &\quad +\sqrt{2}\sum_{h\neq 1} I_{ch}\sin(h\omega_o t+\alpha_{ch}+120^o h) \end{aligned} \tag{7.6}$$

where V_{a1}, V_{b1}, V_{c1}, and I_{a1}, I_{b1}, I_{c1} are three-phase rms voltages and currents at the fundamental frequency, respectively, V_{ah}, V_{bh}, V_{ch}, and I_{ah}, I_{bh}, I_{ch} are three-phase voltages and currents, respectively at any integer and noninteger number harmonics order h, and α_{ah}, α_{bh} and α_{ch} are respective phase angles. Note that according to the IEEE Standard 1459-2010, the power quantities for three-phase systems with nonsinusoidal waveforms are summarized and grouped as fundamental, nonfundamental and combined power components which we will discuss in the following contents.

1) Fundamental Power Components: The fundamental effective rms voltage and current for three-phase three-wire systems are defined as:

$$V_{e1}=\sqrt{\frac{V_{a1}^2+V_{b1}^2+V_{c1}^2}{3}};\quad I_{e1}=\sqrt{\frac{I_{a1}^2+I_{b1}^2+I_{c1}^2}{3}} \tag{7.7}$$

Therefore, fundamental effective apparent power S_{e1}, positive sequence apparent power S_I^+ and fundamental unbalance power for three-phase systems are defined as follows:

$$S_{e1} = 3V_{e1}I_{e1}; \quad S_I^+ = 3V_1^+I_1^+; \quad SU1 = \sqrt{S_{e1}^2 - (S_1^+)^2} \tag{7.8}$$

where V_1^+ and I_1^+ are the positive-sequence voltage and current, respectively.

The fundamental positive sequence active power P_1^+, reactive power Q_1^+, power factor PF_1^+ and load unbalance LU are expressed as:

$$P_1^+ = 3V_1^+I_1^+\cos\theta_1^+; \quad Q_1^+ = 3V_1^+I_1^+\sin\theta_1^+ \tag{7.9}$$

$$PF_1^+ = \frac{P_1^+}{S_1^+}; \quad LU = \frac{SU1}{S_1^+} \tag{7.10}$$

where θ_1^+ is the phase angle difference between fundamental positive sequence voltage and current.

2) Nonfundamental Power Components: The nonfundamental effective rms voltage V_{eH} and current I_{eH} for three-phase three-wire systems are defined as:

$$V_{eH} = \sqrt{\frac{V_{ah}^2 + V_{bh}^2 + V_{ch}^2}{3}}; \quad I_{eH} = \sqrt{\frac{I_{ah}^2 + I_{bh}^2 + I_{ch}^2}{3}} \tag{7.11}$$

The equivalent total harmonic distortion for voltage THD_{eV} and current THD_{eI} based on the effective rms fundamental and nonfundamental voltage and current are defined as:

$$THD_{eV} = \frac{V_{eH}}{V_{e1}}; \quad THD_{eI} = \frac{I_{eH}}{I_{e1}} \tag{7.12}$$

Therefore, nonfundamental power components such as effective current distortion power D_{eI}, voltage distortion power D_{eV}, harmonic apparent power S_{eH}, nonfundamental effective apparent power S_{eN}, harmonic active power P_H, effective harmonic distortion power D_{eH}, and harmonic pollution HP are expressed in the following equations:

$$D_{eI} = 3V_{e1}I_{eH}; \quad D_{eV} = 3V_{eH}I_{e1}; \quad S_{eH} = 3V_{eH}I_{eH} \tag{7.13}$$

$$S_{eN} = \sqrt{D_{eI}^2 + D_{ev}^2 + S_{eH}^2}; \quad P_H = P - P_1 \tag{7.14}$$

$$D_{eH} = \sqrt{S_{eH}^2 - P_H^2}; \quad HP = \frac{S_{eN}}{S_{e1}} \tag{7.15}$$

Note that harmonic active power P_H is obtained by subtracting the fundamental active power P_1 from the total active power $P = Pa + P_b + P_c$, which may lead to erroneous assessment of the P_H since harmonic active power is usually very small part of the total active power [30].

3) Combined Power Components: Finally, combined power components effective apparent power S_e, total active power P, nonactive power N, and power factor PF contained in the IEEE Standard 1459-2010 can be obtained as follows:

$$S_e = 3V_e I_e; \quad P = P_a + P_b + P_c \tag{7.16}$$

$$N = \sqrt{S_e^2 - P^2}; \quad PF = \frac{P}{S_e} \tag{7.17}$$

where $V_e = \sqrt{V_{e1}^2 + V_{eH}^2}$ and $I_e = \sqrt{I_{e1}^2 + I_{eH}^2}$ are the effective rms voltage and current, respectively and P_a, P_b, and P_c are the three-phase active power assessed as:

$$\begin{aligned} P_a &= \frac{1}{T}\int_0^T v_a(t) i_a(t) dt; \quad P_b = \frac{1}{T}\int_0^T v_b(t) i_b(t) dt \\ P_c &= \frac{1}{T}\int_0^T v_c(t) i_c(t) dt \end{aligned} \tag{7.18}$$

7.3 Redefined Three-Phase Power Components

In this section, the definitions of three-phase power components introduced earlier in Section 7.2 are redefined in the time-frequency domain using the time marginal property of Page TFD. The method in [25] is employed for the decomposition of the fundamental and nonfundamental components of PQ disturbance signals, and sequence components are obtained from three phase voltages and currents using the transformation in [101].

1) TM Based Fundamental Power Components: The three-phase effective fundamental

rms voltage and current based on the TM marginal property of TFD are defined as:

$$V_{e1}^{TM} = \sqrt{\frac{(V_{a1}^{TM})^2 + (V_{b1}^{TM})^2 + (V_{c1}^{TM})^2}{3}} \tag{7.19}$$

$$I_{e1}^{TM} = \sqrt{\frac{(I_{a1}^{TM})^2 + (I_{b1}^{TM})^2 + (I_{c1}^{TM})^2}{3}} \tag{7.20}$$

where V_{a1}^{TM}, V_{b1}^{TM}, V_{c1}^{TM}, and I_{a1}^{TM}, I_{b1}^{TM}, I_{c1}^{TM} are the three-phase rms voltages and currents at the fundamental frequency based on the TM property of the TFD.

Therefor, TM property based fundamental effective apparent S_{e1}^{TM}, positive sequence apparent power $(S_1^+)^{TM}$, and fundamental unbalance power SU1 can obtained as:

$$S_{e1}^{TM} = 3V_{e1}^{TM} I_{e1}^{TM}; \quad S_1^{+TM} = 3V_1^{+TM} I_1^{+TM} \tag{7.21}$$

$$SU1^{TM} = \sqrt{(S_{e1}^{TM})^2 - ((S_1^+)^{TM})^2} \tag{7.22}$$

The fundamental positive sequence active power $(P_1^+)^{TM}$, reactive power Q_1^{+TM}, power factor PF_1^{+TM}, and load unbalance LU^{TM} based on the time-marginal property of the TFD and CTFD can be expresses in the following manner:

$$P_1^{+TM} = \frac{1}{2} \cdot \frac{1}{T} \int_0^T \Re\left\{ TM_{V_1^+ I_1^+} \right\} dt \tag{7.23}$$

$$Q_1^{+TM} = \frac{1}{2} \cdot \frac{1}{T} \int_0^T \Im\left\{ TM_{V_1^+ I_1^+} \right\} dt \tag{7.24}$$

$$PF_1^{+TM} = \frac{P_1^{+TM}}{S_1^{TM}}; \quad LU1^{TM} = \frac{SUI^{TM}}{S_1^{+TM}} \tag{7.25}$$

where $TM_{V_1^+ I_1^+}$ is the TM property of the cross time-frequency distribution of the fundamental positive sequence voltage and current.

2) TM Based Nonfundamental Power Components: Based on the TM property of the TFD, the nonfundamental effective rms voltage V_{eH}^{TM} and current I_{eH}^{TM} for three-phase systems are defined as:

$$V_{eH}^{TM} = \sqrt{\frac{(V_{aH}^{TM})^2 + (V_{bH}^{TM})^2 + (V_{cH}^{TM})^2}{3}} \tag{7.26}$$

$$I_{eH}^{TM} = \sqrt{\frac{(I_{aH}^{TM})^2 + (I_{bH}^{TM})^2 + (I_{cH}^{TM})^2}{3}} \tag{7.27}$$

where V_{aH}^{TM}, V_{bH}^{TM}, V_{cH}^{TM}, and I_{aH}^{TM}, I_{bH}^{TM}, I_{cH}^{TM} are three phase nonfundamental rms voltages and currents based on the TM property of the TFD.

The TM based effective THD for voltage THD_{eV}^{TM} and current THD_{eI}^{TM} are assessed as:

$$THD_{eV}^{TM} = \frac{V_{eH}^{TM}}{V_{e1}^{TM}}; \quad THD_{eI}^{TM} = \frac{I_{eH}^{TM}}{I_{e1}^{TM}} \tag{7.28}$$

Therefore, Page TM-based effective current distortion power D_{eI}^{TM}, voltage distortion power D_{eV}^{TM}, harmonic apparent power S_{eH}^{TM}, nonfundamental effective apparent power S_{eN}^{TM}, harmonic active power P_{H}^{TM}, effective harmonic distortion power D_{eH}^{TM}, and harmonic pollution HP^{TM} can be obtained as follows:

$$D_{eI}^{TM} = 3V_{e1}^{TM} I_{eH}^{TM}; \quad D_{eV}^{TM} = 3V_{eH}^{TM} I_{e1}^{TM} \tag{7.29}$$

$$S_{eH}^{TM} = 3V_{eH}^{TM} I_{eH}^{TM} \tag{7.30}$$

$$S_{eN}^{TM} = \sqrt{(D_{eI}^{TM})^2 + (D_{eV}^{TM})^2 + (S_{eH}^{TM})^2} \tag{7.31}$$

$$P_{H}^{TM} = P_{aH}^{TM} + P_{bH}^{TM} + P_{cH}^{TM} \tag{7.32}$$

$$D_{eH}^{TM} = \sqrt{(S_{eH}^{TM})^2 - (P_{H}^{TM})^2}; \quad HP^{TM} = \frac{S_{eN}^{TM}}{S_{e1}^{TM}} \tag{7.33}$$

where harmonic active power for any phase $x = a, b, c$ can be calculated as follows:

$$P_{xH}^{TM} = \frac{1}{2T} \int_0^T \Re \left\{ TM_{V_{xH} I_{xH}} \right\} dt \tag{7.34}$$

Note that TM based harmonic active power P_{H}^{TM} is assessed directly from the TM of the cross TFD of the harmonic voltage and current in order to obtain more accurate result.

3) TM Based Combined Power Components: Finally, combined power components effective apparent power S_{e}^{TM}, total active power P^{TM}, nonactive power N^{TM}, and power factor PF^{TM} based on the TM property are redefined for the PQ disturbance events as:

$$S_{e}^{TM} = 3V_{e}^{TM} I_{e}^{TM}; \quad P^{TM} = P_{a}^{TM} + P_{b}^{TM} + P_{c}^{TM} \tag{7.35}$$

$$N^{TM} = \sqrt{(S_{e}^{TM})^2 - (P^{TM})^2}; \quad PF^{TM} = \frac{P^{TM}}{S_{e}^{TM}} \tag{7.36}$$

where

$$V_{e}^{TM} = \sqrt{(V_{e1}^{TM})^2 + (V_{eH}^{TM})^2}; \quad I_{e}^{TM} = \sqrt{(I_{e1}^{TM})^2 + (I_{eH}^{TM})^2} \tag{7.37}$$

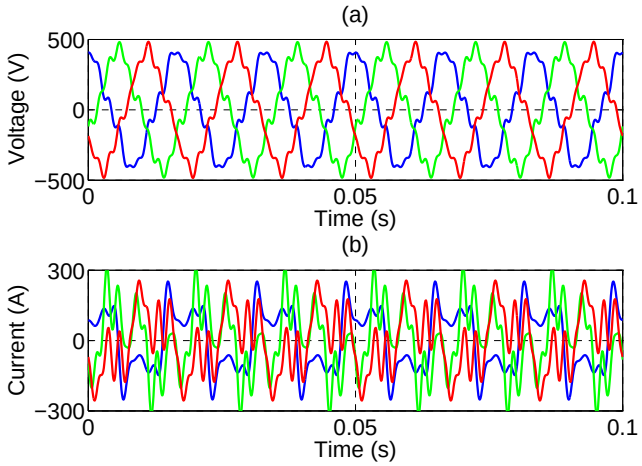

Figure 7.1: A steady state, nonsinusoidal and unbalanced PQ (a) Voltage, and (b) Current disturbance waveforms

7.4 PQ Disturbance Case Study Analysis

In this section, we will analyze two numerical PQ disturbance events in order to justify the efficacy of CW, RID, and Page TFDs in defining three-phase power components. The sampling frequency of the PQ disturbance events is 10 kHz.

Three-Phase Stationary PQ Disturbance:

Fig. 7.1 represents three-phase non-sinusoidal and unbalanced voltage and current PQ disturbances which are composed of 60 Hz, 3rd, 5th, 7th, and 9th harmonic components. In current PQ disturbance signal, high values of harmonic components are considered intentionally in order to justify the efficacy of CW, RID, and Page TFDs in minimizing cross-terms, and cross-power under highly nonlinear situations.

Three-phase power components obtained via various TFDs for the PQ disturbance event are summarized in Table 7.1. Table 7.1 justifies that the results acquired through various TFDs are close to actual values.

In order to compare the accuracy of the TFDs, the percentage errors associated with them in computing combined power components are summarized in the bar plot as shown Fig. 7.2. Bar plot in Fig. 7.2 confirms that Page result in very smaller percentage errors

Table 7.1: Three-Phase Power Components in pu Obtained via various TFDs for Stationary PQ Disturbance case study ($S_{base} = 100$ kVA, $V_{base} = 380$ V)

Components	Analysis Methods			
Combined	Actual Value	CW	RID	Page
	$S_e = 4.2149$	4.2168	4.2167	4.2139
	$P = 2.9062$	2.8673	2.8673	2.8657
	$N = 3.0528$	3.0919	3.0919	3.0894
	$PF = 0.6895$	0.6800	0.6800	0.6801
Fund.	$S_{e1} = 2.9375$	2.9399	2.9398	2.9374
	$S_1^+ = 2.8866$	2.8918	2.8917	2.8894
	$SU1 = 0.5447$	0.5298	0.5298	0.5292
	$P_1^+ = 2.8611$	2.8663	2.8662	2.8639
	$Q_1^+ = 0.3828$	0.3831	0.3831	0.3828
	$PF_I^+ = 0.9912$	0.9912	0.9912	0.9912
	$LU = 0.1887$	0.1832	0.1832	0.1831
Nonfund.	$S_{eN} = 3.0227$	3.0230	3.0230	3.0213
	$S_{eH} = 0.4701$	0.4698	0.4698	0.4697
	$P_H = 0.0413$	0.0412	0.0412	0.0412
	$D_{eI} = 2.9490$	2.9493	2.9493	2.9476
	$D_{eV} = 0.4682$	0.4683	0.4683	0.4681
	$D_{eH} = 0.4683$	0.4680	0.4680	0.4679
	$HP = 1.0290$	1.0283	1.0283	1.0285
Time	t_c (s)	268.353478	289.335297	35.3866

than the CW and RID TFDs. Also, computational time t_c associated with Page TFD is 35.3866 s which is much smaller than the CW and RID TFDs.

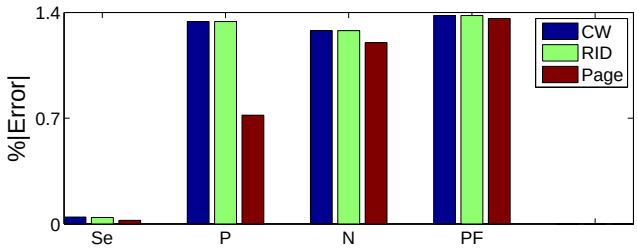

Figure 7.2: Percentage errors associated with various TFDs for three-phase stationary PQ disturbance case study

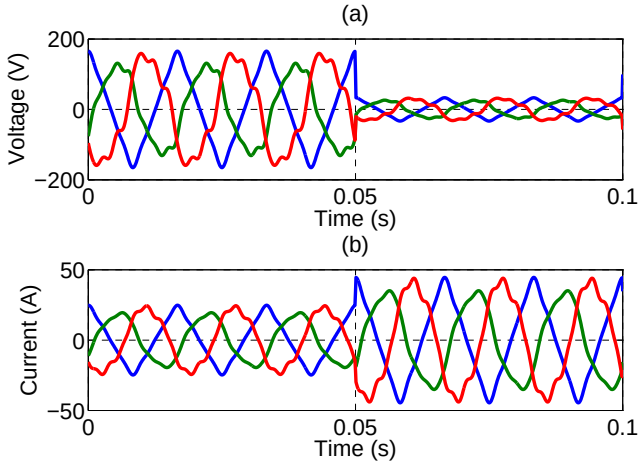

Figure 7.3: Three-phase nonstationary PQ disturbance-(a) Voltage sag, and corresponding (b) Current disturbance waveforms

Three-Phase Nonstationary PQ Disturbance:

In order to justify the efficacy of various TFDs under nonstationary PQ disturbance events, three-phase voltage sag and corresponding current disturbances shown in Fig. 7.3 are considered. In this case study, the voltage and current signals are consist of 60 Hz, 3rd, 5th, and 7th harmonic components.

The results of the voltage sag case study are summarized in Table 7.2. Table 7.2 shows that all the TFDs provide very accurate results, however, Page TFD provides more accurate results in the assessment of most of the power components. To illustrate further, the percentage errors associate with various TFDs in computing combined power components are shown in Fig. 7.4. Bar plot in Fig. 7.4 justifies that in computing combined power components such as S_e, P, and N the percentage errors associated with Page TFD are much

Table 7.2: Three-Phase Power Components in pu Obtained via various TFDs for nonstationary PQ disturbance case study ($S_{base} = 100$ kVA, $V_{base} = 380$ V)

Components	Analysis Methods			
Combined	Actual Value	CW	RID	Page
	$S_e = 4.8302$	4.8270	4.8270	4.8294
	$P = 3.1043$	3.0782	3.0783	3.0818
	$N = 3.7005$	3.7181	3.7180	3.7182
	$PF = 0.6427$	0.6377	0.6377	0.6381
Fund.	$S_{e1} = 4.7563$	4.7530	4.7531	4.7554
	$S_1^+ = 4.7129$	4.7210	4.7210	4.7221
	$SU1 = 0.59289$	0.55103	0.55146	0.56191
	$P_1^+ = 3.0558$	3.0620	3.0629	3.0646
	$Q_1^+ = 3.5962$	3.5934	3.5930	3.5926
	$PF_I^+ = 0.6475$	0.6486	0.6487	0.6490
	$LU = 0.1256$	0.1185	0.1168	0.1190
Nonfund.	$S_{eN} = 0.84172$	0.84161	0.84162	0.84189
	$S_{eH} = 0.071508$	0.071530	0.071532	0.071544
	$P_H = 0.027490$	0.027633	0.027634	0.027647
	$D_{eI} = 0.51203$	0.51186	0.51187	0.51205
	$D_{eV} = 0.664424$	0.664215	0.66425	0.66443
	$D_{eH} = 0.066012$	0.065977	0.065980	0.065987
	$HP = 0.1770$	0.1771	0.1771	0.1770
Time	t_c (s)	257.2129	279.1455715	33.637336

smaller than the CW and RID TFDs. Also, computational speed in Page TFD is faster than the CW and RID TFDs. Therefore, Page TFD can be employed in defining three-phase power components under both steady state and nonstationary PQ disturbance events which minimizes cross-terms, and cross-power efficiently, provides very accurate results and faster computational speed.

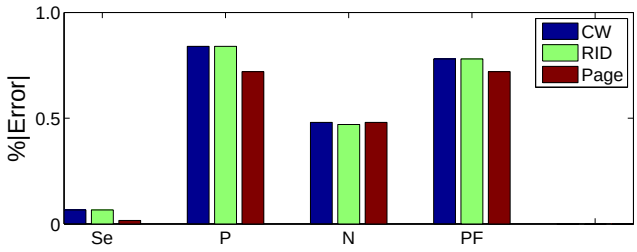

Figure 7.4: Percentage errors associated with various TFDs for three-phase voltage sag case study

Utilizing the proposed method, one can also estimate the three-phase power components for other types of nonstationary PQ disturbance events, such as voltage swell, transients, etc. However, the method will have the limitation as there is no TFD method that can minimize the cross-terms in TFD, and cross-power in cross TFD completely. Therefore, the efficacy of other bilinear TFD methods, such as Born-Jordan, Rihaczek, Zhao-Altas-Mark, that can minimize the cross-terms [16] and cross-power as well, can be investigated in computing three-phase components according to the IEEE Standard 1459-2010.

7.5 Conclusion

In this chapter, three-phase power components are redefined in the time-frequency domain according to the IEEE Standard 1459-2010 based on the time marginal property of Page TFD. Utilizing time-marginal property, Page TFD preserves simultaneous time and variable frequency information, and provides very accurate assessment of three-phase power components under PQ disturbance events. The efficacy of the proposed method has been justified by employing it to stationary and nonstationary PQ disturbances.

Also, the accuracy of the proposed Page TFD based power components assessment method has been compared to CW and RID TFDs for the PQ disturbances. The three-phase power components for stationary and nonstationary PQ disturbances confirm that the proposed Page TFD-based method provides more accurate results, and faster computational speed than the CW and RID methods. Therefore, the proposed page TFD based method

can be a viable alternative for the assessment of three-phase power components according to the IEEE Standard 1459-2010.

CHAPTER 8

A NEW PERSPECTIVE FOR WIND POWER GRID CODES UNDER POWER QUALITY DISTURBANCES

8.1 INTRODUCTION

With increased penetration of wind energy, Federal Energy Regulatory Commission (FERC) in the US sets forth requirements and grid codes specific to wind generating plants. The grid codes issued by the FERC for a wind generating plant interconnection are summarized into three main kinds as follows [77]:

1. **Low Voltage Ride Through (LVRT) Capability:** The first grid code focuses on the low voltage ride through (LVRT) capability of a wind generating plant. As seen in the LVRT curve provided in Fig. 8.1, the two key aspects of this regulation are - a wind generating plant must have the LVRT capability down to 15 % of the rated line voltage for 0.625 s, and must be able to operate continuously at 90 % of the rated line voltage, measured at the high voltage side of the wind generating plant substation transformer(s).

2. **Power Factor Design Criteria:** According to the second grid code, the power factor of a wind generating plan shall remain within the range of 0.95 leading to 0.95 lagging measured at the point of common coupling (PCC) in order to ensure electric power system reliability.

3. **Supervisory Control and Data Acquisition Capability:** To ensure system reliability, the wind generating plant should have supervisory control and data acquisition (SCADA) system to transmit data and receive instructions from the transmission provider. The LVRT capability of a wind generating plant has been heavily studied in recent years

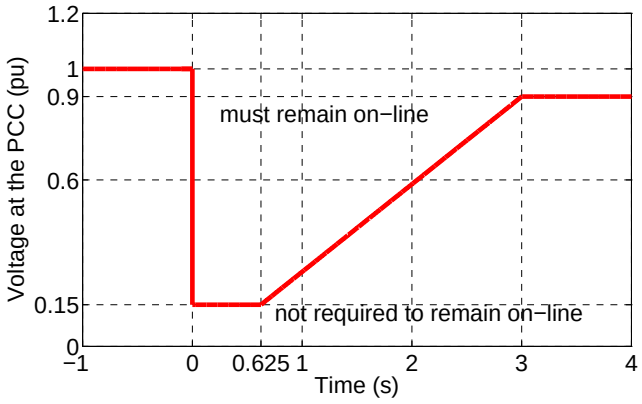

Figure 8.1: Low voltage ride through curve by FERC.

[102]-[106]. In order to enhance the LVRT capability of a wind generating plant, the rms voltage caused by a wind generating plant at the PCC should be assessed accurately. Inaccurate assessment of rms voltage may lead to unnecessary trip of the wind generating plant from the grid. Also, to ensure electric power system reliability and fulfill the grid codes, power factor and supervisory data acquisition of a wind generating plant should be obtained precisely. FFT-based method is commonly used to assess rms voltage, power factor and provide useful information for SCADA system such as real power, reactive power, apparent power, total harmonic distortion (THD) of a wind generating plant.

The FFT requires the signal to be periodic in nature, and only provides accurate assessment in steady state [25]. However, a wind generating plant may introduce low voltage at the PCC caused by uneven power production or a power system fault. Also, transient voltage disturbances are introduced by wind generating plants when they are connected to or disconnected from the grid [80], [107]-[108] and by events as capacitors switching [109]. Furthermore, harmonics are injected into the grid by variable speed wind generating plants due to the switching of power electronic converters. Therefore, from the electrical grid perspective, wind generating plants are perceived as fluctuating power sources, and can be best described as transient, nonsinusoidal and unbalance in nature [110]-[113]. Under such conditions, the signal becomes aperiodic, and the frequency contents of the signal change

with time as well. Hence, the FFT-based method provides erroneous results in the presence of wind generating plant disturbance events [25], and also it cannot provide any time information which may be a challenge for transmission providers to verify wind power grid codes and protect power system reliability.

With regards to the aforementioned issues, time-frequency analysis (TFA) can play a significant to conform wind power grid codes requirement since it has the ability to provide simultaneous time and variable frequency information of wind generating plant disturbance events. The application of the TFA in wind power has been demonstrated in several works [23]-[24], [114]. However, assessments of rms voltage, power factor, and data acquisition for supervisory control system under transient, nonsinusoidal and unbalanced conditions have not been addressed in these works. Also, in [23]-[24], TFD-based THD is employed for grid PQ analysis of wind power. The method defines the THD based on the energy ratio of the fundamental and harmonic components instead of the rms values, nonetheless, [23]-[24] provide inaccurate assessments of wind PQ.

In this chapter, a new method is proposed for the verification of wind power grid codes based on TFA. Unlike the FFT, the method is able to assess the LVRT capability and power factor of a wind generating plant, and acquire data for SCADA system accurately under transient, nonsinusoidal, and unbalanced conditions. In addition, employing the proposed method, the instantaneous direction of active and reactive power flow in a wind generating can be determined by which transmission provider can take necessary steps to protect system reliability in case of large amount of reverse active power flow from the grid to a wind generating plant under PQ disturbance events. The effectiveness of the proposed method will be justified by applying it to real-world wind generating plant disturbance events collected from 150 MW Trent Mesa wind project in Texas.

8.2 Power Quality Indices for Wind Power Grid Codes

In this section, we will utilize a set of PQ indices based on time-frequency analysis (TFA) which will be used to verify the first two wind power grid codes, and data acquisition for supervisory control system under transient, non-sinusoidal and unbalanced conditions.

1. TFA Based Effective RMS Voltage: The first grid code which provides information about LVRT capability can be verified by defining the effective rms voltage V_e under transient, nonsinusoidal and unbalanced conditions according to the IEEE Standard 1459-2010 [13] as follows:

$$V_e = \sqrt{\frac{(V_a^{TFA})^2 + (V_b^{TFA})^2 + (V_c^{TFA})^2}{3}} \tag{8.1}$$

where V_a^{TFA}, V_b^{TFA} and V_c^{TFA} are TFA based effective rms voltage of phase A, phase B, and Phase C of wind generating plant disturbance events, respectively.

2. TFA Based Effective Power Factor: The second grid code emphasizes on wind generating plant power factor requirement and can be verified by defining the effective power factor PF_e under transient, nonsinusoidal and unbalanced conditions based on the TFA method as follows:

$$PF_e = \frac{P}{S_e} = \frac{P}{3 \cdot V_e \cdot I_e} \tag{8.2}$$

where

$$I_e = \sqrt{\frac{(I_a^{TFA})^2 + (I_b^{TFA})^2 + (I_c^{TFA})^2}{3}} \tag{8.3}$$

$$P = P_a^{TFA} + P_b^{TFA} + P_c^{TFA} \tag{8.4}$$

where I_e and P are the effective rms current and total active power of the wind generating plant, respectively.

3. TFA Based Data Acquisition for SCADA System: SCADA system of a wind generating plant is used to provide long-term databases on the farm level so that service engineers can use a central application in the control desk to access and monitor the complete range of up-to-the-minute data from all connected wind turbine generator units to

carry out any kind of comparative analysis. For the instantaneous analysis and monitoring purpose of a wind generating plant data, in this chapter we will obtain voltage and current THDs, active power, apparent power, reactive power and harmonic pollution information for the SCADA system employing the TFA method.

Equivalent Total Harmonic Distortion

THD is the commonly used power quality factor to quantify harmonics injection into grid by a variable speed wind generating plant. The equivalent voltage THD_{eV} and current THD_{eI} for a variable speed wind generating plant can be assessed as:

$$THD_{eV} = \frac{V_{eH}^{TFA}}{V_{e1}^{TFA}} \tag{8.5}$$

$$THD_{eI} = \frac{I_{eH}^{TFA}}{I_{e1}^{TFA}} \tag{8.6}$$

where V_{e1}, V_{eH} and I_{e1}, I_{eH} are TFA based effective fundamental and harmonics rms voltage and current, respectively. Harmonics and fundamental frequency components are separated employing the method in [25].

Active Power

The positive sequence active power P_1^+, harmonic active power P_H, and the total active power P of a wind generating plant are obtained as:

$$P_1^+ = \frac{1}{2T}\int_{t-T}^{t} \Re\left\{ \int_{\omega} CTFD_{v_1^+ i_1^+}(t,\omega;\phi)d\omega \right\} dt \tag{8.7}$$

$$P_H = \frac{1}{2T}\int_{t-T}^{t} \Re\left\{ \int_{\omega} CTFD_{v_H i_H}(t,\omega;\phi)d\omega \right\} dt \tag{8.8}$$

$$P = P_a + P_b + P_c \tag{8.9}$$

where $CTFD_{v_1^+ i_1^+}(t,\omega;\phi)$ and $CTFD_{v_H i_H}(t,\omega;\phi)$ are the cross time-frequency distributions of the positive sequence and harmonic voltage and current, respectively, and P_a, P_b, and P_c

are three-phase power obtained via cross time-frequency distributions of respective voltage and current, respectively.

Apparent Power

The TFA based effective harmonic apparent power S_{eH}, non-fundamental apparent power S_{eN} and total apparent power S_e [13] for a wind generating plant are defined as:

$$S_{eH} = S_{e1}^{TFA} \cdot THD_{eV} \cdot THD_{eI} \tag{8.10}$$

$$S_{eN} = S_{e1}^{TFA} \cdot \sqrt{THD_{eV} + THD_{eI} + THD_{eV} \cdot THD_{eI}} \tag{8.11}$$

$$S_e = \sqrt{S_{e1}^2 + S_{eN}^2} \tag{8.12}$$

Reactive Power

The most suggested reactive power expression is the fundamental positive sequence reactive power [13] which is defined as:

$$Q_1^+ = 3 \cdot \frac{1}{2} \cdot \frac{1}{T} \int_{t-T}^{t} \Im \left\{ \int_{\omega} CTFD_{v^+i^+}(t, \omega; \phi) d\omega \right\} dt \tag{8.13}$$

Harmonic Pollution

The harmonic pollution injected by a variable speed wind generating plant into the grid can be obtained for SCADA system as:

$$HP = \frac{S_{eN}}{S_{e1}} \tag{8.14}$$

The TFA based method discussed in this section will be employed to computer simulated and real-world power quality disturbance events for wind power grid codes under transient, nonsinusoidal, and unbalanced conditions in the next section.

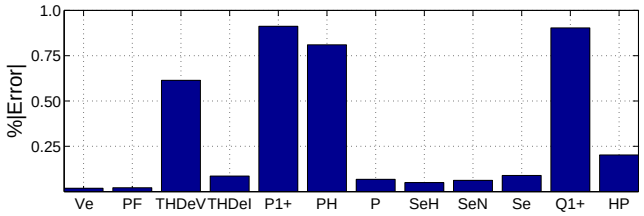

Figure 8.2: Percentage errors associated with the simulated state case study analysis.

8.3 Simulated Case Study

In order to justify the efficacy of the proposed method, the following computer simulated three-phase nonsinusoidal and unbalanced voltage signals are considered:

$$v_a(t) = 1\sqrt{2}\cos(\omega_1 t - 0.74^0) \tag{8.15}$$
$$+ 0.2\sqrt{2}\cos(\omega_3 t + 6.76^0) + 0.1\sqrt{2}\cos(\omega_5 t + 142.3^0)$$
$$v_b(t) = 1.1\sqrt{2}\cos(\omega_1 t - 121.2^0) \tag{8.16}$$
$$+ 0.15\sqrt{2}\cos(\omega_3 t + 6.28^0) + 0.05\sqrt{2}\cos(\omega_5 t + 167.4^0)$$
$$v_c(t) = 1.05\sqrt{2}\cos(\omega_1 t + 121.3^0) \tag{8.17}$$
$$+ 0.1\sqrt{2}\cos(\omega_3 t + 9.7^0) + 0.15\sqrt{2}\cos(\omega_5 t + 157.7^0)$$

The respective three-phase currents signals are as follows:

$$i_a(t) = 1\sqrt{2}\cos(\omega_1 t - 22^0) \tag{8.18}$$
$$+ 0.25\sqrt{2}\cos(\omega_3 t + 120^0) + 0.2\sqrt{2}\cos(\omega_5 t - 175^0)$$
$$i_b(t) = 0.95\sqrt{2}\cos(\omega_1 t - 120.8^0) \tag{8.19}$$
$$+ 0.15\sqrt{2}\cos(\omega_3 t + 99.49^0) + 0.1\sqrt{2}\cos(\omega_5 t + 65.09^0)$$
$$i_c(t) = 0.9\sqrt{2}\cos(\omega_1 t + 120.3^0) \tag{8.20}$$
$$+ 0.01\sqrt{2}\cos(\omega_3 t + 100.01^0) + 0.05\sqrt{2}\cos(\omega_5 t + 57.7^0)$$

As seen in the Eqs. (8.15)-(8.20), the voltage and currents signals are unbalanced and composed of fundamental, 3rd and 5th harmonic components. The percentage errors associated

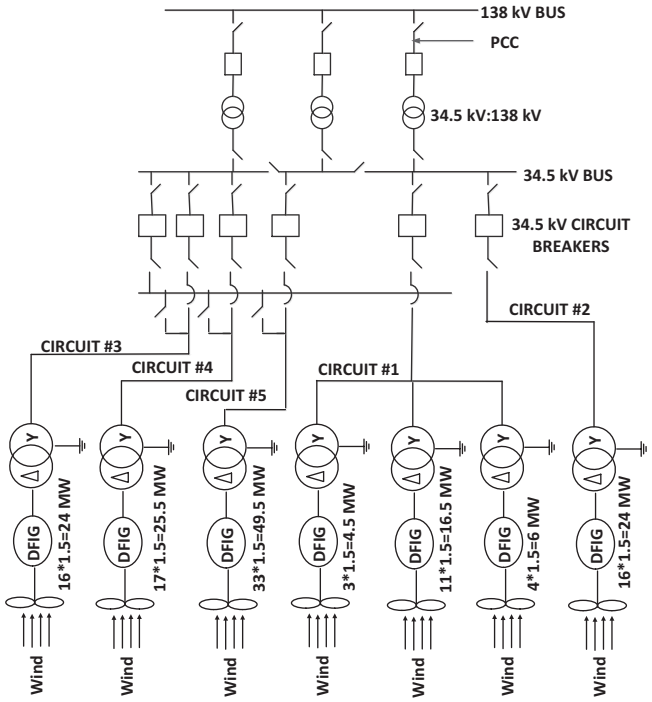

Figure 8.3: Simplified one-line diagram of Trent Mesa wind project.

with the Page TFD-based method for the simulated case study are summarized in Fig. 8.2. We utilize the Page TFD as it provides more accurate results, and faster computational speed than the RID and CW TFDs as discussed in the previous chapter. Fig. 8.2 shows that Page TFD-based method results in very small percentage errors (less than 1%), therefore, the proposed method can be employed for wind power grid codes which we will discuss in the next section.

8.4 Studied Wind Generating Plant

The Real-world wind generating plant PQ disturbance events were recorded from Trent Mesa wind project in Texas, and provided by the courtesy of National Renewable Energy Laboratory (NREL). The one-line diagram of the Trent Mesa wind generating plant is provided in Fig. 8.3. The wind generating plant consists of 100 General Electric (GE) 1.5 MW wind turbine generators for a total capacity of 150 MW. The disturbance events are measured from the high voltage side of the substation transformer at the point of common

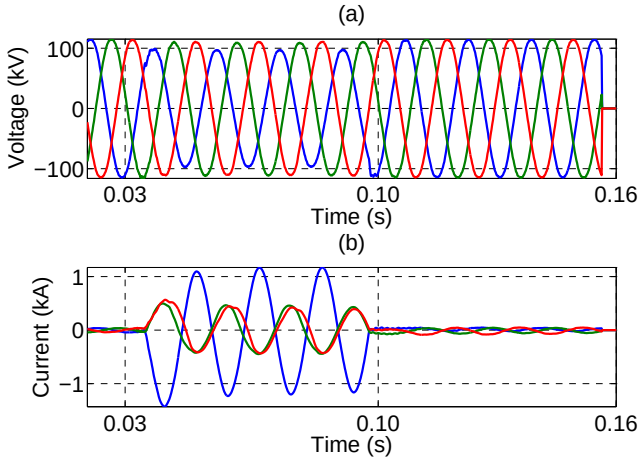

Figure 8.4: (a) Voltage sag, and (b) Current disturbance waveforms.

coupling (PCC) as seen in the figure, and the sampling frequency of the disturbance waveforms is 7678.99 Hz. We will analyze three different disturbance events to demonstrate the efficacy of the proposed TFA based method for wind power grid codes - a voltage sag, a transient and an oscillatory type disturbances.

Voltage Sag Case Study

Figs. 8.4 (a) and (b) show voltage sag, and corresponding current disturbance waveforms, respectively. The following observations are summarized based on the TFA based analysis of the voltage sag case study provided in Fig. 8.5.

Fig. $8.5(a_1)$ shows the effective rms voltage at the PCC stays above 0.9 pu both in steady state and sag conditions, and meets the first grid code requirement by the FERC.

As seen in Fig. $8.5(a_2)$, the power factor is lagging in steady state and leading during the voltage sag. In both conditions, power factor of the wind generating plant is below 0.95 leading to 0.95 lagging, and does not conform the second grid code requirement issued by the FERC.

Figs. $8.5(a_3)$ and (a_4) illustrate that voltage THD increases and current THD decreases during the voltage sag because of the decrease in the fundamental voltage and increase in

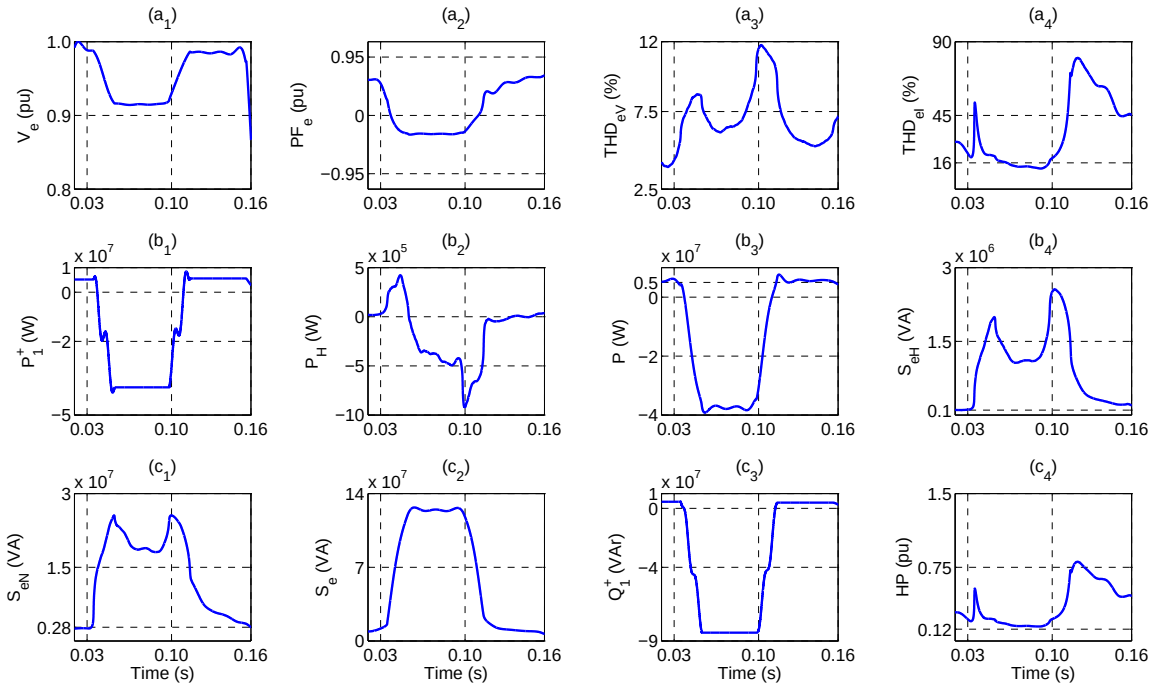

Figure 8.5: Results of voltage sag case study analysis - Effective (a_1) rms voltage, (a_2) power Factor, (a_3) Voltage THD, (a_4) Current THD, (b_1) Positive sequence active power, (b_2) Harmonic active power, (b_3) Total active power, (b_4) Harmonic apparent power, (c_1) Non-fundametnal apparent power, (c_2) Total apparent power, (c_3) Positive sequence reactive power, and (c_4) Harmonic pollution factor.

the fundamental current, respectively. In addition, the voltage THD is above 2.5% limit recommended by the IEEE Standard 519 [10] for 138 kV system.

The positive sequence active power P_1^+, harmonic active power P_H, and total active power P flow from the grid to the wind farm during voltage sag as observed in Figs. 8.5(b_1)-(b_3), respectively. Also, in the steady state the wind generating plant delivers approximately 5 MW power only whereas 40 MW power flows from grid to the wind farm during the voltage sag. This reverse power flow may increase the rotor speed, and result in mechanical damage of wind generating units in the plant. Under such condition, disconnection of a wind generating plant may be required by the transmission provider in order to protect system reliability even though the wind generating plant satisfies the LVRT capability shown in Fig. 8.5(a_1).

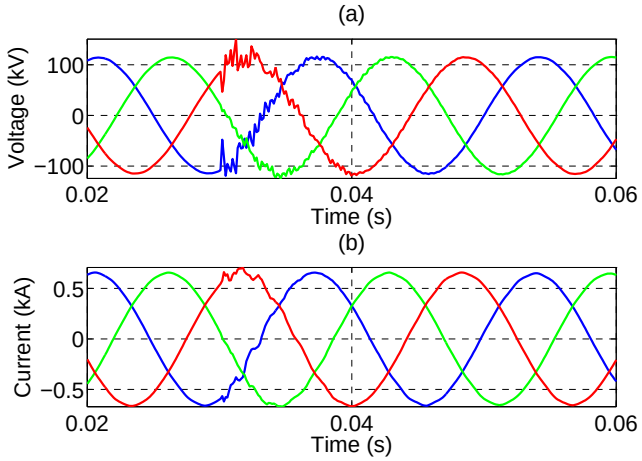

Figure 8.6: Transient (a) Voltage, and (b) Current disturbance waveforms.

The effective harmonic apparent power S_{eH}, non-fundamental apparent power S_{eN} and total apparent S_e of the wind generating plant are summarized in Figs. 8.5(b_4), (c_1) and (c_2), respectively. The total apparent power of the wind generating plant is increased to approximately 140 MVA by the voltage sag disturbance as seen in Fig. 8.5(c_2).

The positive sequence reactive power of the wind generating plant is positive in the steady state, however, is negative and flows from grid to the wind generating plant during the sag as seen in Fig. 8.5(c_3).

Fig. 8.5$(c_{4)}$ shows that harmonic pollution injected by the Trent Mesa wind generating plant into 138 kV grid is above 0.12 pu.

Transient Case Study

The transient voltage and current disturbances for the study of wind power grid codes are incorporated in Figs. 8.6 (a) and (b), respectively. The results of the transient disturbance case study are provided in Fig. 8.7, and summarized in the following contexts.

Fig. 8.7(a_1) shows that transient disturbance causes overvoltage at the PCC, however, the effective rms voltage V_e is above 0.9 pu both in normal and transient operating conditions, and meets the first grid code requirement.

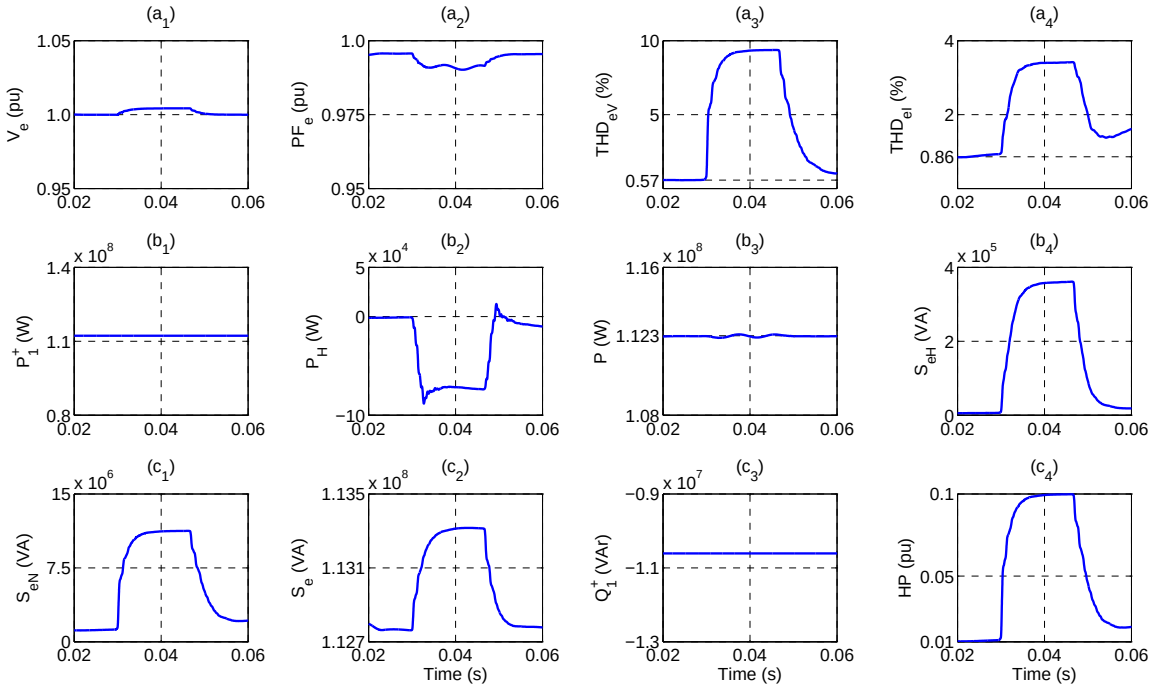

Figure 8.7: Results of trasient case study analysis - Effective (a_1) rms voltage, (a_2) power Factor, (a_3) Voltage THD, (a_4) Current THD, (b_1) Positive sequence active power, (b_2) Harmonic active power, (b_3) Total active power, (b_4) Harmonic apparent power, (c_1) Non-fundametnal apparent power, (c_2) Total apparent power, (c_3) Positive sequence reactive power, and (c_4) Harmonic pollution factor.

The effective power factor PF_e in Fig. 8.7(a_2) is lagging and above 0.95 pu, hence, reliability of the wind farm is not compromised by the transient disturbance according to the second grid code.

Fig. 8.7(a_3) and (a_4) show that the voltage THD at the PCC is below 2.5% in steady state, however, transient disturbance causes the voltage and current THDs increase to approximately 10% and 4%, respectively because of the presence of high harmonic components in the transient voltage and current disturbances.

Unlike the voltage sag, in case of the transient case study, both the positive sequence active power P_1^+ and total active power P flow from wind farm to the grid, only the harmonic active power P_H flows in the opposite direction as observed in Fig. 8.7(b_1)-(b_3). Also, the wind generating plant delivers almost 112.3 MW power into the grid out of rated

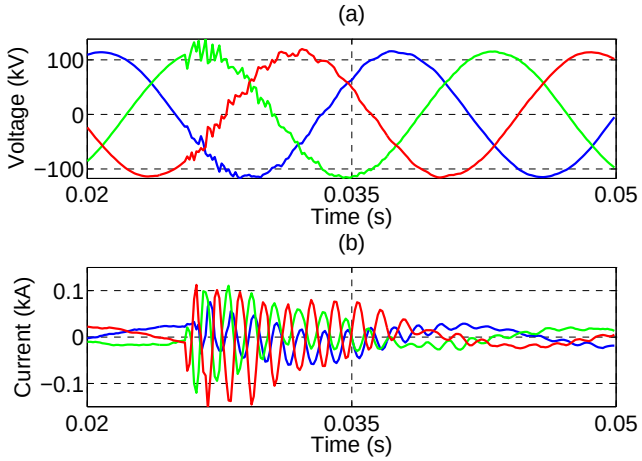

Figure 8.8: Oscillatory (a) Voltage, and (b) Current disturbance waveforms.

150 MW power.

Figs. 8.7(b_4)-(c_2) illustrates that the apparent power of the wind generating plant are increased by the transient disturbance. The positive sequence reactive power of the wind generating plant is negative and flows from grid to the wind generating plant as seen in Fig. 8.7(c_3). Fig. 8.7(c_4) shows that the transient disturbance increases the harmonic pollution injection into the grid to 0.1 pu approximately.

Oscillatory Case Study

A wind generating plant typically consists of vast underground cables, reactive compensation equipment, transformers, wind turbine generators with internal power factor correction capacitors. The energy exchange between inductive and capacitive elements of a wind generating plant may lead to harmonic resonance and introduce oscillatory type disturbance into the grid. Figs. 8.8(a)-(b) represent oscillatory type voltage and current disturbance waveforms recorded from the Trent Mesa wind project. The corresponding TFA based analysis results are summarized in Fig. 8.9, and the following perceptions are made based on the case study analysis.

In the oscillatory case study, the effective rms voltage in Fig. 8.9(a_1) is above 0.9

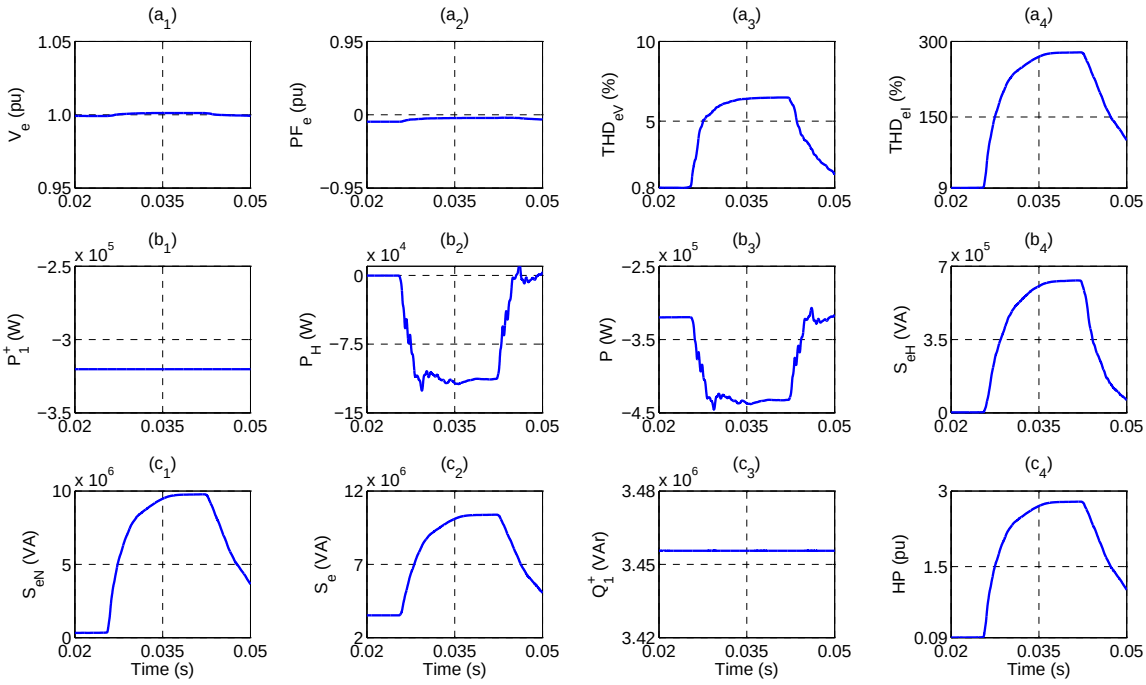

Figure 8.9: Results of oscillatory case study analysis - Effective (a_1) rms voltage, (a_2) power Factor, (a_3) Voltage THD, (a_4) Current THD, (b_1) Positive sequence active power, (b_2) Harmonic active power, (b_3) Total active power, (b_4) Harmonic apparent power, (c_1) Non-fundametnal apparent power, (c_2) Total apparent power, (c_3) Positive sequence reactive power, and (c_4) Harmonic pollution factor.

pu, and the wind generating plant fulfills the first grid code requirement, however, the effective power factor is leading and close to zero, and fails to meet the required power factor criteria according to the second grid code as observed in Fig. 8.9(a_2). Also, in Figs. 8.9(a_3)-(a_4), the effective voltage THD is low compared to very high value of current THD (approximately 300%) during the oscillation. This is an indication of series resonance, where very high value of harmonic current is observed, in the wind generating plant.

All the positive sequence active power P_1^+, harmonic active power P_H and total active power P flow from the grid to the wind generating plant as seen in Figs. 8.9(b_1)-(b_3), respectively. The apparent power information for the SCADA system are incorporated in Figs. 8.9(b_4)-(c_2). As we can see in Figs. 8.9(b_4)-(c_1), the oscillatory disturbance increases the harmonic and non-fundamental apparent power from 0 to 0.7 MVA and 10

Table 8.1: Summary of Case Study Analysis Results

Case Study Analysis				
SCADA DATA	Indices	Volt. sag	Tran.	Osc.
RMS Volt. (pu)	V_e	0.9556	1.002	1.0002
Power Factor (pu)	PF_e	0.1136	0.9937	-0.0576
THD%	THE_{eV}	6.990	4.567	4.234
	THD_{eI}	35.18	2.010	174.7
Active Power (MW)	P_1^+	-12.96	112.23	-0.3203
	P_H	-0.1590	-0.0319	-0.0622
	P	-12.34	112.27	-0.3816
Apparent Power (MVA)	S_{eH}	0.9755	0.1469	0.3353
	S_{eN}	13.51	5.731	6.136
	S_e	62.79	112.98	7.462
Reactive Power (MVAr)	Q_1^+	-33.34	-10.61	3.456
Harmonic Pollution (pu)	HP	0.3634	0.0508	1.751
Grid Codes	I^{st}	yes	yes	yes
	2^{nd}	no	yes	no

MVA, respectively.

Fig. 8.9(c_3) represents the positive sequence reactive power is constant, and flows from the wind generating plant to the grid. Also, the oscillatory disturbance causes the harmonic pollution to increase to a relatively high value of 3 pu approximately compared to the previous two case studies.

The TFA based method provides instantaneous assessment of the effective rms voltage, power factor and supervisory data for a wind generating plant. However, in order to provide more informative and convenient comparison of the three case studies analysis, TFA based PQ (TFAPQ) indices for wind power grid codes are quantified as a single value which is defined as follows:

$$\overline{TFAPQ} = \frac{1}{T}\int_0^T TFAPQ(t)dt \tag{8.21}$$

The results of the three wind generating plant PQ disturbance events are provided in Table 8.1. As seen in the table, the effective rms voltage is above 0.9 pu in all three PQ disturbances, therefore, the wind generating plant meets the first grid code requirement. However, the plant maintains the required power factor criteria in case of the transient disturbance only which is 0.9937 pu lagging. Also, in the transient disturbance, voltage and current THDs are lower at the PCC, the wind generating plant delivers more power, and harmonic pollution injected by the wind generating plant into the grid is much lower than the voltage sag and oscillatory disturbances. Therefore, from PQ point of view, the wind generating plant will have less impact on the electrical grid for the transient disturbance.

8.5 Conclusion

In this chapter, a new time-frequency analysis method is proposed for wind power grid codes under transient, nonsinusoidal and unbalanced PQ disturbance events. The efficacy of the proposed method has been justified by employing it to a computer simulated and real-world wind generating plant PQ disturbances. Unlike the traditional FFT-based method, the proposed technique extracts time information, and provides instantaneous and accurate assessment of effective rms voltage, power factor to verify wind power grid codes under transient, nonsinusoidal, and unbalanced conditions. Also, employing the proposed method, dynamic signature of the wind generating plant PQ disturbance events can be extracted for SCADA system to protect system reliability. For example, in the voltage sag case study, where large amount of reverse active power flows into the plant, disconnection of the wind generating plant may be required to ensure system reliability. In addition, based on the SCADA information provided in this chapter, one can develop a supervisory control system for a wind generating plant to fulfill the grid codes requirements which will be discussed in the scope of future work.

CHAPTER 9

CONCLUSION

This dissertation has the following novel and significant contributions in the area of power quality (PQ) and time-frequency distribution (TFD) which are summarized as follows:

- Although, TFDs have been frequently utilized for the detection, classification, and assessment of PQ disturbances, there is no work devoted to defining rms value, average active power, and reactive power correctly employing TFDs. In this dissertation, rms value, active power and reactive power are defined in the time-frequency domain correctly by introducing the scale factors which will play a significant role for correct assessment of PQ disturbances.

- Also, the existing transient PQ indices are redefined correctly for PQ disturbances which provide much more accurate results than the FFT-based method for nonstationary PQ disturbances.

- Another novel contribution of this dissertation is redefining the single-phase and three-phase power components according to the IEEE Standard 1459-2010 under transient, sinusoidal, nonsinusoidal, balanced, or unbalanced conditions employing TFD method. Utilizing the proposed method, one can find the direction of harmonic active power flow to the network or to the load with time. Also, harmonic active power is assessed directly utilizing time marginal property of the XTFD which provides very precise result.

- Utilizing the concept of TFD-based redefined three-phase power components, a new perspective for wind power grid codes is proposed that is able to accomplish in-

stantaneous verification of wind power grid codes, issued by the FERC, under PQ disturbances.

The TFD-based PQ analysis method provided in this dissertation can play a significant role in the following future works:

- The redefined PQ indices provided in this dissertation can be employed to detect and classify PQ disturbances as the PQ indices extract dynamic signature of PQ disturbances.

- In this dissertation, the existing PQ index instantaneous frequency is utilized to estimate the fundamental frequency deviation of fixed speed wind energy conversion systems. The instantaneous frequency can also be employed to variable speed wind energy conversion systems to assess fundamental frequency deviation once fundamental frequency component is separated from the harmonic components.

- In [75], WV TFD method is employed for direction finding of capacitor switching in electric power systems which may lead to erroneous results due to the presence of cross-power as discussed in this dissertation. For more accurate assessment, RID, CW, and Page TFDs can be employed for direction finding of capacitor switching.

- In this dissertation, frequency components responsible for transient disturbances are identified. Therefore, the impact of transient disturbances on electric power systems can be minimized by designing and employing appropriate filter to remove the transient frequency components.

- Also, time-varying active power and reactive power information are provided utilizing the XTFD which can be employed to design super capacitor energy storage system, and reactive power compensator, respectively to enhance the PQ in electric power systems.

BIBLIOGRAPHY

[1] S. M. Peeran, and C. W. P. Cascadden, "Application, Design, and Specification of Harmonic Filters for Variable Frequency Drives," *IEEE Transactions on Industry Applications*, vol. 31, no. 4, pp.841-847, July/August 1995.

[2] P. W. Hammond, "A New Approach to Enhance Power Quality for Medium Voltage AC Drives," *IEEE Transactions on Industry Applications*, vol. 33, no. 1, pp. 202-208, January/February 1997.

[3] Y. Liu, G. T. Heydt, and R. F. Chu, "The Power Quality Impact of Cycloconverter Control Strategies," *IEEE Transactions on Power Delivery*, vol. 20, no. 2, pp. 1711-1718, April 2005.

[4] J. Mazumdar, R. G. Harley, and F. C. Lambert, and G. K. Venayagamoorthy, "Neural Network Based Method for Predicting Nonlinear Load Harmonics," *IEEE Transactions on Power Electronics*, vol. 22, no. 3, pp.1036-1045, May 2007.

[5] B. M. Dehkordi, M. Moallem, and A. Parsapour, "Predicting Foaming Slag Quality in Electric Arc Furnace Using Power Quality Indices and Fuzzy Method," *IEEE Transactions on Instrumentation and Measurement*, vol. 60, no. 12, pp. 3845-3852, December 2011.

[6] S. K. Jain, S. N. Singh, and J. G. Singh, "An Adaptive Time-Efficient Technique for Harmonic Estimation of Nonstationary Signals," *IEEE Transactions on Industrial Electronics*, vol. 60, no. 8, pp. 3295-3303, May 2012.

[7] D. Somayajula, and M. L. Crow, "An Ultracapacitor Integrated Power Conditioner for Intermittency Smoothing and Improving Power Quality of Distribution Grid," *IEEE Transactions on Sustainable Energy*, vol. 5, no. 4, pp. 1145-1155, October 2014.

[8] K. Koziy, B. Gou, and J. Aslakson, "A Low-Cost Power-Quality Meter With Series Arc-Fault Detection Capability for Smart Grid," *IEEE Transactions on Power Delivery*, vol. 28, no. 3, pp. 1584-1591, July 2013.

[9] G. T. Heydt, and W. T. Jewell, "Pitfalls of Electric Power Quality Indices," *IEEE Transactions on Power Delivery*, vol. 13, no. 2, pp. 570-578, April 1998.

[10] *IEEE Recommended Practice for power and Grounding Electronic Equipment*, 1999. IEEE Std. 1100-1999, IEEE Press.

[11] IEC61400-21, *Measurement and Assessment of Power Quality Characteristics of Grid-Connected Wind Turbines*, Ed. 1, 2008.

[12] *IEEE Trial-Use Standard Definitions for the Measurement of Electric Power Quantities Under Sinusoidal, Non-sinusoidal, Balanced, Or Unbalanced Conditions*, IEEE Standard 1459-2000, 2000.

[13] *IEEE Standard Definitions for the Measurement of Electric Power Quantities Under Sinusoidal, Non-sinusoidal, Balanced or Unbalanced Conditions*, IEEE Standard 1459-2010, March 2010.

[14] C. Gherasim, J. V. den Keybus, J. Driesen, and R. Belmans, "DSP Implementatin of Power Measurements According to the IEEE Trial-Use Standard 1459," *IEEE Transactions on Instrumentation and Measurement*, vol. 53, no. 4, pp. 1086-1092, August 2004.

[15] A. Mansour, Z. Chengning, and H. Nasry, "Measurement of Power Components in Balanced and Unbalanced Three-Phase Systems Under Nonsinusoidal Operating Conditions by Using IEEE Standard 1459Ď1d'72010 and Fourier Analysis," *2013 International Conference on Technological Advances in Electrical, Electronics and Computer Engineering (TAEECE)*, pp. 166-171, 9-11 May 2013.

[16] L. Cohen, *Time-Frequency Signal Analysis*, Prentice Hall, New York, 1995.

[17] W. G. Morsi, and M. E. El-Hawary, "Reformulating Power Components Definitions Contained in the IEEE Standard 1459-2000 Using Discrete Wavelet Transform," *IEEE Transactions on Power Delivery*, vol. 22, no. 3, pp. 1910-1916, July 2007.

[18] W. G. Morsi and M. E. El-Hawary, "Reformulating Three-Phase Power Components Definitions Contained in the IEEE Standard 1459-2000 Using Discrete Wavelet Transform," *IEEE Transactions on Power Delivery*, vol. 22, no. 3, pp. 1917-1925, July 2007.

[19] W. G. Morsi, and M. E. El-Hawary, "A New Perspective for the IEEE Standard 1459-2000 Via Stationary Wavelet Transform in the Presence of Nonstationary Power Quality Disturbance," *IEEE Transactions on Power Delivery*, vol. 23, no. 4, pp. 2356-2365, October 2008.

[20] W. G. Morsi, and M. E. El-Hawary, "Wavelet Packet Transform-Based Power Quality Indices for Balanced and Unbalanced Three Phase Systems Under Stationary and Nonstationary Operating Conditions," *IEEE Transactions on Power Systems*, vol. 24, no. 4, pp. 2300-2310, October 2009.

[21] W. G. Morsi, C. P. Diduch, L. Chang, Koziy, and M. E. El-Hawary, "Wavelet Based Reactive Power and Energy Management in the Presence of Power Quality Disturbances", *IEEE Transactions on Power Systems*, vol. 26, no. 3, pp. 1263-1271, August 2011.

[22] Y. J. Shin, E. J. Powers, W. M. Grady, and A. Arapostathis, "Power Quality Indices for Transient Disturbances," *IEEE Transactions on Power Delivery*, vol. 21, no. 1, pp. 253-261, January 2006.

[23] P. Stone, M. Islam, and Y. J. Shin, "Power Quality Impact of Wind Turbine Generators on the Electrical Grid," *Energy Tech, 2012 IEEE*, Cleaveland, Ohio, USA, pp. 1-6, May 2012.

[24] M. Islam, H. A. Mohammadpour, P. Stone, and Y. J. Shin, "Time-frequency Based Power Quality Analysis of Variable Speed Wind Turbine Generators," *Industrial Electronics Society, IECON 2013 - 39th Annual Conference of the IEEE*, vol., no., pp. 6426-6431, 10-13 November 2013.

[25] M. Islam, H. A. Mohammadpour, A. Ghaderi, C. Brice, and Y. J. Shin, "Time-frequency-Based Instantaneous Power Components for Transient Disturbances According to IEEE Standard 1459," *IEEE Transactions on Power Delivery*, vol., no. 99, pp., October 2014.

[26] H. Kim, F. Blaabjerg, and B. Bak-Jensen, "Spectral Analysis of Instantaneous Powers in Single-Phase and Three-Phase Systems with Use of p-q-r Theory," *IEEE Transactions on Power Electronics*, vol. 17, no. 5, pp. 711-720, September 2002.

[27] J. I. Leon, R. Portillo, S. Vazquez, J. J. Padilla, L. G. Franquelo, and J. M. Carrasco, "Simple Unified Approach to Develop a Time-Domain Modulation Strategy for Single-Phase Multilevel Converters," *IEEE Transactions on Industrial Electronics*, vol. 55, no. 9, pp. 3239-3248, September 2008.

[28] W. A. Omran, H. S. K. El-Goharey, M. Kazerani, and M. M. A. Salama, "Identification and Measurement of Harmonic Pollution for Radial and Nonradial Systems," *IEEE Transactions on Power Delivery*, vol. 24, no. 3, pp. 1642-1650, July 2009.

[29] A. E. Emanuel, and D. L. Milanez, "Clarke's Alpha, Beta, and Zero Components: A Possible Approach for the Conceptual Design of Instrumentation Compatible with IEEE Std. 1459-2000," *IEEE Transactions on Instrumentation and Measurement*, vol. 55, no. 6, pp. 2088-2095, December 2006.

[30] A. Cataliotti, and V. Cosentino, "A Time-Domain Strategy for the Measurement of IEEE standard 1459-2000 Power Quantities in Nonsinusoidal Three-Phase and Single-Phase Systems," *IEEE Transactions on Power Delivery*, vol. 23, no. 4, pp. 2113-2123, October 2008.

[31] A. Cataliotti, V. Cosentino, and S. Nuccio, "A Virtual Instrument for the Measurement of IEEE Std. 1459-2000 Power Quantities," *IEEE Transactions on Instrumentation and Measurement*, vol. 57, no. 1, pp. 85-94, Janruary 2008.

[32] A. Pigazo, and V. M. Moreno, "Accurate and Computationally efficient Implementation of the IEEE 1459-2000 Standard in Three-Phase Three-Wire Power Systems," *IEEE Transactions on Power Delivery*, vol. 22, no. 2, pp. 752-757, April 2007.

[33] J. J. Tomić, and M. D. Kušljević, "An Adaptive Resonator-Based Method for Power Measurements According to the IEEE Trial-Use Standard 1459-2000," *IEEE Transactions on Intrumentation and Measurement*, vol. 59, no. 2, pp. 250-258, February 2010.

[34] L. Angrisani, P. Daponte, M. D'Apuzzo, and A. Testa, "A Measurement Method Based on the Wavelet Transform for Power Quality Analysis," *IEEE Transactions on Power Delivery*, vol.13, no.4, pp.990-998, October 1998.

[35] G. Zwe-Lee, "Wavelet-Based Neural Network for Power Disturbance Recognition and Classification," *IEEE Transactions on Power Delivery*, vol. 19, no. 4, pp. 1560Ď1d'71568, October 2004.

[36] J. G. M. S. Decanini, M. S. Tonelli-Neto, F. C. V. Malange, and C. R. Minussi, "Detection and Classification of Voltage Disturbances Using a Fuzzy-ARTMAP-Wavelet Network," *Electric Power System Research*, vol. 81, no. 12, pp. 2057Ď1d'72065, December 2011.

[37] C. H. Lin, and C. H. Wang, "Adaptive Wavelet Networks for Power-Quality Detection and Discrimination in a Power System," *IEEE Transactions on Power Delivery*, vol. 21, no. 3, pp. 1106-1113, July 2006.

[38] S. J. Huang, T. M. Yang, and J. T. Huang, "FPGA Realization of Wavelet Transform

for Detection of Electric Power System Disturbances," *IEEE Transactions on Power Delivery*, vol. 17, no. 2, pp. 388-394, April 2002.

[39] U. D. Dwivedi, and S. N. Singh, "Enhanced Detection of Power-Quality Events Using Intra and Interscale Dependencies of Wavelet Coefficients," *IEEE Transaction on Power Delivery*, vol.25, no. 1, pp. 358-366, January 2010.

[40] A. Andreotti, A. Bracale, P. Caramia, and G. Carpinelli, "Adaptive Prony Method for the Calculation of Power-Quality Indices in the Presence of Nonstationary Disturbance Waveforms," *IEEE Transactions on Power Delivery*, vol. 24, no. 2, pp. 874-883, April 2009.

[41] A. Bracale, P. Caramia, and G. Carpinelli, "Adaptive Prony Method for Waveform Distortion Detection in Power Systems," *Int. Journal of Electricl Power and Energy Systems*, vol. 29, no. 5, pp. 371-379, June 2007.

[42] H. C. Lin, "Intelligent Neural Network-Based Fast Power System Harmonic Detection," *IEEE Transactions on Industrial Electronics*, vol. 54, no. 1, pp. 43-52, February 2007.

[43] I. Y.-H. Gu, and M. H. J. Bollen, "Estimating Interharmonics by Using Sliding-Window ESPRIT," *IEEE Transactions on Power Delivery*, vol. 23, no. 1, pp. 13-23, January 2008.

[44] A. Bracale, G. Carpinelli, Z. Leonowicz, T. Lobos, and J. Rezmer, "Measurement of IEC Groups And Subgroups Using Advanced Spectrum Estimation Methods," *IEEE Transactions on Instrumentation and Measurement*, vol. 57, no. 4, pp. 672-681, April 2008.

[45] G. W. Chang, C.-I. Chen, and Q.-W. Liang, "A Two-Stage ADALINE for Harmonics and Interharmonics Measurement," *IEEE Transactions on Industrial Electronics*, vol. 56, no. 6, pp. 2220-2228, June 2009.

[46] C. I. Chen, G. W. Chang, R. C. Hong, and H. M. Li, "Extended Real Model of Kalman Filter for Time-Varying Harmonics Estimation," *IEEE Transactions on Power Delivery*, vol. 25, no. 1, pp. 17-26, January 2010.

[47] G. W. Chang, C.-I. Chen, and Y.-F. Teng, "Radial-Basis-Function-Based Neural Network for Harmonic Detection," *IEEE Transactions on Industrial Electronics*, vol. 57, no. 6, pp. 2171-2179, June 2010.

[48] N. K*ö*se, *Ö* Salor, and K. Leblebicioğlu, "Interharmonics Analysis of Power Signals with Fundamental Frequency Deviation Using Kalman Filtering," *Electric Power System Research*, vol. 80, no. 9, pp. 1145-1153, September 2010.

[49] S. K. Jain and S. N. Singh, "Exact Model Order ESPRIT Technique for Harmonics And Interharmonics Estimation," *IEEE Transactions on Instrumentation and Measurement*, vol. 61, no. 7, pp. 1915-1923, July 2012.

[50] A. Bracale, G. Carpinelli, I. Y.-H. Gu, and M. H. J. Bollen, "A New Joint Sliding-Window ESPRIT And DFT Scheme for Waveform Distortion Assessment in Power Systems," *Electric Power Systems Research*, vol. 88, pp. 112-120, July 2012.

[51] S. K. Jain, and S. N. Singh, "Fast Harmoinc Estimation of Stationary and Time-Varying Signals Using EA-AWNN", *IEEE Transactions on Instrument and Measurement*, vol. 62, no. 2, pp. 335-343, February 2013.

[52] M. V. Chilukuri, and P. K. Dash, "Multiresolution S-Transform-Based Fuzzy Recognition System for Power Quality Events," *IEEE Transactions on Power Delivery*, vol. 19, no. 1, pp. 323-330, January 2004.

[53] P. K. Dash, K. B. Panigrahi, and G. Panda, "Power Quality Analysis Using S-Transform," *IEEE Transactions on Power Delivery*, vol. 18, no. 2, pp. 406-411, April 2003.

[54] P. K. Dash, K. B. Panigrahi, D. K. Sahoo, and G. Panda, "Power Quality Disturbance Data Compression, Detection, and Classification Using Integrated Spline Wavelet and S-Transform," *IEEE Transactions on Power Delivery*, vol. 18, no. 2, pp. 595-600, April 2003.

[55] S. Mishra, C. N. Bhende, and K. B. Panigrahi, "Detection and Classification of Power Quality Disturbances Using S-Transform and Probabilistic Neural Network," *IEEE Transactions on Power Delivery*, vol. 23, no. 1, pp. 280-287, January 2008.

[56] H. Shunfan, L. Kaicheng, and M. Zhang, "A Real-Time Power Quality Disturbances Classification Using Hybrid Method Based on S-Transform and Dynamics," *IEEE Transactions on Instrumentation and Measurement*, vol. 62, no. 9, pp. 2465-2475, September 2013.

[57] P. K. Ray, S. R. Mohanty, and N. Kishor, "Classification of Power Quality Disturbances Due to Environmental Characteristics in Distributed Generation System," Sustainable Energy, IEEE Transactions on , vol.4, no.2, pp.302,313, April 2013.

[58] C. Y. Lee, and Y. X. Shen, "Optimal Feature Selection for Power-Quality Disturbances Classification," *IEEE Transactions on Power Delivery*, vol. 26, no. 4, pp. 2342-2351, October 2011.

[59] P. S. Wright, "Short-time Fourier Transforms and Wigner-Ville Distributions Applied to the Calibration of Power Frequency Harmonic Analyzers," *IEEE Transactions on Instrumentation and Measurement*, vol. 48, no. 2, pp. 475-478, April 1999.

[60] G. T. Heydt, P. S. Fjeld, C. C. Liu, D. Pierce, L. Tu, and G. Hensley, "Applications of the Windowed FFT to Electric Power Quality Assessment," *IEEE Transactions on Power Delivery*, vol. 14, no. 4, pp. 1411-1416, October 1999.

[61] S. H. Iaramillo, G. T. Heydt, and E. O. Neill Carrello, "Power Quality Indices for Aperiodic Voltages and Currents," *IEEE Transactions Power Delivery*, vol. 15, no. 2, pp. 784-790, April 2000.

[62] S. Santoso, W. M. Grady, E. J. Powers, J. Lamoree, and S. C. Bhatt, "Characterization of Distribution Power Quality Events with Fourier and Wavelet Transforms," *IEEE Transactions on Power Delivery*, vol. 15, no. 1, pp. 247-254, January 2000.

[63] Y. H. Gu, and M. H. J. Bollen, "Time-Frequency and Time-Scale Domain Analysis of Voltage Disturbances," *IEEE Transactions on Power Delivery*, vol. 15, no. 4, pp. 1279-1284, October 2000.

[64] A. Abdullah, AR.; Sha'ameri, AZ.; Sidek, AR.M.; Shaari, M.R., "Detection and Classification of Power Quality Disturbances Using Time-Frequency Analysis Technique," *5th Student Conference on Research and Development, 2007*, vol., no., pp. 1-6, 12-11 December 2007

[65] A. R. Abudullah, and A. Z. Sha'ameri, "Power Quality Analysis Using Linear Time-Frequency Distribution," *2nd IEEE International Conference on Power and Energy (PECon 08)*, Johor Baharu, Malaysia, December 1-3, 2008.

[66] Bin W. Sharifudin, W. M. F, and Z. Sharif, "Detection and Analysis of Power Quality Disturbances Using Bilinear Time-Frequency Distribution," *2013 IEEE 9th International Colloquium on Signal Processing and its Applications (CSPA)*, vol., no., pp. 263-268, 8-10 March 2013.

[67] Z. Liu,and Q. Zhang, "An Approach to Recognize the Transient Disturbances With Spectral Kurtosis," *IEEE Transactions on Instrumentation and Measurement*, vol.63, no.1, pp.46-55, January 2014.

[68] W. Liu, and X. Guo,"Detection of Transient Power Quality Disturbances Based EMD Combined with Choi-Williams Distribution," *2012 IEEE International Conference on Automation and Logistics (ICAL)*, vol., no., pp. 588-591, 15-17 August 2012.

[69] H. I. Choi, and W. J. Williams, "Improved Time-Frequency Representation of Multi-component Signals Using Exponential Kernel,"*IEEE Transactions on Acoust., Speech, Signal Processing*, vol. 37, pp. 862-871, 1989.

[70] J. Jeong, and W. J. Williams, "Kernel Design for Reduced Interference Distributions," *IEEE Transactions on Signal Processing*, Vol. 40, no. 2, pp. 402-412, February 1992.

[71] P. Loughlin, L. E. Atlas, and J. Pitton, "Advanced Time-Frequency Representation for Speech Processing," *in: Visual Representation of Speech Signals*, M. Cooke, S. Beete, and M. Crawford (eds.), John Wiley and Sons, 1993.

[72] L. Cohen, "Generalized Phase-Space Distribution Functions", *Jour. Math. Phys.*, Vol. 7, pp. 781-786, 1966.

[73] C. H. Page, "Instantaneous Power Spectra," *Journal of Applied Physics*, vol. 23, pp. 103-106, 1952.

[74] Y. Shin, E. Powers, and W. Grady, "On Definition of Cross Time-Frequency Distribution Function," *in Proc. SPIE-Advanced Signal Processing Algorithms, Architectures, Implementations X*, San Diego, CA, July 2000, pp. 9-16.

[75] Y.-June Shin, E. J. Powers, W. M. Grady, and A. Arapostathis, "Signal Processing-Based Direction Finder for Transient Capacitor Switching Disturbances," *IEEE Transactions on Power Delivery*, vol. 23, no. 4, pp. 2555-2562, October 2008.

[76] Y.-J. Shin, D. Gobert, S.-H. Sung, E. J. Powers, and J. B. Park, "Application of Cross Time-Frequency Analysis to Postural Sway Behavior: The Effects of Aging and Visual Systems," *IEEE Transactions on Biomedical Engineering*, vol. 52, no. 5, pp. 859-868, May 2005.

[77] Federal Energy Regulatory Commission (FERC), United States of America, Docket no. RM05-4-001; Order no. 661-A, Interconnection for Wind Energy, December 12, 2005.

[78] W. J. Williams, "Uncertainty, Information, and Time-Frequency Distributions", *in Advanced Signal Processing Algorithms, Architectures, and Implementations II, SPIE.*, vol. ,1566, pp. 144-156, 1991.

[79] S. Aviyente, and W. J. Williams, "A Centrosymmetric Kernel Decomposition for Time-Frequency Distribution Computation," *IEEE Transactions on Signal Processing,* vol. 52, no. 6, pp. 1574-1584, June 2004.

[80] C. S. Demoulias, and P. Dokopoulos, "Electrical Transients of Wind Turbines in a Small Power Grid," *IEEE Transactions on Energy Conversion*, vol. 11, no. 3, pp. 636-642, September 1996.

[81] D. Gautam, V. Vittal, and T. Harbour, "Impact of Increased Penetration of DFIG-Based Wind Turbine Generators on Transient and Small Signal Stability of Power Systems," *IEEE Transactions on Power Systmes*, vol. 24, no. 3, pp. 1426-1434, August 2009.

[82] V. C. Ganti, B. P. Singh, S. K. Aggarwal, and T. C. Kandpal, "DFIG-Based Wind Power Conversion with Grid Power Leveling for Reduced Gusts," *IEEE Transactions on Sustainable Energy*, vol. 3, no. 1, pp. 12-20, January 2012.

[83] H. Emanuel, M. Schellschmidt, and S. Wachtel, "Power Quality Measurement of Wind Energy Converters with Full-Scale Converter According to IEC 61400-21," *10th International Conference on Electrical Power Quality and Utilisation*, pp. 1-7, September 2009.

[84] Z. Chen, and E. Spooner, "Grid Power Quality with Variable-Speed Wind Turbines," *IEEE Transactions on Energy Conversion*, vol. 16, no. 2, pp. 148-154, June 2001.

[85] J. I. Herrera, T. W. Reddoch, and J. S. Lawler, "Harmonics Generated by Two Variable Speed Wind Generating Systems," *IEEE Transactions on Energy Conversion*, vol. 3, no. 2, pp. 267-273, June 1988.

[86] M. Martinez, T. Itsaso, S. A. Gerardo, and H. Camblong, "Sliding-Mode Control for DFIG Rotor- and Grid-Side Converters Under Unbalanced and Harmonically Distorted Grid Voltage," *IEEE Transactions on Energy Conversion*, vol. 27, no. 2, pp. 328-339, June 2012.

[87] R. Pena, J. C. Clare, G. M. Asher, and A. Arapostathis, "Doubly Fed Induction Generator Using Back-to-Back PWM Converters and Its Application to Variable Speed Wind-Energy Generation," *IEEE Proceedings Electric Power Applications*, vol. 143, no. 3, pp. 231-241, May 1996.

[88] *"20% Wind Energy by 2030"*, Executive Summary, U. S. Department of Energy, December 2008.

[89] A. Sumper, O. Gomis-Bellmunt, A. Sudria-Andreu, R. Villafafila-Robles, and J. Rull-Duran, "Response of Fixed Speed Wind Turbines to System Frequency Disturbances," *IEEE Transactions on Power Systems*, vol. 24, no. 1, pp. 181-192, February 2009.

[90] L. Munteanu, A. L. Bratcu, N. A. Cutululis, and E. Ceangâ, "*Optimal Control of Wind Energy Systems*," Springer, 2008.

[91] C. Luo, and B. T. Ooi, "Frequency Deviation of Thermal Power Plants Due to Wind Farms", *IEEE Transactions on Energy Conversion*, vol. 21, no. 3, pp. 708-716, September 2006

[92] H. Banakar, C. Luo, and B. T. Ooi, "Impacts of Wind Power Minute-to-Minute Variations on Power Systems Operation,"*IEEE Transactions on Power Systems*, vol. 23, no. 1, pp. 150-160, February 2008.

[93] C. Luo, H. G. Far, H. Banakar, and B. T. Ooi,"Estimation of Wind Penetration as Limited by Frequency Deviation", *IEEE Transactions on Energy Conversion*, vol. 22, no. 3, pp. 783-791, September 2007.

[94] L. Jin, S. Yuan-Zhang, P. Sorensen, L. Guo-Jie, and G. Weng-Zhong,"Method for Assessing Grid Frequency Deviation Due to Wind Power Fluctuation Based on Time-Frequency Transformation", *IEEE Transactions on Sustainable Energy*, vol. 3, no. 1, pp. 65-73, January 2012.

[95] S. Heirer, *Grid Integration of Wind Energy Conversion System*, New York: Wiley, 1998.

[96] V, Akhmatova, and H. Knudsenb,"An Aggregate mmodel of a Grid-Connected, Large-Scale, Offshore Wind Farm for Power Stability Investigations - Importance of Windmill Mechanical System," *International Journal of Electrical Power and Energy Systems*, vol. 24, Issue 9, pp. 709-717, November 2002.

[97] IEEE SSR Task Force, "First Benchmark Model for Computer Simulation of Subsynchronous Resonance," *IEEE Transactions on Power Application Systems*, vol. PAS-96, pp. 1562-1572, September/October 1997.

[98] P. M. Anderson, A. Bose, "Stability Simulation Of Wind Turbine Systems," *IEEE Transactions On Power Apparatus And Systems*, vol. 102, no. 12, pp. 3791-3795, December 1983.

[99] Z. Guo, L.-G. Durand, and H. C. Lee, "The Time-Frequency Distributions of Nonstationary Signals Based on a Bessel Kernel," *IEEE Transactions on Signal Processing*, vol. 42, no. 7, pp. 1700-1707, July 1994.

[100] Y. J. Shin, A. C. Parsons, E. J. Powers, and W. M. Grady, "Time-Frequency Analysis of Power System Fault Signals for Power Quality," *Proceedings of IEEE Power Engineering Society Summer Meeting*, Edmonton, Alberta, Canada, pp. 402-407, 1999.

[101] C. L. Fortescue, "Method of Symmetrical Components Applied to the Solution of Polyphase Networks," *AIEE Transactions*, vol. 37, pp. 1027Ď1d'71140, 1918.

[102] C. Rahmann, H. J. Haubrich, A. Moser, R. Palma-Behnke, L. Vargas, and M. B. C. Salees, "Justified Fault-Ride-Through Requirements for Wind Turbines in Power Systems," *IEEE Transactions on Power Systems*, vol. 26, no. 3, pp. 1555-1563, August 2011.

[103] A. O. Ibrahim, T. H. Nguyen, D. C. Lee, and S. C. Kim, "A Variable Speed Wind Turbine Control Strategy to Meet Wind Farm Grid Code Requirements," *IEEE Transactions on Power Systems*, vol. 25, no. 1, pp. 331-340, February 2010.

[104] K. E. Okedu, S. M. Muyeen, R. Takahashi, and J. Tamura, "Wind Farms Fault Ride Through Using DFIG With New Protection Scheme," *IEEE Transactions on Sustainable Energy*, vol. 3, no. 2, pp. 242-254, April 2012.

[105] L. G. Meegahapola, T. Littler, and D. Flynn, "Decoupled-DFIG Fault Ride-Through Strategy for Enhanced Stability Performance During Grid Faults," *IEEE Transactions on Sustainable Energy*, vol. 1, no. 3, pp. 152-162, October 2010.

[106] B. Badrzadeh, and A. Halley, "Challenges Associated With Assessment and Testing of Fault Ride-Through Compliance of Variable Power Generation in Australian National Electricity Market," *IEEE Transactions on Sustainable Energy*, vol., no., pp., June 2014.

[107] A. Moawwad, M. El Moursi, and W. Xiao, "A Novel Transient Control Strategy for VSC-HVDC Connecting Offshore Wind Power Plant," *IEEE Transactions on Sustainable Energy*, vol., no. 99, pp. 1-14, June 2014.

[108] T. Aigner, S. Jaehnert, G. L. Doorman, and T. Gjengedal, "The Effect of Large-Scale Wind Power on System Balancing in Northern Europe," *IEEE Transactions on Sustainable Energy*, vol. 3, no. 4, pp. 751-759, October 2012.

[109] D. Gautam, V. Vittal, and T. Harbour, "Impact of Increased Penetration of DFIG-Based Wind Turbine Generators on Transient and Small Signal Stability of Power Systems," *IEEE Transactions on Power Systems*, vol. 24, no. 3, pp. 1426-1434, August 2009.

[110] M. Black, and G. Strbac, "Value of Bulk Energy Storage for Managing Wind Power Fluctuations," *IEEE Transactions on Energy Conversion*, vol. 22, no. 1, pp. 197-205, March 2007.

[111] J. Lin, Y. Sun, Y. Song, W. Gao, and P. Sorensen, "Wind Power Fluctuation Smoothing Controller Based on Risk Assessment of Grid Frequency Deviation in an Isolated System," *IEEE Transactions on Sustainable Energy*, vol. 4, no. 2, pp. 379-392, April 2013.

[112] L. Ruttledge, N. W. Miller, J. O'Sullivan, and D. Flynn, "Frequency Response of Power Systems With Variable Speed Wind Turbines," *IEEE Transactions on Sustainable Energy*, vol. 3, no. 4, pp. 683-691, October 2012.

[113] L. Trilla, O. Gomis-Bellmunt, A. Junyent-Ferre, M. Mata, J. Sanchez Navarro, and A. Sudria-Andreu, "Modeling and Validation of DFIG 3-MW Wind Turbine Using Field Test Data of Balanced and Unbalanced Voltage Sags," *IEEE Transactions on Sustainable Energy*, vol. 2, no. 4, pp. 509-519, October 2011.

[114] W. Cho, and E. J. Powers, "Time-frquency Analysis for the Grid Power Quality of a Variable Speed Wind Turbine Generators," *Proceedings of IEEE Power Electronics and Machines in Wind Applications*, Lincoln, NE, pp. 1-6, June 2009.